ABSTRACT

Assessing the Magnitude and Frequency of Hydrological Processes
and their Effect on Threshold Channel Morphology, North Bosque River, TX

Samuel T. Barber, M.S.

Mentor: Peter M. Allen, Ph.D.

The North Bosque River (NBR) is a dynamic fluvial system experiencing geomorphic change resulting from hydrological and sedimentological influences. This thesis describes the forces that influence hydrological and geomorphological shifts along the NBR corridor, emphasizing the relationship between the frequency and magnitude of high flow events. An increase in NBR mean daily discharge from 5.6 to 8.4 m^3/s is attributed to a historical 100-yr flood recorded in late 1991. The NBR's geomorphic response to flow increases are primarily observed as planform and slope profile changes. Vertical profile changes are limited by the presence of rigid beds, which degrade at a rate of 0.73 mm/yr. Planform erosional assessments indicate that NBR cutbanks are shearing at 0.5 to 0.75 m/y. The NBR's slope increased and sinuosity decreased from 1995 to 2019. These morphological and hydrological changes characterize the NBR's response to a historical flood event.

Assessing the Magnitude and Frequency of Hydrological Processes
and their Effect on Threshold Channel Morphology, North Bosque River, TX

by

Samuel T. Barber, B.S.

A Thesis

Approved by the Department of Geosciences

_____

Steven G. Driese, Ph.D., Chairperson

Submitted to the Graduate Faculty of
Baylor University in Partial Fulfillment of the
Requirements for the Degree
of

Master of Science

Approved by the Thesis Committee

_____

Peter M. Allen, Ph.D., Chairperson

_____

John A. Dunbar Ph.D.

_____

Joseph D. White, Ph.D.

Accepted by the Graduate School

May 2021

_____

J. Larry Lyon, Ph.D., Dean

Page bearing signatures is kept on file in the Graduate School.

TABLE OF CONTENTS

LIST OF FIGURES

LIST OF TABLES

LIST OF ABBREVIATIONS

CFA	Comprehensive Flow Analysis
CSR	Capacity/Supply Ratio
D	Sediment caliber / distribution
d_{16}	16^{th} percentile sediment caliber
d_{50}	50^{th} percentile sediment caliber
d_{84}	84^{th} percentile sediment caliber
F	Frequency
FDC	Flow duration curve
FFA	Flood-frequency analysis
HEC-RAS	Hydrologic Engineering Center's River Analysis System
IDW	Inverse Distance Weighted interpolation
K_d	*Soil* adsorption coefficient
K_{gr}	Cretaceous Glen Rose Formation
K_{ked}	Cretaceous Edwards Formation
K_{pa}	Cretaceous Paluxy Sand Formation
Ksat	Saturated Hydraulic Conductivity
K_{wa}	Cretaceous Walnut Clay Formation
L	Sedimentary load - transport
M	Magnitude
MCP	Mass curve profile
NBR	North Bosque River, TX
NC	Neils Creek, TX
Q	Hydrologic discharge (flow)
Q_{al}	Quaternary alluvium
Q_{eff}	Effective discharge
RBFI	Richard-Baker Flashiness Index
RD	Root dendrology
REM	Root exposure morphology
RGA	Rapid geomorphic assessment
RI	Return-interval
S	Slope
ΔT	Change over time interval
Tc	Soil strength / shear
v_c	Critical velocity
W	Channel width
α	Alpha parameter
β	Beta parameter

ACKNOWLEDGMENTS

I would like to express my thanks to my committee members Dr. Peter Allen, Dr. John Dunbar, and Dr. Joseph White for providing me with an interesting and unique study, and for pushing my limits as a scientist and student. Without your express mentorship and patience, completing this thesis would have been a near impossible task. Thank you to the many members of Baylor University who have helped me with various aspects of my thesis - to Dr. Joe Yelderman, Mr. Bruce Byars, and Mr. Wayne Hamilton - your assistance made this monumental task possible. For long drives through the North Bosque Watershed with Wayne, your friendship (and driving skills) made that task worth every mile. I would love the chance to get lost on Texas roads with you again. To the geoscience students and faculty who taught me the 'ins and outs' of the laboratory, I thank you. A special thanks those who granted me access to their personal properties in pursuit of my research - to Mr. John Bullion and Mr. Kent Gilbreath; I could not have accomplished this without your help and generosity. To Mr. Michael Danella of the USACE-DFW, for providing crucial HEC-RAS data for the North Bosque River; this data was a great tie in to the thesis and saved weeks of field work. To Dr. Beebe, thank you for giving me access to a quiet place to write and revise. Simply saying that writing this thesis has been challenging would be a huge understatement; there have been so many people who have encouraged me to stay positive and persevere despite the challenges of fatherhood, the global pandemic, the stressors of graduate school, and the added difficulty of working remotely - thank you to all of my friends and family who have always supported me and helped me stay strong every inch of the way.

DEDICATION

To my wife Katherine and my son Thomas, you are both crucial to my success as a student, husband, and father - you both inspire me to push through the hardest of times

CHAPTER ONE

Introduction

Riverine erosion is a fluvial process that has been comprehensively analyzed as it directly impacts the loss of farmable and habitable land (Wilkinson & McElroy, 2007), can adversely affect river ecology (Das et al., 2014), and is costly to mitigate and prevent in large-area tributaries (Roy et al., 2018; Logar, Brouwer, &Pailex, 2019). Riverine erosion is monitored by both federal agencies and private-sector industry to assess impacts on civilians and infrastructure. The cost of this monitoring is large, with inflation adjusted rates for river restoration projects ranging from 3,800 to 24,000 USD per river mile (FEMA 1991). According to Gregory [2006], there are over 3.5 million miles of rivers within the United States, most of which are to some degree impacted by the influence of anthropogenic stressors. The National Rivers and Streams Assessment performed by the EPA [2014] determined that 23% of the US stream riparian zones were in poor physical condition, and therefore are more prone to erosional processes such as degradation or channel shearing. This amounts to approximately 1 to 6.7 billion USD in stream restoration costs depending on impact severity (according to FEMA dollar/river-mile cost estimates). Restoration includes floodplain management, erosion mitigation, structure removal/improvement and other engineering techniques to improve the overall form and function of waterways (Palmer et al., 2007). The immense cost to repair these impacted streams is an economic explanation for the abundance of river erosion studies. However, due to regional differences in stream type, vegetative cover, watershed area and channel form variability, effectively constraining all river functions into a single

study has proven to be a difficult task. In order to group rivers, conceptual models are often utilized in riverine studies.

Conceptual models represent the theoretical function of a system, and are often implemented since they do not strictly rely on measured data. Many applications of these conceptual models are incorporated throughout literature, including fluvial sedimentary processes (Snyder et al., 2004), water-driven soil erosion (Parsons et al., 2004), river changes resulting from in-channel structures (Brandt, 2000), and broad fluvial geomorphologic studies (Biedenhern, Thorne & Watson, 2000). One founding conceptual model is the magnitude and frequency analysis (MFA) developed by Gilbert and Mackin [1914] to describe riverine equilibrium in terms of sedimentary and hydrological inputs and their effect on channel form (Leopold, 1980). This conceptual model was expanded by Lane [1955], who characterized river equilibrium as a balance that shifts according to four interacting variables: Sediment transport (L), sediment size distributions (D), hydrological flow (Q), and river slope (S) change and interact to describe the stability of a river in terms of aggradation (deposition) and degradation (erosional processes) (Lane, 1955) (Figure 1.1).

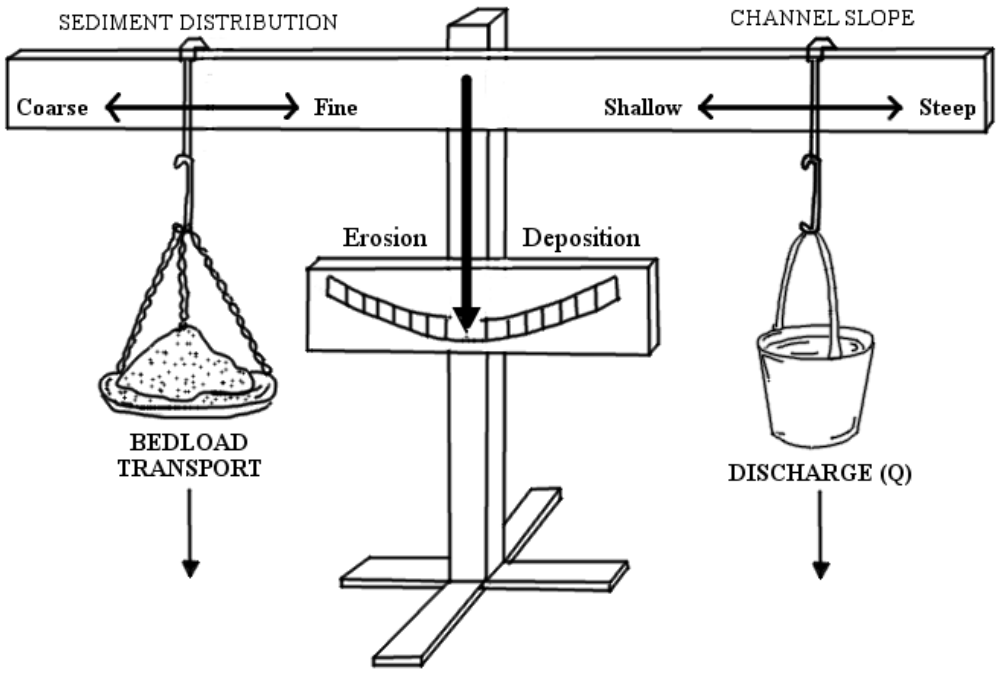

Figure 1.1. Lane's Balance depicting the relationship between S, D, L, and Q. Increasing slope leads to an increase in Q. Inversely, a shallower slope would lead to an increase in in aggradation as flow decreases. Shifts in any one factor can alter the entire river system (modified from Lane, 1955).

Lane's Balance is simplified according to the equation:

$$LD \sim QS \qquad \text{(Equation 1)}$$

This proportional relationship expresses the driving forces that interact and alter the river channel (Lane, 1955). These four variables are still considered the most important in constraining the geomorphic processes within a river.

Wolman and Miller [1960] developed yet another conceptual model to characterize fluvial geomorphologic processes. They used MFA to determine the effective discharge (Q_{eff}) of a river, representing the dominant discharge that most effectively alters river channel form (Wolman and Miller, 1960). Q_{eff} has been used across different regions, river types, and watershed studies (Pickup & Warner, 1976;

Nash, 1994; Leopold et al., 2020). The MFA of hydrological events allows researchers to gauge past, present, and future responses to changing climate, hydrological input variations, anthropogenic stressors, and ecological changes. In this thesis, I implement MFA as a proxy to assess geomorphological changes to a river in a study watershed.

Specific study objectives include to:

1. Establish the relationship between frequency and magnitude of storms and their effect on channel morphology along the North Bosque River, TX.
2. Implement comprehensive hydrological assessments to better characterize the NBRs past, present, and future response to changes in driving mechanisms such as climate and sediment inputs.

This thesis serves as a methodical guide to assess a rivers response to historically large flow volumes.

[1.1] Study Area - The North Bosque River Watershed

This study was conducted in the North Bosque River (NBR) watershed, a sub-basin to the Brazos River Basin of Texas. The NBR originates near Stephenville in Erath County, and drains approximately 3,200 square kilometers of headwaters into Lake Waco. The North Bosque River is approximately 156 river-km long, and passes through Erath, Hamilton, Bosque, and McLennan counties (Figure 1.2).

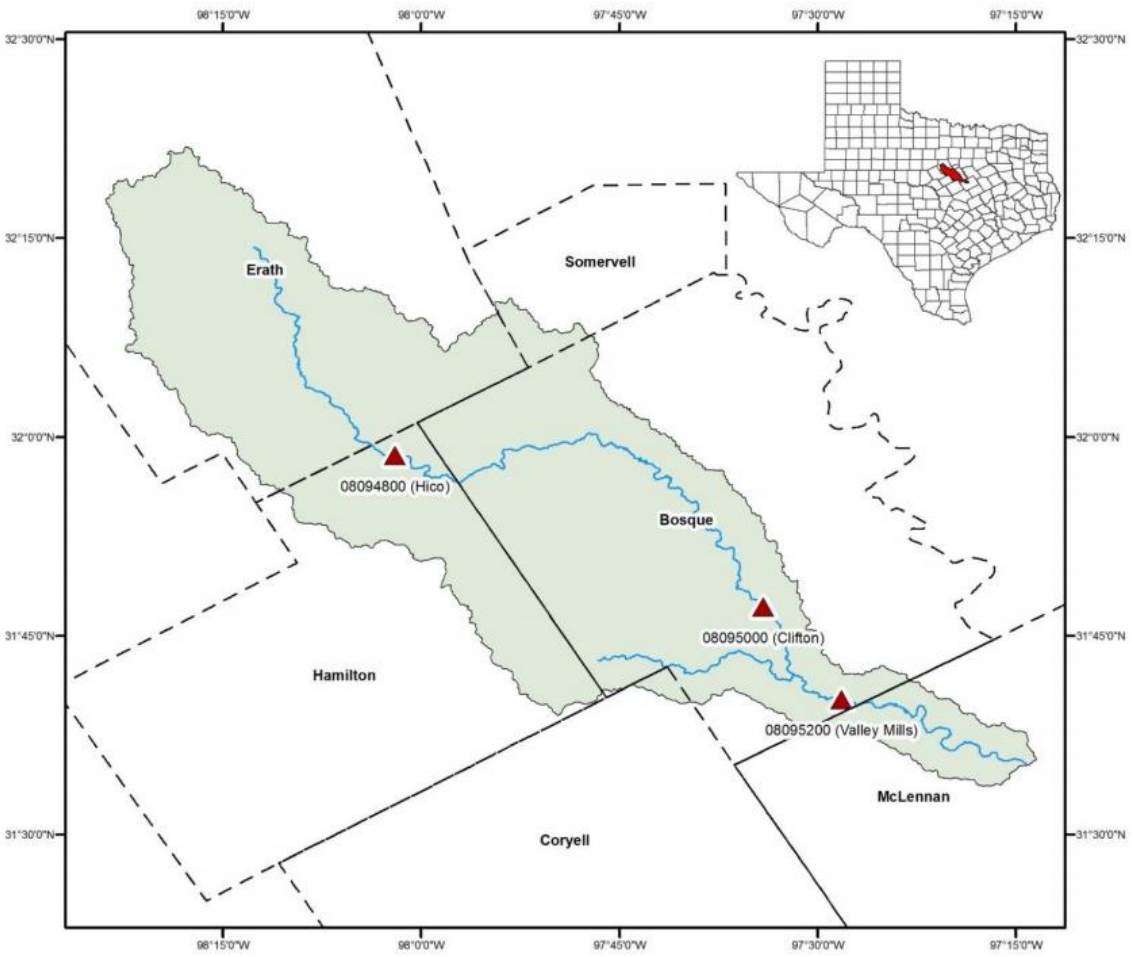

Figure 1.2. The North Bosque River watershed, Central Texas. This map shows the NBR channel and Neils Creek, a high order tributary and secondary contributor of inputs to the NBR. The three USGS gage stations located within the watershed are useful sources for historical and real-time hydrological data.

[1.2] Geological Setting

A comprehensive study of the geomorphic and geological setting of the NBR watershed was completed by Proctor [1969]. Proctor describes the NBR watershed as highly flashy, and notes that flood discharges over 500,000 cubic feet per second are a realistic potential. The NBR is in a geomorphically variable location, and includes four physiographic regions (Washita Prairie, Lampasas Cut Plain, Paluxy Cross-Timbers, and

the Glen Rose Prairie). Each of these regions is characterized by different geological units. A map of the NBR watershed geological formations are shown in Figure 1.3.

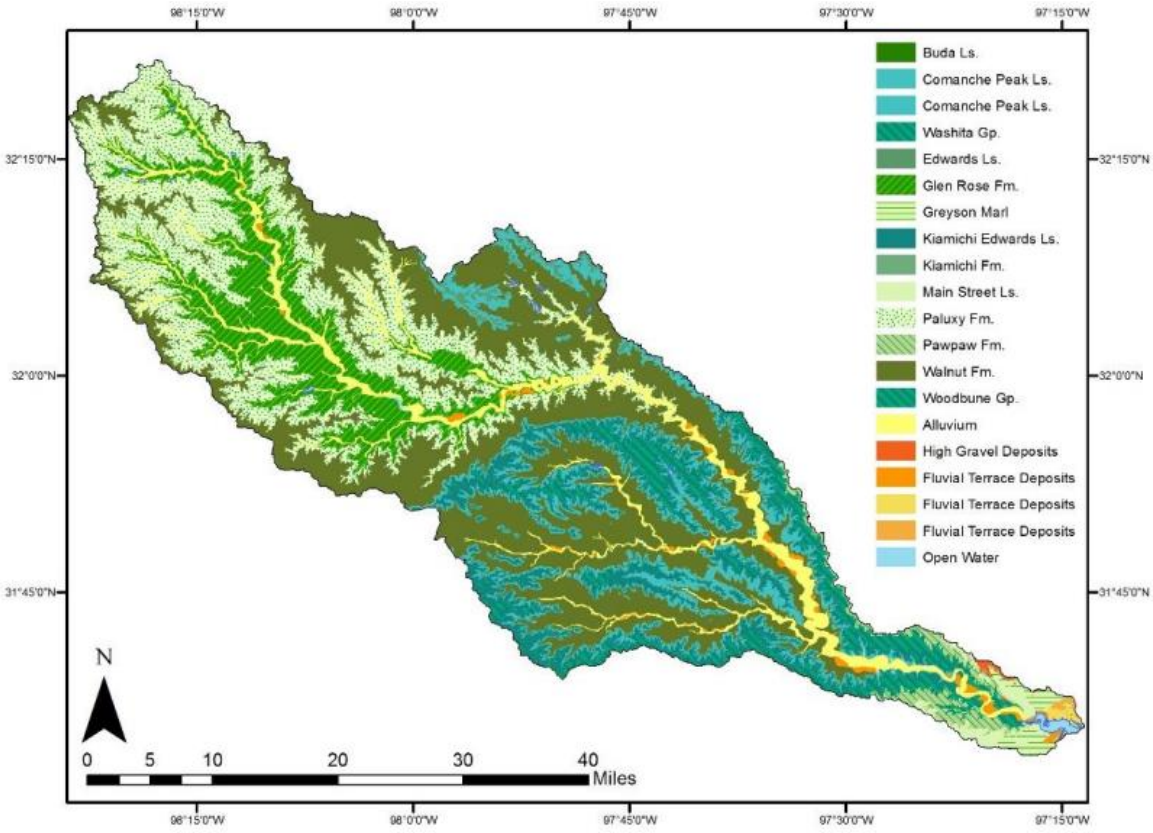

Figure 1.3. Geological map of the NBR watershed developed in ArcMap 10.8 from USGS and TNRIS datasets (2007). The NBR and its adjacent floodplain are bound by fluvial alluvium generated from the surrounding geological units.

Proctor notes that the Georgetown Formation, Edwards Limestone, Comanche Peak Limestone, Paluxy Sand, and Glen Rose Formations are the most geomorphically important formations of the watershed. Channel beds of the NBR are commonly bound by these geological formations - NBR watershed geologies were mapped according to their relative longitudinal slope profile by Proctor [1969] (Figure1.4).

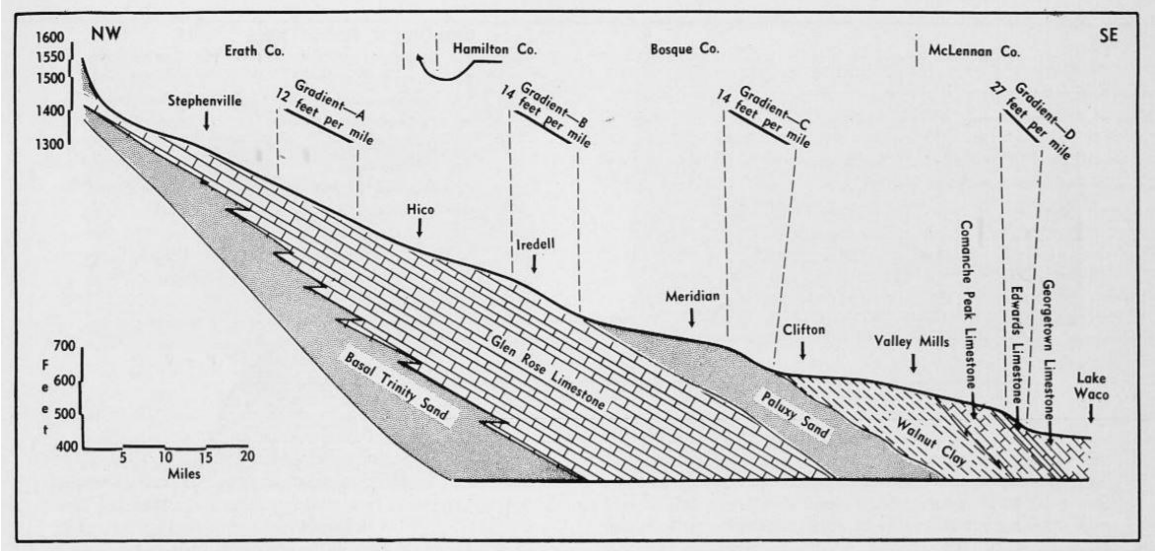

Figure 1.4. Slope profile developed by Proctor, 1969. The NBR originates within the Glen Rose formation near Stephenville, draining into the Paluxy Sand, Walnut Clay, and Comanche Peak Limestone formations.

Slope variations along the NBR are associated with the different lithologic dips that influence the channel bottom slope. The Georgetown Formation, which comprises the lower portions of the NBR watershed (Washita Prairie), is described as one of the least geomorphically significant groups. Streams in this region are widespread and have shallow gradients. Washita Prairie soils are limestone-derived and are poorly developed. In contrast, the Lampasas Cut Plain (Which includes the Edwards, Comanche Peak, and Walnut formations) occupies a majority of the NBR watershed. Of particular note, the Walnut Clay is described to be located along the valley floor of the watershed, and is often the channel bottom of NBR streams. Once again, poor soil development characterizes the watershed, this correlates to the Cretaceous limestones that dominate the region. The Paluxy Sand is located further upstream, and is characterized by slightly more developed soils and friable sands. Streams in this region are often choked by sand due to porous beds, and are described as indistinct with unremarkable boundaries. The

headwaters near Stephenville, TX represent the Glen Rose formation. The Glen Rose is described as 'benched' due to differential weathering of marls and limestones.

[1.3] Hydrological History of the NBR and Climate

The hydrology of the NBR is best described by its climate, which drives the rainfall and subsequent runoff into the watershed. The surrounding climate of the NBR watershed is classified as a 'subtropical-humid', with 30-year normal mean temperatures ranging from 18 to 20 C° (from 1981-2010 data records, normalized) (PRISM, 2020). Average annual mean rainfall rates range between 711 to 812 mm (30-yr mean normalized records) (PRISM Climate Group, Oregon State University, http://prism.oregonstate.edu, created 10 Jan, 2020.). Annual precipitation was discretized into monthly averages to determine the presence of seasonal patterns as presented in Figure 1.5.

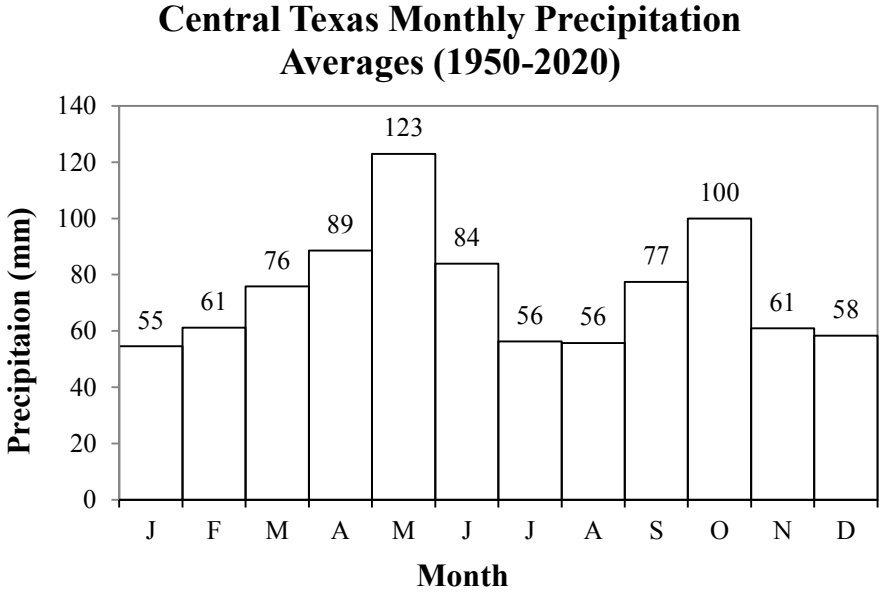

Figure 1.5. Monthly rainfall averages for Central Texas. Data was gathered from NOAA at Dallas Fort Worth; Period of record from 1950 to 2020

Monthly rainfall increases from the beginning of the year, peaking in May at 123mm. Precipitation attenuates towards the summer, with another small spike in precipitation in October. The following observations are made regarding seasonality of precipitation; (1) Summer months, particularly July and August, represent the driest periods in Central Texas. (2) Rainfall averages gradually increase during spring (March-May). (3) Winter precipitation rates remain relatively stable, averaging at 58 mm/month between November and January, and (4) precipitation in Central Texas exhibits a bimodal pattern, with peak precipitation in May and October. To better link precipitation averages to the magnitude of rainfall, depth duration recurrence intervals (RI's) were developed for the NBR watersheds according to Central Texas hydrological mean flow data compiled by Asquith [2004] (Table 1.1) .

Table 1.1. Depth-Frequency of Precipitation Maxima for the North Bosque River Watershed. Modified from Asquith et al., 2004.

24-hour Duration	
Recurrence Interval (Yr)	Rainfall Depth (mm)
2	86
5	119
10	145
25	178
50	203
100	234
250	279

Trends in monthly rainfall data closely mirror monthly flow averages as seen in Figure 1.6, monthly flow data were compiled from the Valley Mills USGS gage station 08095200.

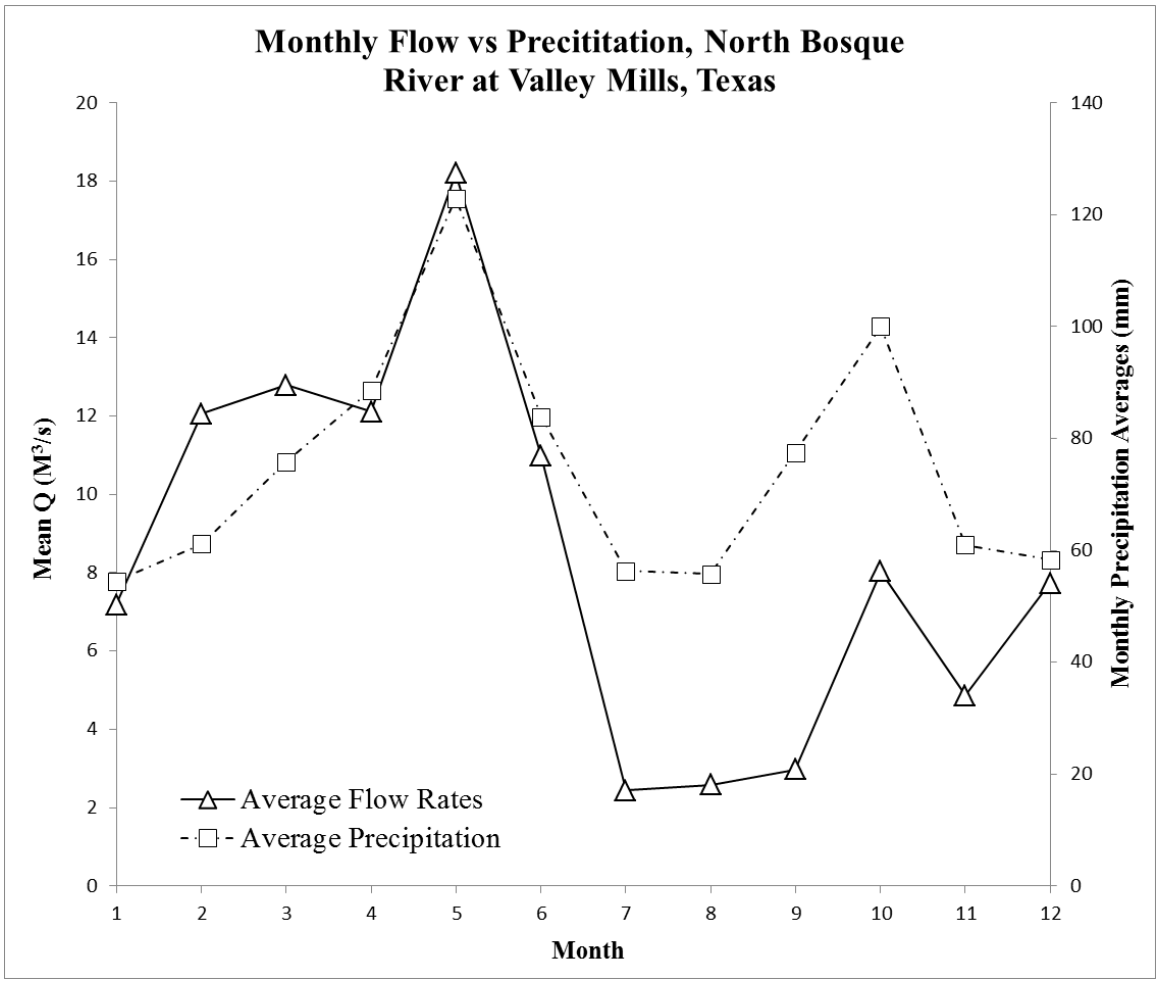

Figure 1.6. Monthly mean daily flow averages along the North Bosque River at Valley Mills (USGS gage 08095200) from 1960 to 2020. Precipitation data from figure 5 is paired to show the direct relationship between rainfall and river discharge.

Rainfall and river discharge are closely linked; both precipitation and discharge exhibit seasonally driven trends. July and August (late summer) represent the lowest average flow months along the NBR watershed. Higher flow conditions are observed during March-May, with average Q peaks in May (spring).

CHAPTER TWO

Methods

Five major facets of the NBR were studied to evaluate morphological channel change: (1) an assessment of the hydrological inputs to the NBR (cumulative flow trends, flood frequency analyses, flow duration curves, and flashiness indices). (2) The characterization of the watershed sedimentary inputs (classification of sediment sources, dominant channel sediment distributions, and effective discharges). (3) Identifying the boundary conditions of the NBR (bank composition and erodibility, confining geological units and their erodibility, and vegetation profiles of the channel). (4) An assessment of channel geometry (slope and sinuosity profiles). (5) The determination of planform and lateral migration rates (historical aerial imagery analysis, predictive erosion modelling, and root dendrology assessments).

In order to further characterize the hydrological/sedimentological regime of the NBR watershed, a scaled survey approach was implemented. This scaled approach first focuses on the entire watershed in the form of a rapid geomorphic assessment (RGA - see section 3.2.1). The RGA serves to identify dominant watershed characteristics including the sedimentary and hydrologic inputs, channel boundaries (bed and bank materials), and vegetation profiles that must be assessed to support observations made at smaller spatial scales. Information collected from this survey includes channel geometry, vegetation profiles, and bed/bank compositions. The RGA provided an observational glimpse at the processes that influence and resist channel change, but was limited in quantifiable data. This informational gap was bridged by conducting an intensive study of the NBR

between the Clifton and Valley Mills USGS gage stations, deemed the NBR Reach. The NBR Reach provided a detailed view of the river channel, the sediments and hydrology that influence it, and the boundary conditions that resist change within the channel.

The frequency and magnitude of channel form change along the NBR channel is achieved by investigating the contributing factors that act on the boundaries of the river channel. The relationship between driving and resisting forces is the primary stressor that results in channel change (width/depth, longitudinal profile, and planform). The foundation of this methodology was derived from a USACE channel stability assessment, which simplified the explanation of channel variance in the following diagram (USACE, 1994) (Figure 2.1).

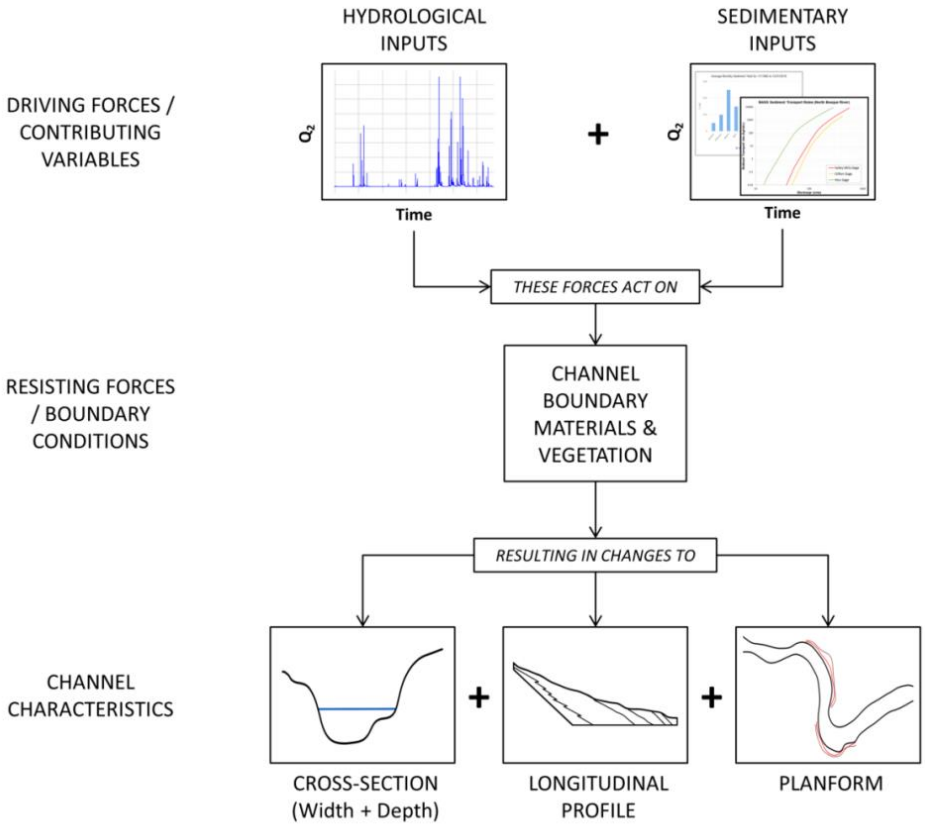

Figure 2.1. A detailed analysis of the hydrological and sedimentary inputs is completed in order to understand their effect on the channel boundaries. Establishing a relationship between these variables contextualizes channel change (Modified from USACE, 1994).

Hydrological and sedimentary inputs are characterized as the primary factors that contribute to a fluvial system; these inputs act on the channel banks and bed, resulting in changes to the channel (USACE, 1994).

[2.1] Assessment of Hydrological Inputs

Several methodologies were completed in order to characterize the historical hydrology of the NBR watershed; (1) historical data was processed to identify deviations in cumulative flow rates, (2) flood frequency analyses, (3) determination of the frequency and magnitude of historical flows via discretized Flow Duration Curves (FDC's), and (4) an assessment of stream flashiness.

To identify potential historical changes to the NBR's hydrology, a Mass Curve Profile (MCP) was developed. The MCP is a measure of cumulative mean daily flow over cumulative time, and was originally established to characterize the hydrological flow regime of a river (Searcy & Hardison, 1960). Three scenarios can be observed with a mass curve; (1) A steepening in the mass curve would indicate an increase in flowrate over time, (2) low flow conditions are observed as a reduction in the mass curve profile, and, (3) a stable balance between flow and time denotes little change to the hydrology of a river. Any distinguishable changes between these scenarios could indicate historical changes to the NBR's hydrologic flow regime. In the instance of MCP deviations, a discretized partial flood frequency analysis (PFA) will be performed. The PFA was completed by segmenting historical daily mean flow records to assess temporal variance in flow magnitude; three segments were determined from deviations in the mass curve profile, and were subsequently plotted along a PFA. A plot of flow vs. exceedance days

was developed for these time periods, and was incorporated in the effective discharge assessment in section 3.2.3.

Flood frequency analyses (FFA) of the NBR were completed to identify the magnitude and frequency of significant floods. Additionally, a flow duration curve (FDC) for the Valley Mills USGS gage station was developed to establish the frequency and magnitude of average of flows along the NBR; this FDC will be used as a hydrological input for other methodologies and was constructed with the Comprehensive Flow Analysis web-tool (CFA) (Wible et al., 2014; Wible & Arabi, 2013) which is also discretized for MCP deviations.

An assessment of the NBR's Richard-Baker Flashiness Index (RBFI) was completed to contextualize the rivers' response to precipitation. Flashiness is described as a measure of the frequency and magnitude of a rivers' response to precipitation. High RBFI values indicate that a river is responsive to precipitation, and is likely to experience short-term high magnitude flows more frequently than a river with low a RBFI (Baker et al., 2004). High RBFI values have been attributed to the movement of sediment, and can contextualize the tendency of sediment to be routed through a channel as a result of frequent increases to flow (Bledsoe, 2012). Higher magnitude flows have the ability to move sediments and erode bed/banks; as a result it is important to classify how flashy a river is in order to fully understand the hydrological regime of the river. In other words, flashiness is one way to better identify the tendency of a river to reach critical flood stages that could move channel sediments or cause channel erosion. River flashiness is dependent on regional geology, seasonal variations such as droughts or snowmelt, and storm magnitude and frequency (Bledsoe, 2012). The following equation from Baker et

al. (2004) was used to calculate the Richard-Baker Flashiness Index (RBFI) to characterize discharge inputs vs. outputs:

$$R - B\ Index = \frac{\sum_{i=1}^{n} |q_i - q_{i-1}|}{\sum_{i=1}^{n} q_i} \quad \text{(Equation 2)}$$

Where q represents daily discharge (m^3/s). The absolute change in flow over time is divided by the discharge sum for the same time period. This equation results in a dimensionless representation of flow reactivity for given river, and describes oscillations in discharge as it relates to total cumulative discharge of a river (Baker et al., 2004).

[2.2] Assessment of Sedimentological Inputs

Three primary methods were completed to characterize the sedimentary inputs within the NBR Watershed: (1) A rapid geomorphic assessment (RGA) of the watershed, (2) determination of sedimentary distributions via Wolman Pebble Count (3) a calculation of effective discharge and capacity/supply assessment.

The RGA is an assessment of 100 river crossings within the NBR watershed. The RGA was completed to identify sediment origins and to determine resisting characteristics of the watershed that influence stability along the NBR channel. RGA's allow researchers to describe variations in the boundary conditions (bed/bank material, bank vegetation, etc.) that resist erosion (downcutting/channel shearing), as well as the hydrological and sedimentary sources that move through the watershed. River assessment sites were randomly plotted along the watershed, and were snapped to the nearest road-river intersection in ArcMap 10.8. This process was completed avoid unconscious selection bias of different stream sizes within the watershed.

The density of NBR watershed riparian vegetation was completed during the RGA. This assessment included the identification of locations within the watershed that

are densely vegetated vs. those that lack dense vegetation. An observational vegetation cover rank from I-IV was assigned to each RGA location, where Class I indicates little to no vegetation, and Class-IV denotes dense vegetation.

Dominant channel forming sediments that were observed during the NBR RGA were classified according to their source and size. Sedimentary distributions and classifications were completed according to the methodologies described by Wolman (1954). A Wolman pebble count of five bars within the NBR Reach, in addition to one pebble count at the mouth of Neils Creek, was completed to quantify gravel distributions (d_{16}, d_{50}, and d_{84}) along the NBR. These gravel size distributions are used in the calculation of sediment transport rates and effective discharges. Gravel distributions were calculated via the "Size-classpebblecountanalyzer2007" Excel program (Potyondy & Bunte, 2002).

Sedimentary discharge data paired with annual FDC's were utilized to determine effective discharge rates (Q_{eff}) that affect the NBR channel via the CFA Tool (Biedenharn et al., 2000; Wible et al., 2014; Wible & Arabi, 2013). Q_{eff} can be described as a threshold flow that most effectively routes sediment through a channel (Andrews, 1980). In addition, shear stress values vs. depth profiles for the NBR were developed via USACE HEC-RAS rating curve tool.

A channel stability analysis of the NBR was completed via the Capacity/Supply Ratio (CSR) tool developed by Stroth (2017). The CSR Tool implements known sedimentary distribution data, USGS-derived hydrological FDCs, and trapezoidal channel geometries (Established via USACE HEC-RAS model) to establish a set of stable slope/width profiles (Stroth, 2017). The CSR Tool solves the concept of Lane's Balance,

but instead of being limited by a single discharge, it incorporates the use of FDC data to describe sediment transport for the entire flow regime (Stroth, 2017). The CSR Tool is an adaptation of the Copeland Method (1994) which is limited to both single discharges and sand-bed streams. Stroth's CSR Tool not only accounts for all of the FDC, but has applications in gravel bedded streams as well (Stroth, 2017). The CSR will be used to describe the effect that incoming sediments and water from the 'supply reach' have on a downstream 'design reach.' In this case, the NBR Reach is the 'design,' while sedimentary and hydrological inputs from Clifton are considered the 'supply reach.'

[2.3] Characterizing the Boundary Conditions

Five techniques were completed to assess the NBR resisting boundary conditions: (1) Determination of bank sediment distributions and USDA and USCS soil classifications, (2) MiniJet soil erodibility assessment, (3) an assessment of the geological beds of the NBR, (4) the calculation of NBR geological physical properties via slake analysis, and (5) the characterization of riparian bank vegetation profiles.

Bank soil classifications and grain size analysis were completed for 9 soil samples via Mastersizer 2000 analyses, the resulting classifications are plotted on a USDA Sand-Silt-Clay ternary diagram and were classified with the USCS classification scheme. An additional classification of primary soils within the watershed was completed to determine general variations in soil characteristics (plasticity, K-sat, K-factor, bulk density, liquid limit); data for these soils was compiled from the Web Soil Survey web-tool (Proctor, 1969; NRCS Web Soil Survey, 2020). NBR soil erodibility data was determined by comparing the established soil groups with data provided by Briaud (2017), soil groups were plotted along Briaud's Soil Erodibility Indices plot to describe

their relative erodibility. To further contextualize erodibility of the NBR banks, 2 soil samples were collected for Jet Erosion assessments in accordance with methodology described by Hanson and Cook (2004). Erosional time/depth data were input into the 'Jet Erosion Test Spreadsheet version 2.1.1' by Daly (2014). This spreadsheet determines τ_c and K_d values for the soil samples, which were averaged according to the three solutions produced by the Excel program (Blaisdell Solution, Scour Depth, and Iterative Solution), and were plotted along Perera and Wu's 2016 compilation of erosional data to provide further context to the erodibility of the NBR banks.

A compilation of confining geological data was gathered to assess physical characteristics, slake durability, and erodibility of the NBR watershed geological formations (Crawford, 2020; Lamb et al., 2015; Proctor, 1969). In addition, predictive scour erosion methodologies described by Dickenson and Baillie (1991) were implemented by utilizing HEC-RAS derived parameters (stream power and stream velocity) to determine average erosion rates for geological formations in Central Texas with similar lithological properties to those within the NBR watershed. USGS mean daily flow values at the Valley Mills gage station (09805200; 60 years) were converted into stream power in order to calculate degradation rates. These methods were completed to assess the degree of erosion (in the form of downcutting/vertical degradation) along the channel-bottom of the NBR via slake durability and degradative analyses described by Dickenson and Baillie (1999). This method can be used to assess the likelihood of slope change within the NBR as a result of degradation, and provides critical comparisons to channel bank erodibility assessments.

The presence and percentage of riparian vegetation cover within the watershed was noted during the RGA. Bank vegetation profiles were assessed along the NBR watershed in order to better classify and characterize the degree of bank protection provided by roots and vegetation. Riparian vegetation can reduce erosion and channel shearing - researchers have described densely vegetated banks to be as reinforced as a bank with riprap cover (Smith, 1976). Other researchers have focused on vegetation as a proxy for estimating stream width (Anderson, Bledsoe & Hession, 2004). This approach to estimating widths assigns regression parameters (alpha and beta) and mean flow data in the following power law function to predict channel width:

$$w = \alpha Q^{\beta} \qquad \text{(Equation 3)}$$

Where α and β represent the regression coefficients and exponent respectively, Q is a geomorphically significant discharge (m^3/s), and w is the channel width (m). This is a useful calculation that is implemented to show how vegetation could effectively slow the NBR's rate of widening.

Riparian vegetation density was classified according to several schemes compiled by Anderson and Bledsoe; many variations in α and β parameters have been determined in literature (Anderson, Bledsoe & Hession, 2004). This power function is used as a reference to help identify the best fit classification scheme based on established flow conditions and current channel widths of the NBR. The cutbanks and depositional portions of the NBR are classified for the presence of vegetation in order to identify what portions of the river are more susceptible to erosion as a result of low vegetative buffering.

[2.4] Cross-Sectional Geometry and Longitudinal Profile of the NBR

Variations between the driving and resisting forces lead to shifts in channel slope and longitudinal profile. This change was assessed via the following methods: (1) development of the HEC-RAS longitudinal slope profile, and (2) an assessment of historical channel sinuosity via centerline analyses.

A slope profile of the North Bosque River was developed by utilizing minimum channel elevations in the HEC-RAS model for the North Bosque River, data for this model was provided from the USACE DFW District (USACE, 1995). Minimum channel elevations were plotted against river mile to develop a slope profile for the entire NBR. Deviations along this plot will indicate changes to the slope, which will be utilized as input data into various models, including sediment transport calculations and the CSR Tool (See section 3.2.3).

Historical air photos were used as a reference for channel centerline analysis, this analysis measures historical change in channel length over time. Changes to centerline length are indicators that the NBR channel is experiencing longitudinal change. This change is often observed in regards to sinuosity. Channels that elongate experience a reduction in slope. Inversely, a decrease in centerline length indicates that a channel is becoming shorter, mirrored by an increase in channel slope. Aerial photo analysis is a useful tool for determining centerline profiles, and has been used in as a cost-effective high-resolution approach to river dynamics research (Fisher, Bookhagen & Amos, 2013).

[2.5] Channel Form - Planform and Lateral Migration.

Lateral migration rates were determined via three methodologies: (1) Historical aerial imagery analysis, (2) Briaud's Observation Method, and (3) Root Dendrology Analysis.

Historical aerial imagery was used to calculate annual erosion rates along the cutbanks of the NBR reach. A total of eight aerial imageries were digitized and orthorectified in ArcMap 10.8 (photo metadata is available in Appendix A). A brief aerial assessment of the channel was made to identify active portions of the channel. Migration was most common along the cutbank portions of the NBR channel. For this reason only the cutbanks within the reach were delineated for lateral migration assessments. These cutbanks represent the most active portions of the channel and were selected to establish the maximum end of erosion rates within the channel. A total of 20 cutbanks (described as Cells in Figure 2.2) were observed for this assessment.

Similar methodologies have been implemented for stream surveys that utilize aerial imagery to determine historical changes to a rivers' profile (Beaver Watershed Alliance, 2017). Air-photo based methodologies have also been implemented for coastal erosion studies (Stafford, 1971). Stafford implemented measurement reference points along the coastline that would be used to establish average erosion rates (Stafford, 1971). Similarly, this method requires reference zones in order to determine erosion rates between each photo-year. Cutbanks were discretized into box-like 'cells' in order to assess the same spatial extent of each cutbank.

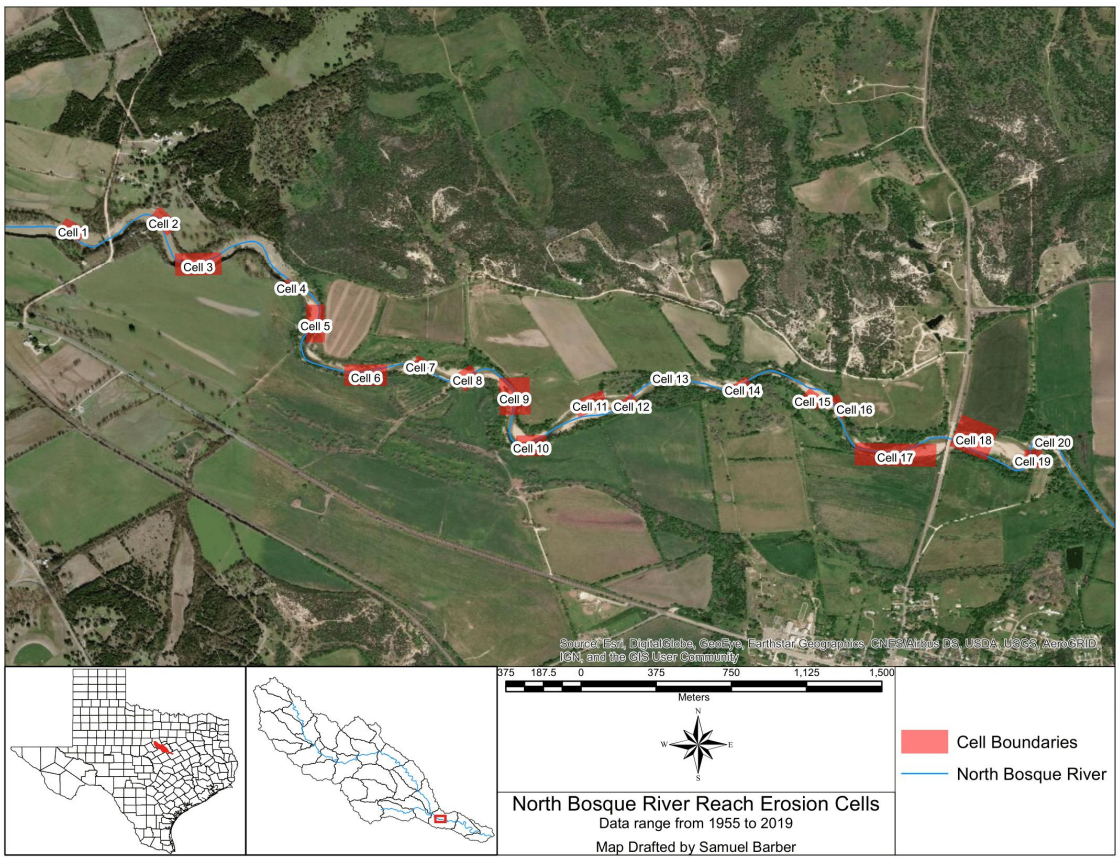

Figure 2.2. Erosion corridor cells along the NBR reach. Twenty cutbanks were selected for delineation and aerial imagery analysis, however only the last 16 cutbanks were fully processed due to lack of spatial overlap between all available imagery years.

Each cutbank cell varies in size due to differences in meander geometry; therefore, cells were sub-divided into 10 equally spaced sections to determine average erosion rates between each photo-year. Bank profiles were delineated by digitizing the boundary between the upper banks from the main bank slope, this boundary was determined for each imagery dataset (Figure 2.3).

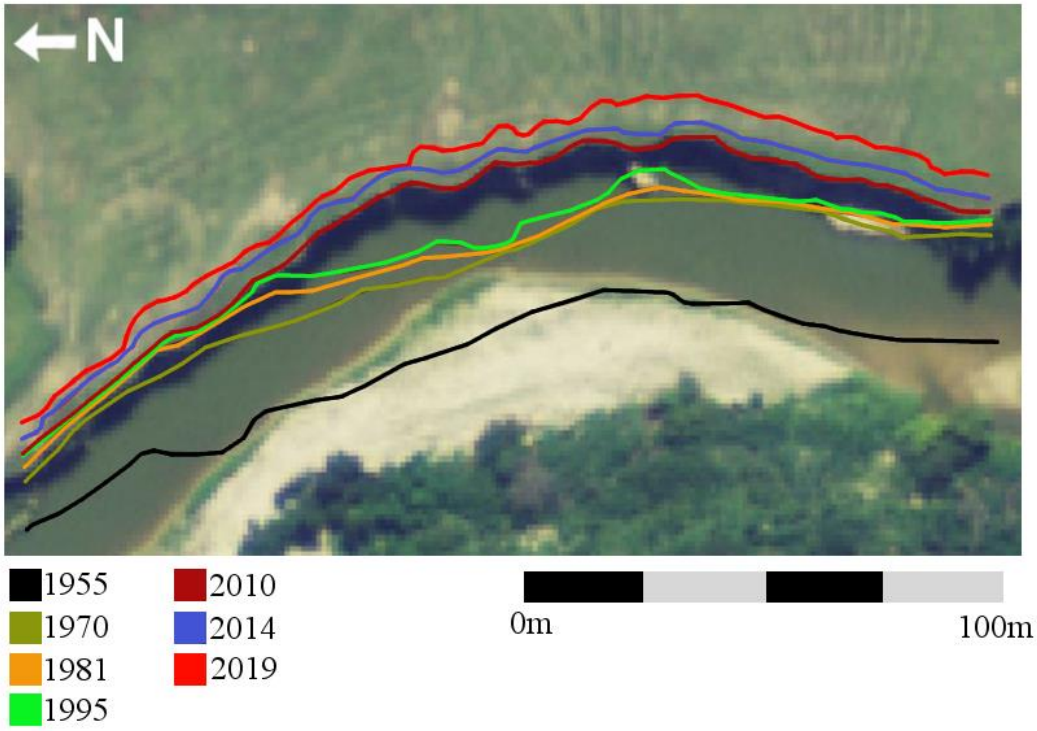

Figure 2.3. Cutbank delineation exercise example. Erosion along cutbank 9 was delineated for each aerial imagery dataset. This bank is shearing to the East. Profiles from 1955 to 2019 are noted accordingly. 2010 aerial imagery is used as the basemap for this figure.

While the air-photo delineation provides a historical look at erosion, some methods have been developed that provide predictive context to erosional events. The Observation Method was proposed as a predictive method that could determine erosion rates based on aerial photo derived erosion rates, channel geometries, water flow, and soil erodibility (Briaud & Montalvo-Bartolomei, 2014). The Observation Method serves as a 'check' for the observed aerial imagery erosion rates, and can be used to predict channel migration rates by inputting real and hypothetical data into the model. Briaud's Observation Method was utilized for the NBR with the same temporal range as the Air-Photo delineation method; however additional analyses can be easily input into the model for hypothetical hydrological events.

The final method used to assess lateral migration rates is referred to as Root Dendrogeomorphology (RD Method). The RD method allows for the calculation of erosion rates based on morphological changes to the root paired with field measured bank profiles over decadal timescales. The cell structure of roots change in response to exposure, this shift was used to identify how long ago exposure via erosion has occurred. The upper slope of the bank was projected down to the water level, and the horizontal distance from this projection to the root sample was measured. This measurement provides a distance that represents the total bank lost from erosion. Erosion rates were calculated for each sample by dividing the measured distance by the date to exposure. A total of 20 roots were collected along the NBR reach for analysis, samples were collected upon availability, and in some cases the same tree was sampled multiple times (Figure 2.4).

The NBR has a low density of suitable root samples; many of the roots along the reach were located in the upper portions of the channel and were not immediately accessible from kayak. Fourteen different trees were sampled, with a species diversity of seven. Species identifications, specific locations, and general sample notes are available in Appendix B. Root 'pucks' 2-5 cm thick were cut with an electric Ryobi chainsaw. Samples were alphanumerically labeled for orientation along the river, as features such as scarification may be related to the position of the root along the channel (Figure 2.5).

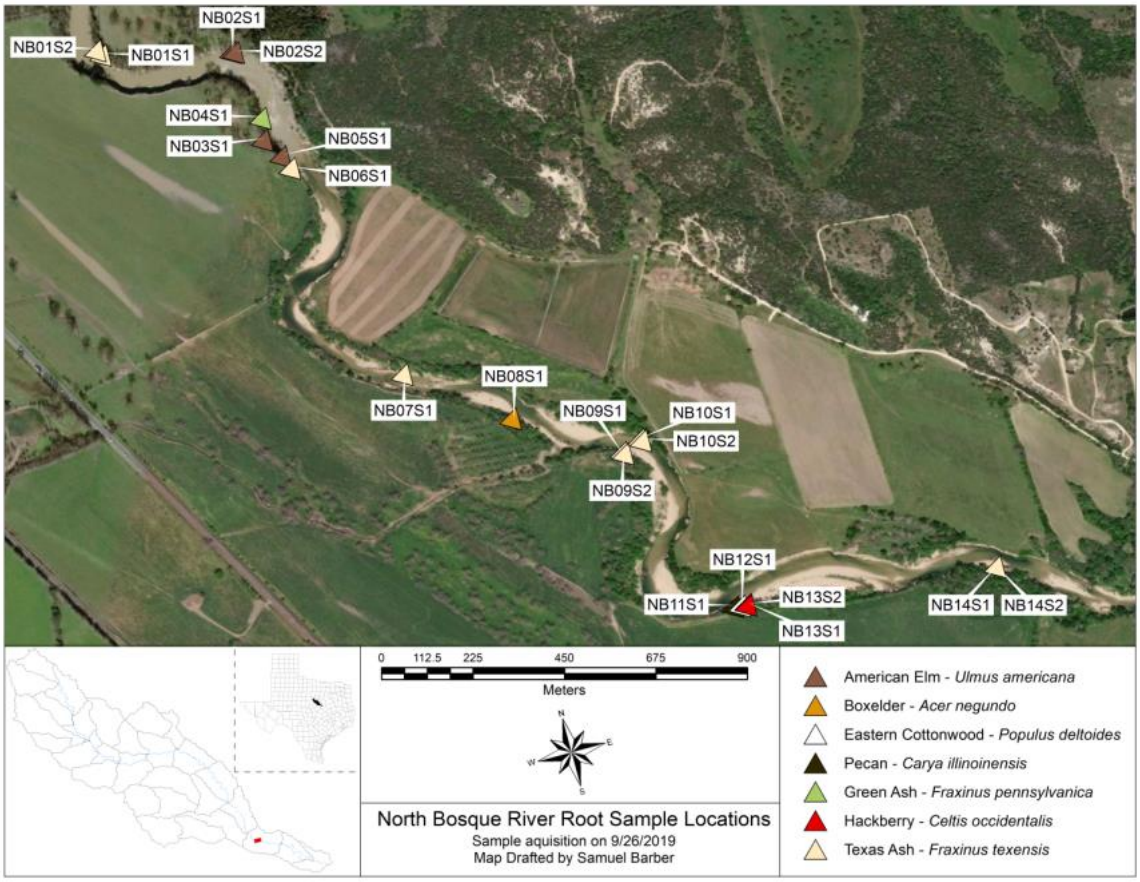

Figure 2.4. Location map of the collected root samples within the NBR reach, with tree species identification labels. Soil samples taken from the reach share the same alphanumeric IDs and are located with the corresponding root sample.

Additional channel metrics were recorded, including channel-bottom widths - which were measured to the nearest foot with a digital rangefinder. Ideally samples should be collected from similar locations within the channel (all samples from cutbanks, point bars, or straight portions of the channel) to account for variable erosion rates associated with different locations within a channel. For example, roots collected along a meandering cutbank are likely to have associated erosion rates much higher than those calculated for straight portions of the channel. In addition, sampling roots within a similar stage height is appropriate; roots were collected along bank heights that would be submerged in bankfull conditions (1.5 year flood range). Collecting roots that are in the

upper channel may not be appropriate due to the decreased probability of submersion and associated erosion within the channel.

Figure 2.5. Example of root orientation in the field: Top and Bottom portions are labeled. Upstream and downstream orientations are labeled to identify possible features related to sediment transport scarification.

Root samples were placed in an oven at 100 C° to remove excess moisture that may affect the polishing process or warp the sample over time. Dehydrated root samples were rough sanded with a 60-grit belt sander to remove major gouges from the initial chainsaw cut. A palm sander was used to progressively sand the samples up to 320-grit to remove remaining gouges and polish the surface. Samples were then hand-sanded up to 1,200-grit in order to achieve a fine polish necessary for microscopic analysis. Figure 2.6 shows the raw labelled roots, with corresponding polished surfaces observed under microscope. Root anatomy was observed for each sample. Features such as scarification, compression and partial burial were recorded. Age to exposure morphology was recorded

by counting the yearly rings of the sample to the root exposure morphology (REM). Overall root ages were also recorded.

Figure 2.6. (Top) initially exposed face of roots labeled according to orientation along the streambank. (Bottom) Sanded and processed root pucks prepared for morphology analysis.

The REM is indicated by a morphological shift from root-like ring-porous cell walls to stem-like diffuse-porous cell structures (Robert, Mencuccini & Vilalta, 2017). This change in cell structure is a natural response to prevent excess water loss. Erosion rates were calculated for each sample by dividing the REM age by the measured horizontal distance to the projected bank location. These erosion rates were then used to determine a mean erosion rate for the NBR reach. A frequency plot of root exposure dates was developed with a cell range of 2 years to assess the relationship between storm recurrence and erosional events. In addition, a frequency histogram of erosion exposure dates was developed in excel. Exposure rate by year were plotted to identify potential trends in erosional magnitude over time. Finally, a linear regression of erosion rates was plotted as an alternative method to determine lateral erosion rates. This linear regression implements average rates of erosion for each year where samples were exposed. These averages represented the erosion rate over time until a new erosion rate was calculated. Erosion rates on this graph were plotted according to their cumulative sum over time to as a proxy to determine erosion rates from the period of record.

CHAPTER THREE

Results

The frequency and magnitude of hydrological events and their resulting impact on the channel are assessed by determining the relationship between hydrological and sedimentological inputs on the resisting channel boundaries. This relationship was further supported by investigating lateral migration rates and changes to the NBR channel profile.

[3.1] Hydrological Inputs to the North Bosque River

[3.1.1] Mass Curve Profile

A mass curve of cumulative mean daily flow vs. cumulative time was developed for the USGS Valley Mills gage station 08095200. This curve, illustrated in Figure 3.1, depicts three distinct periods of flow. These periods, which are identified as observable deviations in the mass curve slope, are indicative of changes to the flow regime along the North Bosque River. These three periods are described as the Initial, Intermediate, and Current Periods. Each period represents a distinct temporal range associated with hydrologic shifts in long term flow rate.

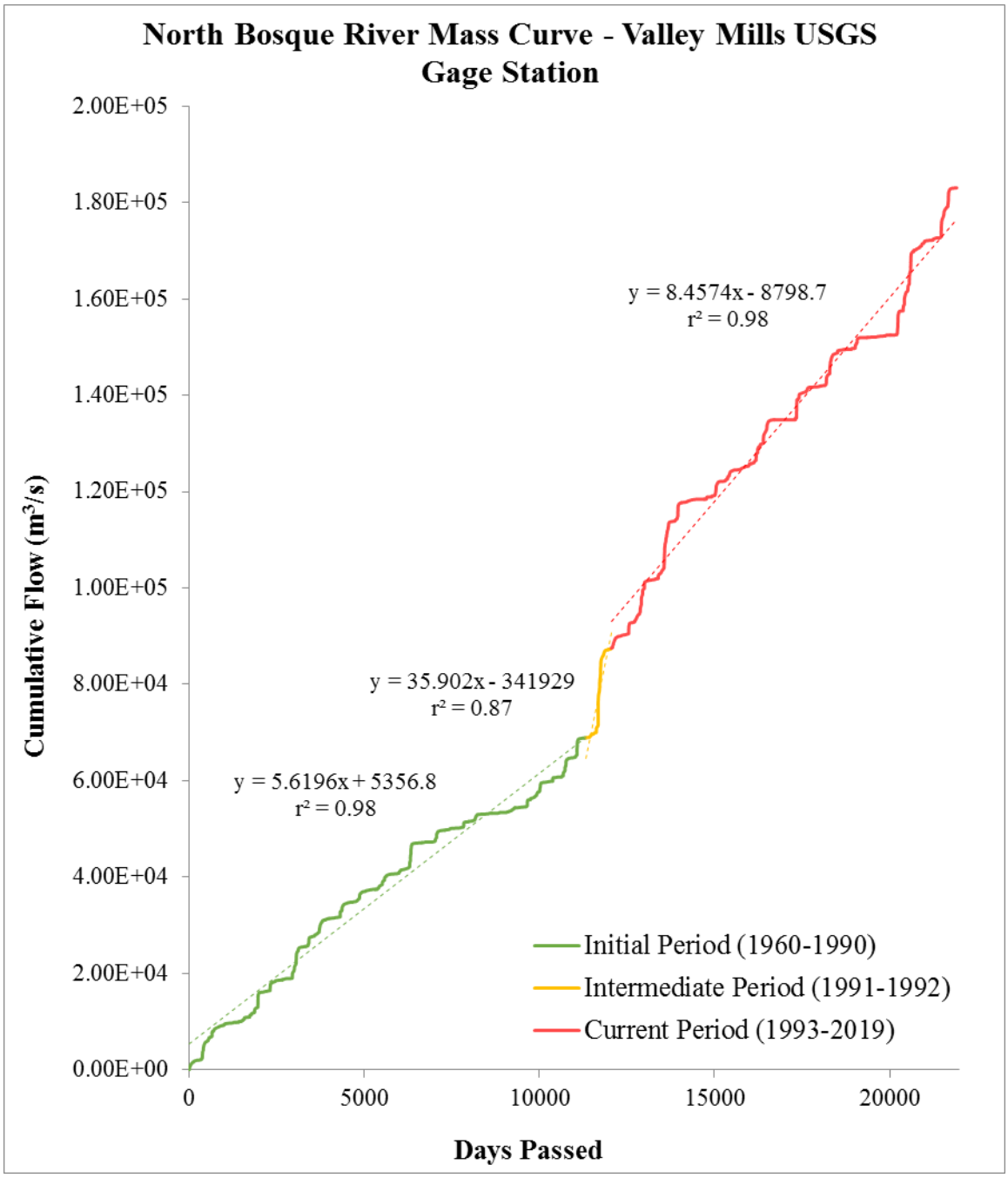

Figure 3.1. Mass curve profile depicting cumulative flow vs. cumulative time along the North Bosque River at Valley Mills, TX (Flow Data interval 1/1/1960 to 12/31/2019). A major transitional period from 1991 to 1992 was identified to change the flowrate of the NBR basin.

The Initial Period from 1960 to 1990 had an average daily flow rate of 5.62 m^3/s (r^2 = 0.98). An increase was observed from 1991-1992, flow rates were dramatically

higher (daily average of 35.9 m^3/s) s (r^2 = 0.87) which steepened the MCP. This transitional increase is described as the Intermediate Period. Lastly, an average flow rate equal to 8.46 m^3/s (r^2 = 0.97) from 1993 to 2019 characterizes the Current Period.

[3.1.2] NBR Flood Frequency Analysis

A flood frequency analysis (FFA) was developed by utilizing Valley Mills USGS gage station flow data to classify the magnitude of major floods along the NBR from 1-1-1990 to 12-31-2019 [Gage #08095200 located at Latitude 31°40'10", Longitude 97°28'09" NAD27]. The FFA identifies flow magnitude for each flood return interval (RI). The FFA for the NBR (1960 to 2019) is presented in Figure 3.2, including the largest flow events recorded during the period of record.

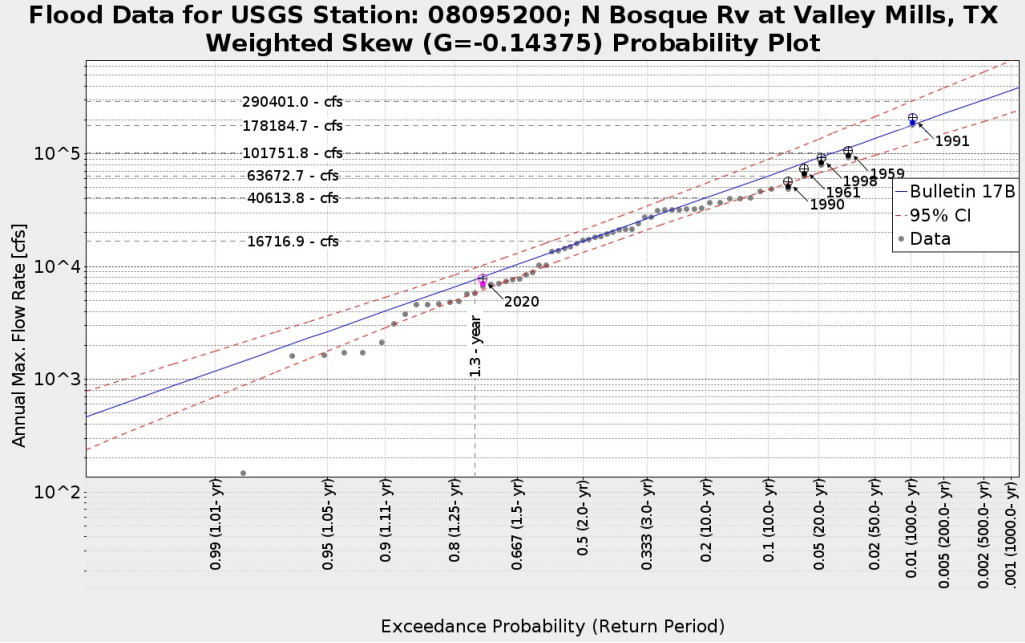

Figure 3.2. Flood frequency data derived from the USGS Valley Mills gage, developed in the CFA tool with data from 1960 to 2020. This FFA denotes 1991 as the most notable flood of record between the historical data observed. The 1991 flood is equivalent to the upper 95% confidence interval associated with the 100-year return period. The increase in channel flow is observed in both the Mass Curve Profile and Partial Frequency Analysis.

This FFA analysis shows that the flow rate of the 1991 flood was higher than all other flooding events identified for the analysis period - the 1991 flood was found to have 100-year RI. Mean flow rates and the 95% Confidence Interval flow rates for each RI are presented in Table 3.1, this table shows the range of flows associated with each RI.

Table 3.1. Data summary for the FFA at Valley Mills. These data were determined from the CFA tool - units converted to metric.

Return Period (Year)	Lower 95% Flowrate (m^3/s)	Mean Flowrate (m^3/s)	Upper 95% Flowrate (m^3/s)
200	4034.1	6094.4	10472.2
100	3278.6	4825.1	7984.4
50	2602.3	3724.3	5916.6
40	2400.8	3403.7	5332.8
25	2001.2	2779.6	4224.1
20	1822.9	2506.7	3752.1
10	1314.3	1750.0	2491.8
5	869.6	1121.7	1513.5
2	367.3	464.9	589.2
1.5	226.9	293.4	371.6
1.25	137.5	185.2	238.6
1.01	19.1	32.9	49.8

The NBR FFA at Valley Mills shows bankfull discharge estimates (RI = 1.5) of 290 m^3/s. This flow rate closely resembles the discharge associated with the 1.5 year flood from the USACE HEC-RAS flood stage/discharge rating curve in Figure 3.3, which shows bankfull discharges at 240 m^3/s.

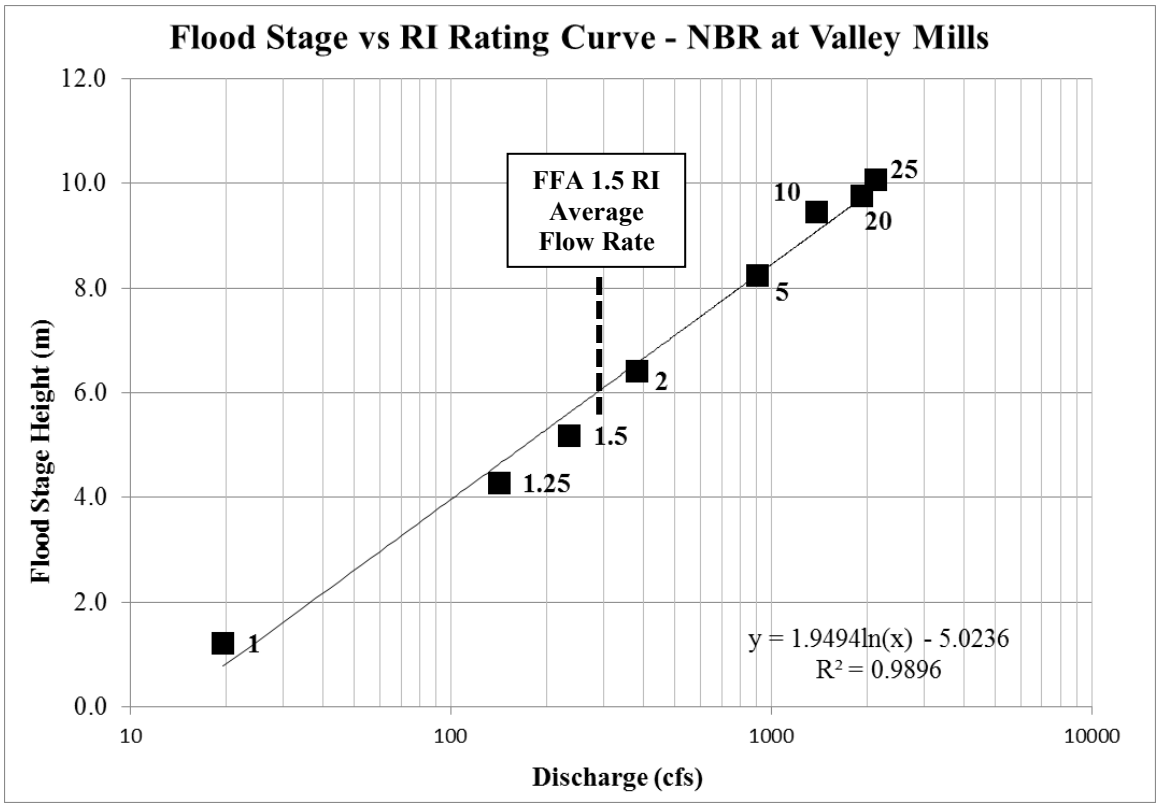

Figure 3.3. Flood stage height (m) vs Recurrence Interval Flowrates for the NBR at Valley Mills, developed in HEC-RAS with NBR data provided by the USACE-DFW. Flow volumes associated with the 1.5 year flood derived from the FFA are plotted as a dotted line.

The NBR bankfull averages were plotted along with data compiled by Chuan et al. [2014], who gathered river bankfull metrics for 230 river reaches in various countries (in particular channel slope, bankfull depth, and bankfull width) to describe how alluvial rivers are controlled by water and sediments (Figure 3.4).

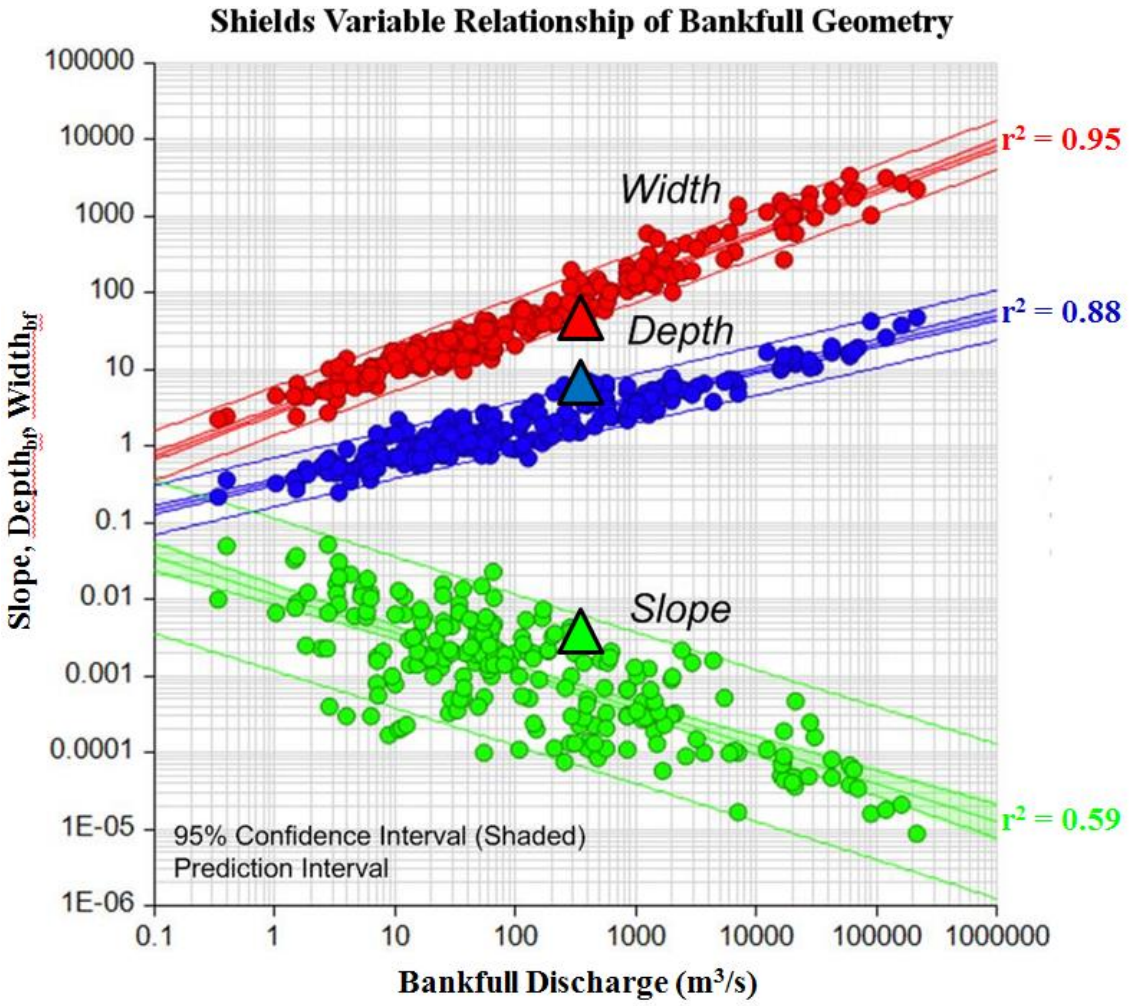

Figure 3.4. Shields variable relationship of 230 river reaches ranging from silt-bed to cobble beds (data from Chuan et al., 2014). This log-log plot presents slope, bankfull depth and bankfull width as groups against bankfull discharge. Bankfull metrics for the NBR were plotted along this chart to observationally contextualize the NBR into rivers of similar channel forming discharges, indicated by triangles or respective color.

This figure contextualizes the NBR to other watersheds with similar bankfull discharges, in addition to a range of watershed types. The NBR plots outside of the 95% Confidence Interval for all three metrics. Bankfull depth (approximately 5m) and bankfull width (appx. 30m) were selected according to bankfull flow volumes and cross section geometry from the NBR HEC-RAS model.

[3.1.3] Flow Duration Profiles of the NBR

The following section outlines the flow duration curves developed for these periods, which were developed to assess potential changes to the NBR resulting from this historical storm in 1991.

Average flow duration curves for the Initial, Intermediate, and Current Periods were developed and plotted to identify long-term changes to flow exceedance that may be linked to the 1991 flood (Figure 3.5). These data show the magnitude (flow volume) of flows and the frequency (percentage of time) that these flows are moving through the channel.

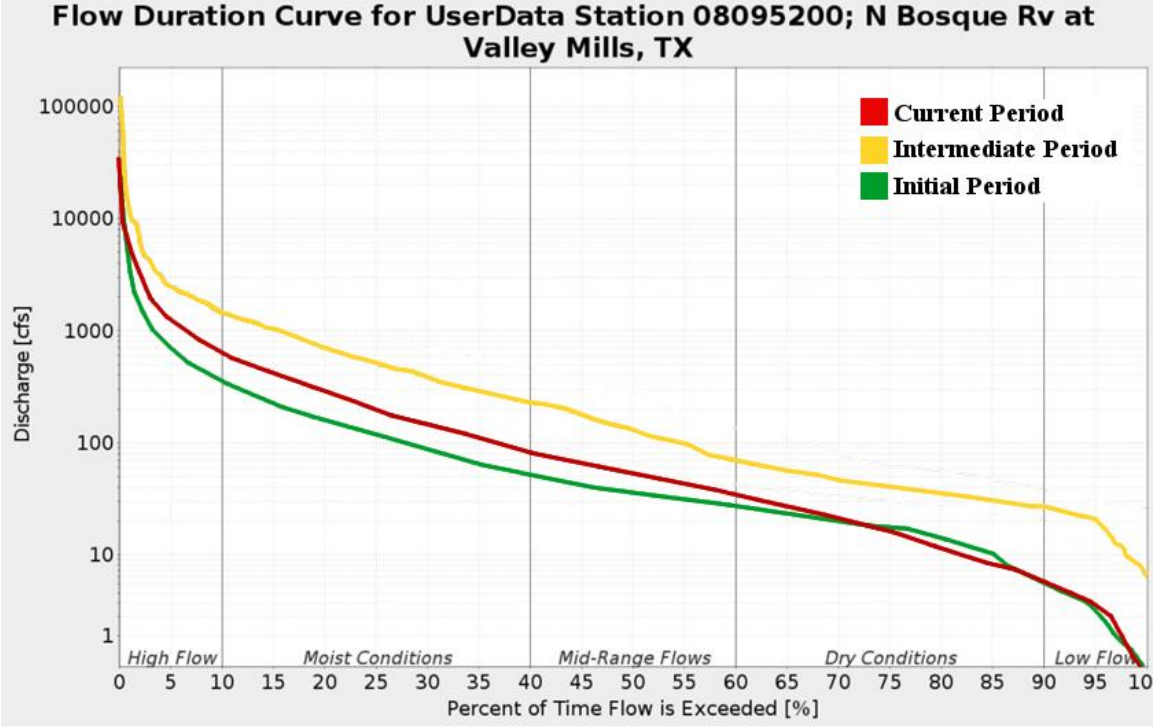

Figure 3.5. Mean FDC data for the Initial (green; 1960-1990), Intermediate (yellow;1991-1992) and Current (red; 1993-2016) flow periods. The intermediate period shows increased frequency of high flow conditions. In addition, an increase in flow conditions is noted between the Initial and Current Periods.

'High Flow' conditions represent the upper 10 percent of flow volumes, which can be described as the flows resulting from storm events and runoff. On the opposite end of the spectrum are 'Low Flow' conditions, which are associated with drought and seasonally dry periods. Each of the three flow periods has unique exceedance percentiles that express the likelihood a flow threshold will be met, these data are provided for each period in Table 3.2.

Table 3.2. Average FDC exceedance percentiles for the NBR Flow Periods. These data present flow volumes associated with each flow frequencies. [Flow Unit = m^3/s]

Exceedance Percentile	Initial Period Flowrate	Intermediate Period Flowrate	Current Period Flowrate
99	0.202	8.231	0.11
95	2.695	20.517	2.75
90	5.593	26.729	5.366
75	18.137	40.792	16.045
50	37.092	129.25	52.113
25	123.45	513.5	192.536
10	357.609	1439	626.45
5	698.57	2489	1288.5
1	3067.7	10681.5	6319.6

The flow rates associated with the Initial Period from 1991-1992 are remarkably higher than the other periods (99^{th} percentile flows are an order of magnitude higher than the other Periods). This information is critical to determine shear stress values within the NBR channel. Establishing a relationship between the flow frequencies and in-channel shear stress is useful for describing the frequency and magnitude of channel change in the NBR reach, as increases shear stress leads to the erosion of geomaterials - in this case the beds and banks of the NBR (Turowski et al., 2007).

[3.1.4] Stream Flashiness (R-B Indices)

The RBFI assessment was completed for the three time periods associated with the MCP to determine if the NBR is more or less reactive to incoming floodwaters, these indices are presented in Table 3.3 below.

Table 3.3. R-B indices for the Initial (1960-1990), Intermediate (1991-1992), and Current (1993-2019) Periods. The R-B Index for the entire record from 1960 to 2019 also calculated. Drainage area for the Valley Mills USGS gage station 09805200 was included for future comparison to other similarly sized watersheds.

Stream	Period of Record	R-B Index
North Bosque River: Initial Period	1/1/1960 - 12/31/1990	0.65
North Bosque River: Intermediate Period	1/1/1991 - 12/31/1992	0.76
North Bosque River: Current Period	1/1/1993 - 12/31/2019	0.61
North Bosque River (Average)	1960 - 2019	0.65

A slight decrease in RBFI is denoted from the Initial to Current Period, which is bound by a notably high RBFI value during the Intermediate Period. The R-B indices for the NBR were comped to data from Baker's study of six northern states (Illinois, Indiana, Iowa, Michigan, Ohio and Vermont - referred to as the Six-State Area) (Baker et al., 2004). First, the NBR flashiness index was plotted against the 515 measured streams and their associated R-B values vs. watershed area in Figure 3.6.

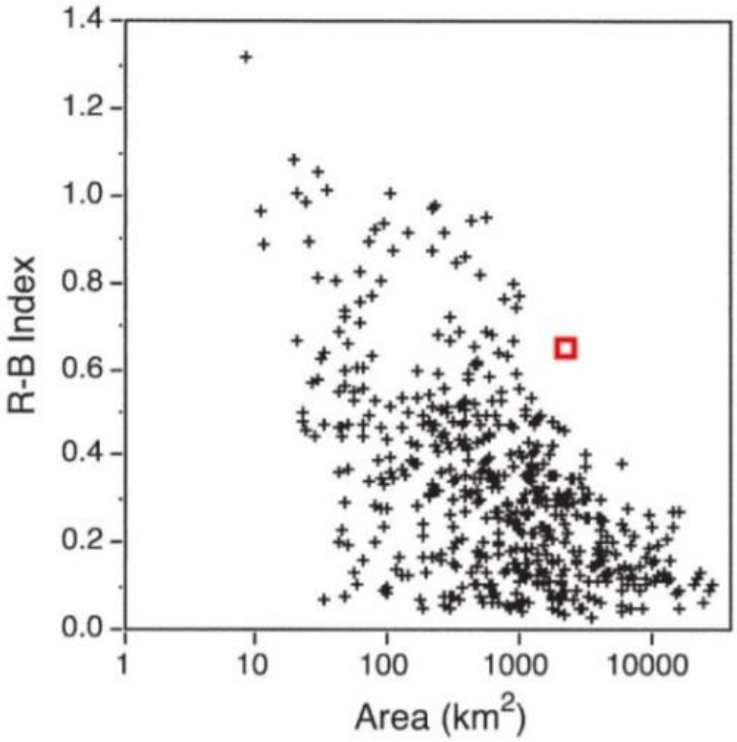

Figure 3.6. Comparison of the NBR RBFI (Indicated by the red box) compared to the 515 streams within the Six-State area. Modified from Baker et al., 2014.

This graph shows that the NBR is notably more reactive to hydrological events (rainfall events and flooding) when compared to rivers of similar watershed size in the Six-State Area, as it plots as an outlier to the main study group. The NBR's RBFI was then compared to watersheds of a similar size classification. This graphic was developed by Baker to describe the range of RBFI values associated with the rivers in the Six-State Area (Figure 3.7).

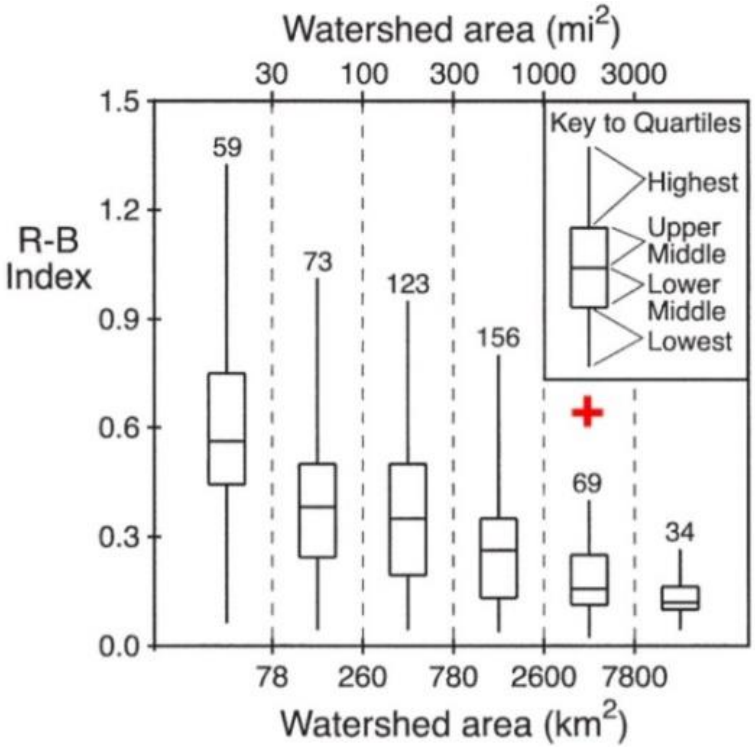

Figure 3.7. NBR RBFI vs. average watershed areas of the Northern United States. The NBR (indicated by the red cross) exhibits an RBFI notably higher than those within the Six-State Area, indicating this Texas stream is much more reactive to precipitation compared to similarly sized watersheds in the northern US. Adapted from Baker et al., 2014.

This graph shows that smaller watersheds are often flashier, since storms are often able to cover more of the watershed - effectively inputting more water into the channel for a single storm event. When compared to watersheds of a similar size classification, the flashiness value of the NBR more closely resembles RBFI values associated with smaller scale watersheds. This trends further shows that the NBR is remarkably influenced by runoff and flood events. Characterizing flashiness is useful for contextualizing the frequency of critically effective flows that can move sediments and erode the channel.

[3.2] NBR Sedimentary Assessments

The following results detail the transport and classification of sediments within the North Bosque River watershed. Recent studies have noted that the most resistive channel material drives channel form (Dunne and Jerolmack, 2020). Therefore it is important to identify the dominant sediments of the NBR, their origins within the watershed, and the processes associated their transport.

[3.2.1] Classifying Sedimentary Sources (RGA)

Riverine sediments are derived from several sources, namely: 1) from the erosion of upland materials, 2) from the bed of a river via plucking, abrasive forces, and/or entrainment, and 3) from the mining the banks via channel erosion. The RGA is a technique that helps identify the origins of sediment within the NBR watershed. Initially, the RGA was implemented by Heeren [2012] as a method to identify critically impacted streams within a watershed that are more likely to degrade. Heeren incorporated a score sheet based on channel stability - the channel stability index (CSI) - to assess the degree of erosional processes along a watershed. For the NBR, erosional evidence was similarly recorded at each site. An altered erosional classification scheme was developed by rating erosional intensity on a scale from 0 to 3 (where ‘0’ refers to ‘Stable Channels’ and ‘3’ represents channels that are ‘Severely Impacted’ by erosional processes (i.e. undercutting, lateral shearing, and bank exposure). Field photos presented in Figure 3.8 provide examples of erosional references recorded for the RGA.

Figure 3.8. RGA examples of erosion classifications. (Class 3) Photo taken along the main North Bosque River channel; severe erosion was characterized by exposed bedrock, undercut/eroded left and right banks, and bank failure. (Class 2) Photo from tributary with Paluxy Sand exposures; streams with partial bank failure, widening, notable downcutting, and presence of weak vegetative cover were often classified as moderately eroded. (Class 1) Pictured is an unnamed tributary to Neils Creek; slightly eroded streams were classified based on the presence of slight bank/bed exposures, partial bank failures, sparse vegetation, and signs of sedimentation. (Class 0) Pictured is a small order stream located on the NE segment of the watershed; smaller streams and tributaries with dense vegetation, no visible bank or beds, low flow conditions, and little sedimentation were classified as stable, and exhibit little to no erosion.

Three primary trends along the NBR were observed: (1) The RGA indicated severe erosion was more common along wider streams and tributaries, particularly along the main NBR channel. (2) Most smaller streams and tributaries were observed to be stable

as a result of shallow channel depths and dense riparian vegetation. (3) Major bedload inputs are derived from larger order tributaries of the NBR and its' adjacent headwaters (i.e. Neils Creek and Meridian Creek). Utilizing the erosional observations made during the RGA, paired with the erosional classification scheme, an erosion/sediment source map was developed for the NBR watershed (Figure 3.9) to identify locations in the watershed that are more susceptible to erosion. Note that only major named tributaries are included in the map in order to increase contrast. Each 'dot' on the map represents one of the sites located along a tributary.

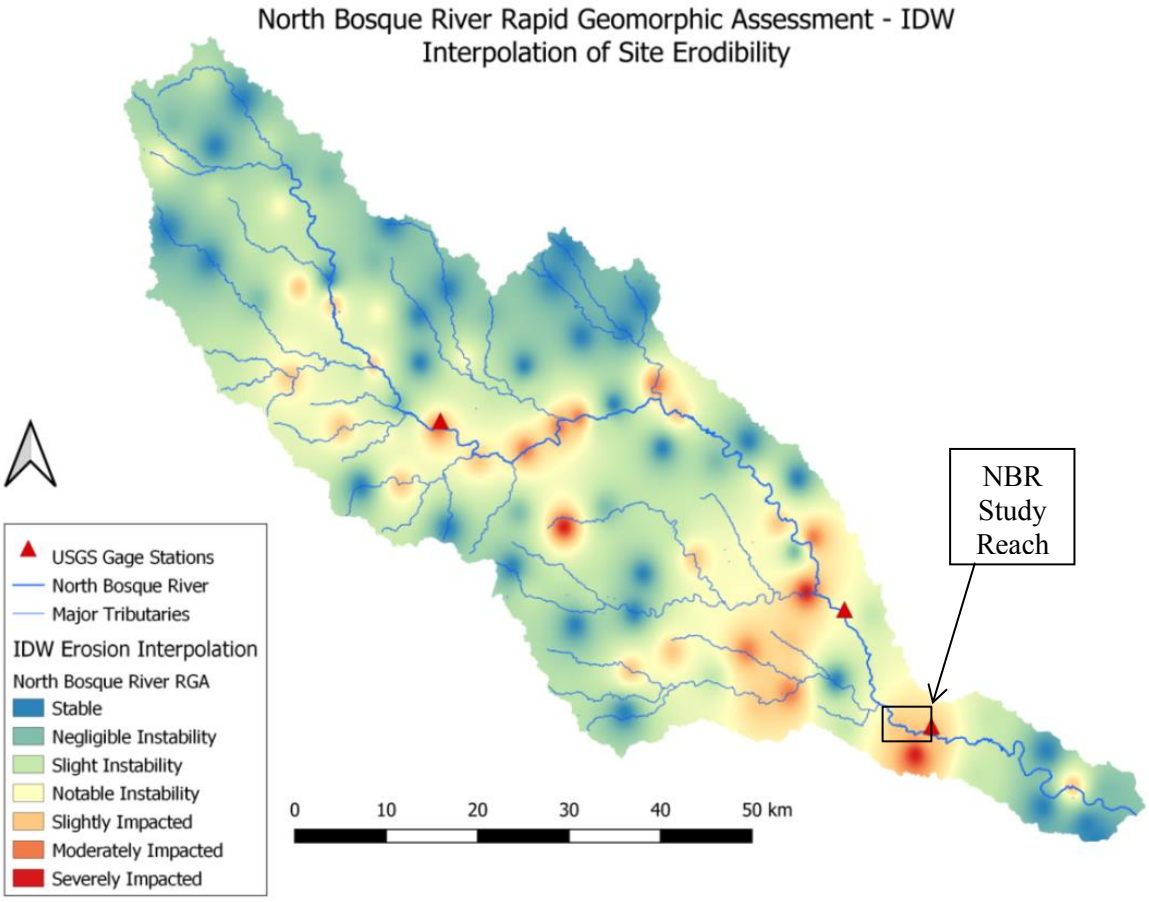

Figure 3.9. IDW interpolation of impacted streams and tributaries along the NBR watershed. IDW weights were assigned to the classification values described in Figure 20, and were plotted to identify potential sediment sources within the watershed. Small headwater streams and tributaries were removed to improve map visibility.

Site locations and general notes are for the RGA analysis are provided in Appendix C. Stable channels characterized by the presence of dense vegetation and few exposed banks/beds were observed along headwaters of the watershed. Stable channel portions often comprised of tributaries no deeper than 1 meter with gentle slopes, low flow conditions, and dense riparian vegetation. Very few signs of sedimentation were observed along the NBR headwaters - this was described as a general lack of channel bottom sediments (gravel and sand) in the NBR headwaters. Larger tributaries of the NBR watershed were often described as erosionally impacted. A general relationship between stream order and erosion severity was observed. Larger tributaries were often characterized by bank erosion, shearing, undercutting of riparian vegetation, and channel widening along the meandering portions of the stream. Channel gravels were observed in these larger tributaries along point bars and in-situ channel deposits. Sand and silt deposits were occasionally noted as overbank deposits, this was mostly observed downstream from outcrops of Paluxy Sand. Larger order tributaries were characterized by bank erosion (in the form of shearing, undercutting, and channel widening); these locations act as sources for gravel, but also contribute bank derived sediments to the study reach.

Neils Creek and Meridian Creek are dominant gravel sources, and were classified as severely impacted based on the RGA erodibility scheme. These larger tributaries are the dominant generators of alluvium-derived gravels; very little sand and silt sized particles were observed within the channel. Streams with exposed bedrock were often classified as impacted; erosional buffering from the geological thresholds causes these streams to widen rapidly as the hydrologic forces are diverted to the less rigid banks. The

NBR was consistently the most severely impacted stream in the watershed. The NBR was characterized by massive gravel beds, wide channel bottoms, impacted banks, undercut vegetation, and was often bound by either exposed bedrock or thick gravel beds.

Several geological formations were observed within the NBR watershed, each with unique physical properties and compositions that can buffer riverbeds from downcutting. These geological units are described in Table 3.4 according to their sedimentary contribution to the watershed.

Table 3.4. Relative tendency of the NBR geologic formations to contribute sediments to the NBR channel.

Formation	Sedimentary Input
Alluvium (Q_{al})	Primary contributor of small gravels, sand, and silt
Edwards Limestone (K_{ked})	Massive limestone blocks, not a notable provider of sediments
Comanche Peak Limestone (K_c)	Small gravels, chert, and fossiliferous fragments
Walnut Clay (K_{wa})	Source for gravels and clay nodules in the NBR Reach
Paluxy Sand (K_{pa})	Primary source of sand and silt, observed as overbank deposits along the adjacent floodplains
Glen Rose Limestone (K_{gr})	Large plucked slabs of limestone - These sediments are not located far from their source

Remarks for each observed geological formation were compiled; these descriptions are provided alongside Proctor's [1969] lithological descriptions of the NBR watershed in Table 3.5.

Table 3.5. Primary geological units of the NBR watershed (modified from Proctor 1969 with supporting RGA derived observations).

Formation	Proctor's Description	RGA Field Descriptions
Alluvium (Q_{al})	Limestone gravels and fossil fragments. Siliceous sediments are characterized as sandy quartz grains with Edwards derived cherty fragments.	Flood plain terrace deposits often composed of eroded Paluxy Sand in downstream segments. Dominant alluvium is limestone gravel and fossil fragments.
Edwards Limestone (K_{ked})	Massively bedded limestone with marl and reef limestone interbedding. Forms resistant ledges and is a major slope controlling formation if the watershed.	Acts as the 'capstone' unit within the watershed, and directly protects the underlying units. Massive eroded blocks result from the undercutting erosion of the Comanche Peak Limestone.
Comanche Peak Limestone (K_c)	Chalky and nodular fossiliferous limestone. Forms steep mid-slopes of the Lampasas Cut Plain. Rarely seen without protective Edwards Limestone	15 to 30 meters thick, often observed directly beneath the Edwards Fm. Friable and notably erodible, primary source for gravels along the NBR watershed.
Walnut Clay (K_{wa})	Alternating clays and nodular limestones. Massive shell beds, characterizes the lower slopes and valley floors of the Lampasas Cut Plain.	Large plucked clay gravels from this formation were noted along the NBR reach. Notably erodible but often buffered by large volumes of overlying gravel deposits.
Paluxy Sand (K_{pa})	Poorly cemented fine-to-medium quartz sand. Contributes abundant sediments to the NBR causing channels to become choked with sediments.	Denoted as highly erodible in the field, however observations of this sediment in the river channel was sparse aside from sites observed in the outcropping unit location. Mostly seen as downstream terrace deposits.
Glen Rose Limestone (K_{gr})	Thin to medium bedded limestones with marly limestone beds.	Provides large slabs of 5-10 cm thick limestone beds. Large source of sediments in the upper portions of the NBR.

Additional gravels from the channel are sourced from the bank alluvium, the presence of bedded gravels in the Paluxy Sand and the Q_{al} was noted during the RGA. Gravels were the most frequently observed sediment within the NBR watershed. Little to

no sand was observed except as overbank deposits downstream from Clifton, TX. Suspended sediment was occasionally observed as silty coat on channel bottom gravels, though this fine sediment does not appear to be a major sedimentary component of the watershed.

Sediment sources were identified by determining the approximate transport distances for the most abundantly observed sediments. The sediment transport distance calculation implements sediment size data to determine the frequency of sediment movement within a channel of known geometry, the calculation of this distance is thoroughly described by Beechie [2000]. Average sediment distributions for gravels and sands were determined from the Mastersizer 2000 (Section 3.3.1) and Wolman Pebble Count Method (Section 3.2.2); these data represent the average particles moving through the NBR channel. FDC data critical force thresholds for the sediments are determined to identify the frequency of sediment entrainment (Beechie, 2000). Sand and gravel travel distances for the Initial, Intermediate, and Current Periods were independently calculated to observe changing trends in the frequency and magnitude of sediment transport distance (Figure 3.10).

		NBR Sediment Travel Distance	
		Gravel (22.4 mm)	Sand (80 µm)
Travel Distance (km/yr)	Initial Period	0.16	98
	Intermediate Period	0.48	214
	Current Period	0.32	135

Figure 3.10. Travel velocities and distances for the NBR sands and gravels for the Initial, Current, and Intermediate periods. Sand moves notably further than gravel in a single year.

These travel distances were plotted with the NBR watershed map to express the linear scale of sediment travel in figure 3.11.

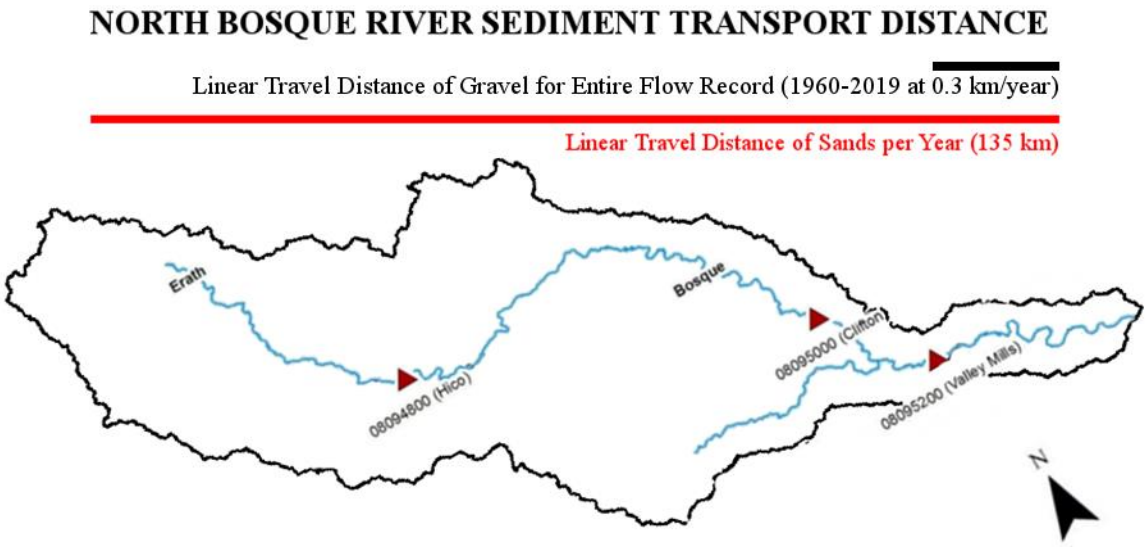

Figure 3.11. Linear sand and gravel transport distances in relation to the NBR watershed. Gravels moving at 0.3 km/yr are commonly observed within the channel bottom, while sands that move 135 km/yr are able to move from their source directly to Lake Waco (or are deposited as overbank deposits) within a single year.

The travel distance data reveals several trends for the NBR hydrologic regime: (1) in all hydrologic time periods, sand is capable of being routed completely thought he watershed (the NBR is approximately 160 km long), sand sized particles are calculated to move at a minimum of 98 km downstream from their initial source. (2) Gravel moves significantly slower through the channel, in a given year for the current hydrological regime of the NBR, gravel is estimated to travel roughly 0.3 km per year - assuming constant annual hydrology in the NBR it would take gravel sized particles 450 years to move the same distance as sand does in 1 year. (3) Peaks in sedimentary travel distances were observed for the Intermediate Period. (4) An increase in the rate of transport for

both sands and gravels is observed between the initial and current periods, indicating a change in flow has occurred between these two periods.

The RGA is a useful observational technique that can be used to contextualize the various potential sources of sediment within a watershed. However the RGA still fails to detail the volume of sediment being transported, and lacks evidence on how much sediment is effectively being routed through the channel. By calculating the effective transport distances of sediment for the NBRs hydrological capacity, it is easier to quantitatively identify the causes for observed trends in channel sediments - in this case the travel distance explains the effective lack of sand sized particles while explaining the presence of gravels. Gravels transport rates are significantly shorter than those calculated for sands, while sand is effectively able to move through the entire NBR watershed within a 2 year period.

[3.2.2] Classification of Channel Sediments

Gravel size distributions and particle size histograms were developed for the NBR and Neils Creek tributary; these gravels represent the dominant observed channel sediment in the NBR reach, and were classified for their usability calculating load, effective discharge, and other metrics for the watershed. A total of 6 point bars were studied to determine sediment distributions (Figure 3.12). Additionally, average d_{16}, d_{50}, and d_{84} values were determined for each point bar along the NBR corridor, the distributions were averaged to identify variations in grain size between the NBR reach and Neils Creek (Figure 3.13).

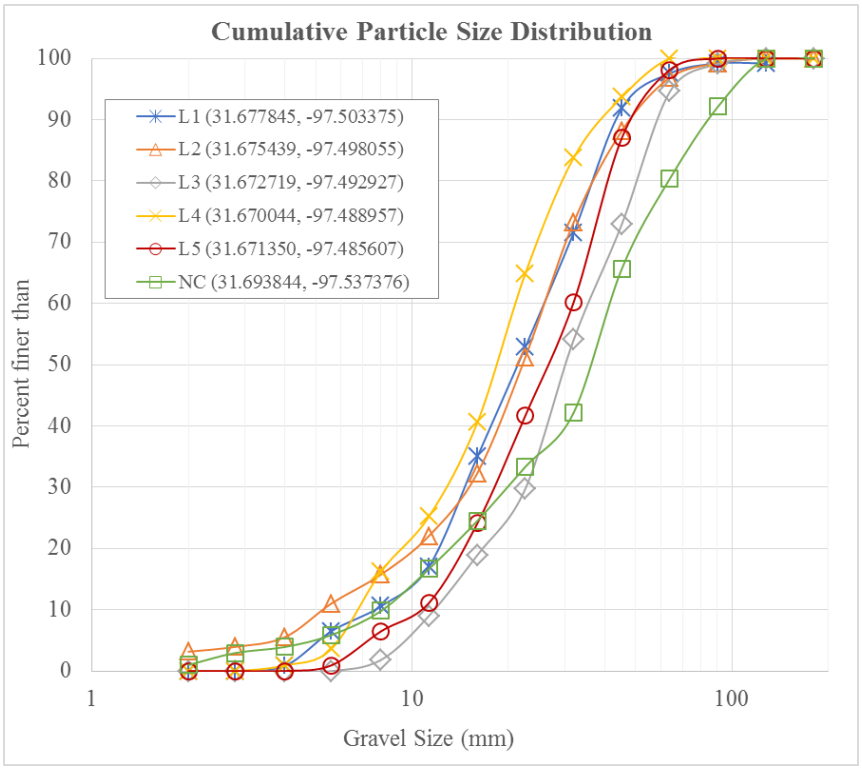

Figure 3.12. Cumulative particle size distribution curves for gravel collected along the 5 North Bosque River corridor sites and Neils Creek tributary.

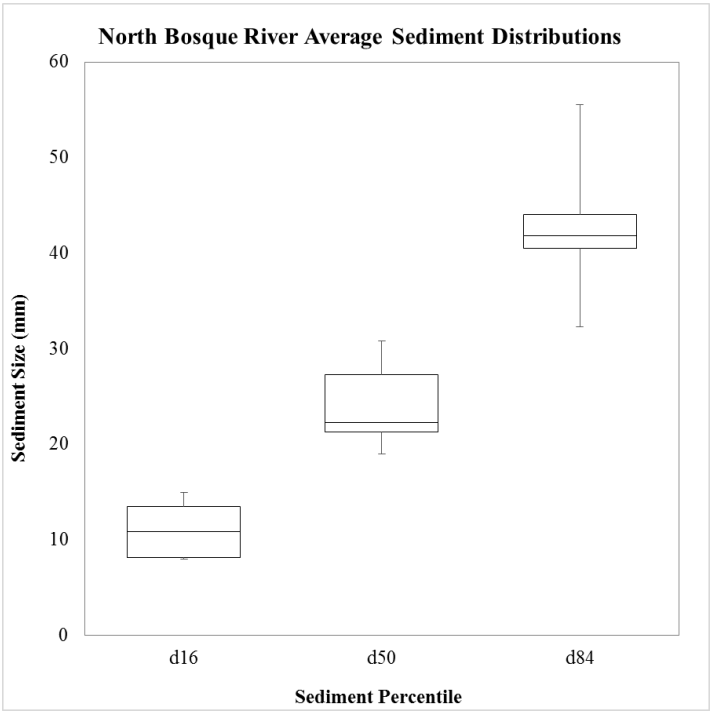

Figure 3.13. Box and whisker profile of d_{16}, d_{50}, and d_{84} gravel size distributions.

Average d_{16} values are 11.1mm, d_{50} values are 24.1mm, and d_{84} averages are 42.8mm. Average values for the North Bosque River are similar to those observed at the mouth of Neils Creek (NC), however d_{84} values for the NC tributary are notably higher at d_{84}=72.5 mm. Refer to Appendix D for tabular Wolman Pebble Count Data determined from the Wolman Pebble Count Excel Macro. No trends in location vs. gravel size were observed from the 6 sample groups.

[3.2.3] Effective Discharge and Stable Channel Designs

A joint assessment of the hydrological and sedimentological inputs of the NBR was completed by determining the NBR's effective discharge (Q_{eff}). Effective discharge can be described as the flow (or range of flows) that most effectively move sediments within the channel. Wolman and Miller [1960] first related this effective force (Q_{eff}) to the frequency and magnitude of flows that do the most "work" in a geomorphic setting. In this case, effective discharge is described as the flow that most effectively routes sediments and water through the NBR channel, and can be described as the channel-forming discharge that drives hydraulic change along the NBR. Q_{eff} can be determined by multiplying flow frequencies of a river by the transport of sediment (Biedenharn et al., 2000) (Figure 3.14).

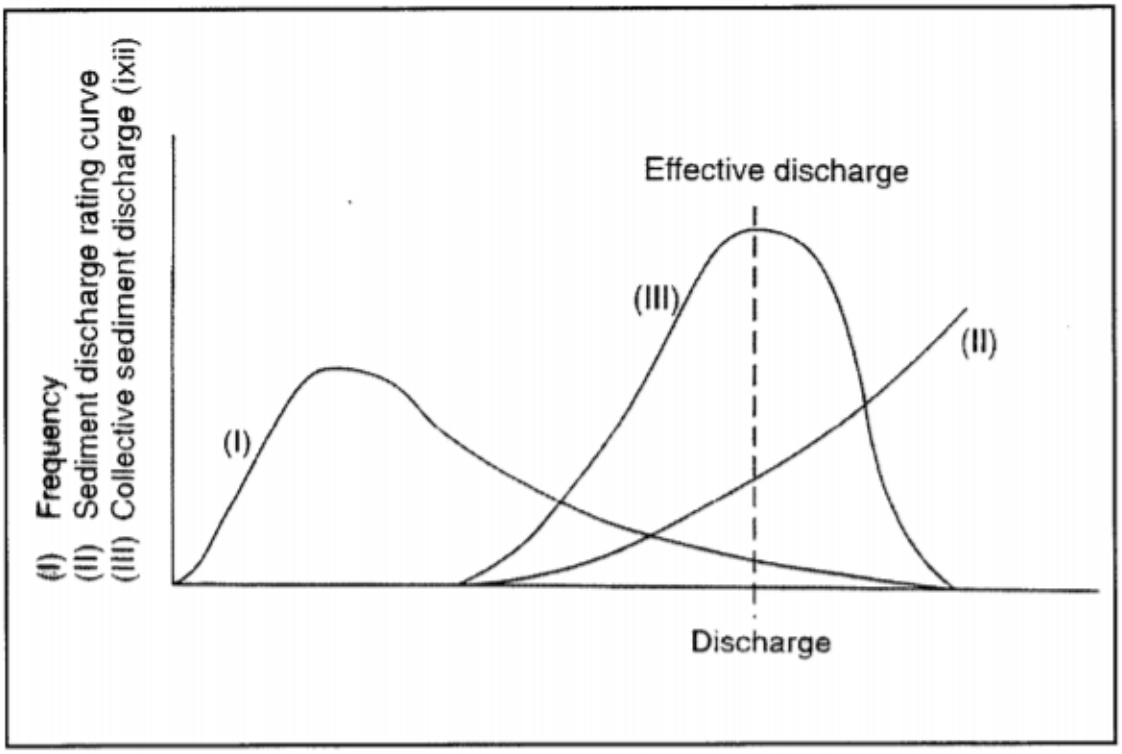

Figure 3.14. Biedenhard's explanation of effective discharge determination. Q_{eff} is derived from both flow frequency and sediment discharge data. Note that as frequency attenuates the effectiveness decreases. Q_{eff} values strike a balance between these two variables. (from Biedenhard, 2000).

Flow duration curves for the three periods established from the Mass Curve Profile and PFA were independently assessed for their associated effective discharge rates in effort to characterize historical trends associated with the observed increase in flow during the Intermediate Period. The following plots depict the resulting effective discharge (Q_{eff}) rates for the Initial, Intermediate, and Current Periods respectively - an increase in effectiveness between the Initial and Current Periods is observed (Figures 3.15 to 3.17):

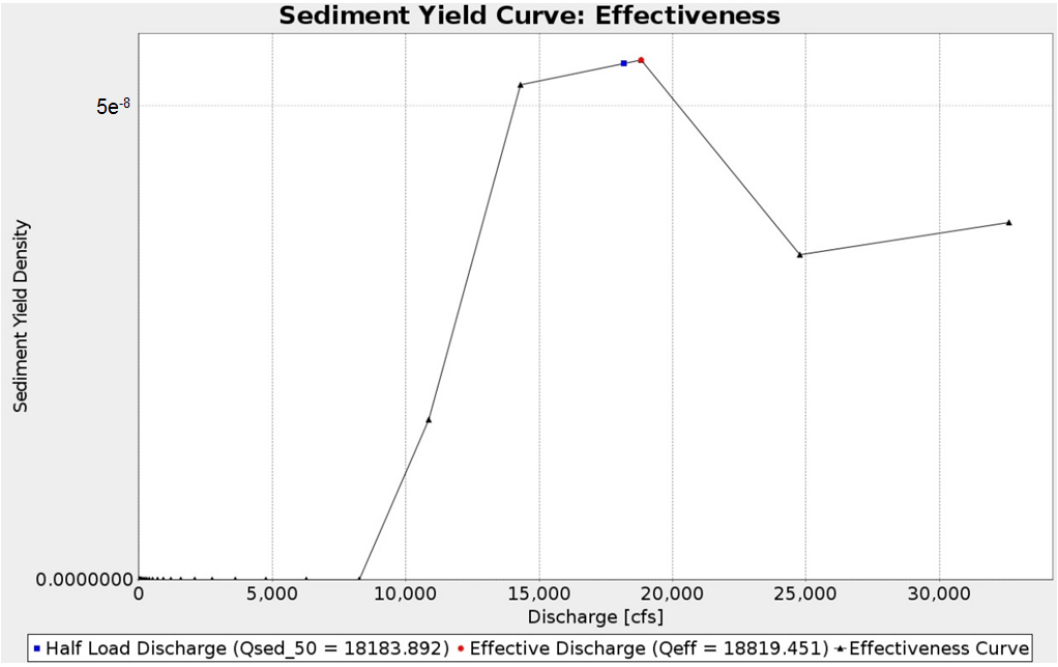

Figure 3.15. Effectiveness curve for the Initial Period from 1960 to 1990. These plots were developed in the eRams tool package according to the methods outlined by Martin and Church [2000].

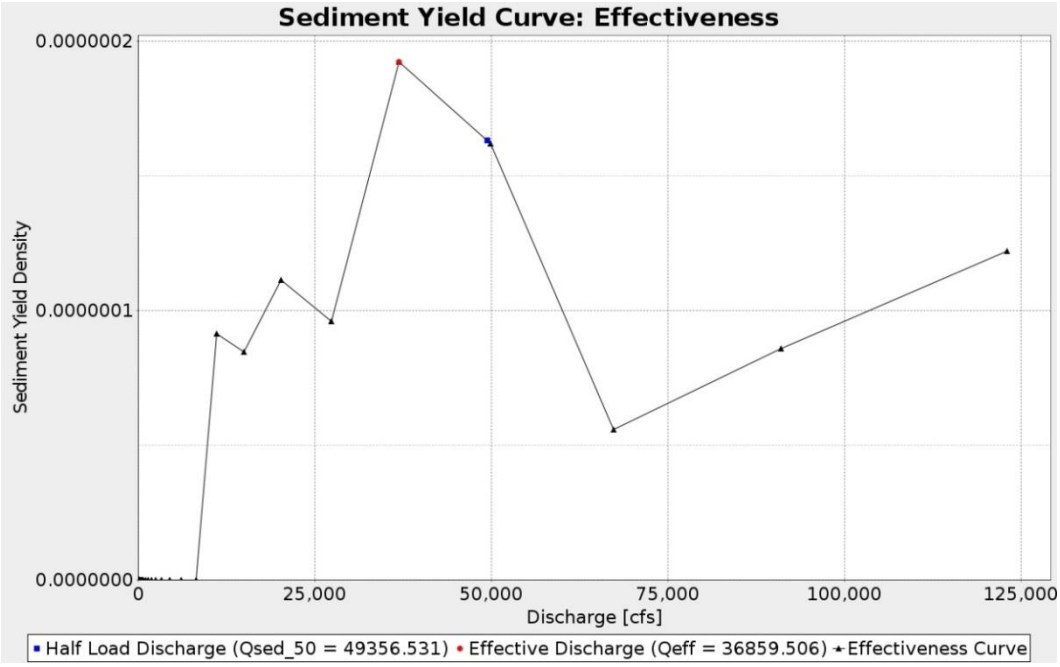

Figure 3.16. Effectiveness profile for the Intermediate Period representing sediment transport between 1991-1992.

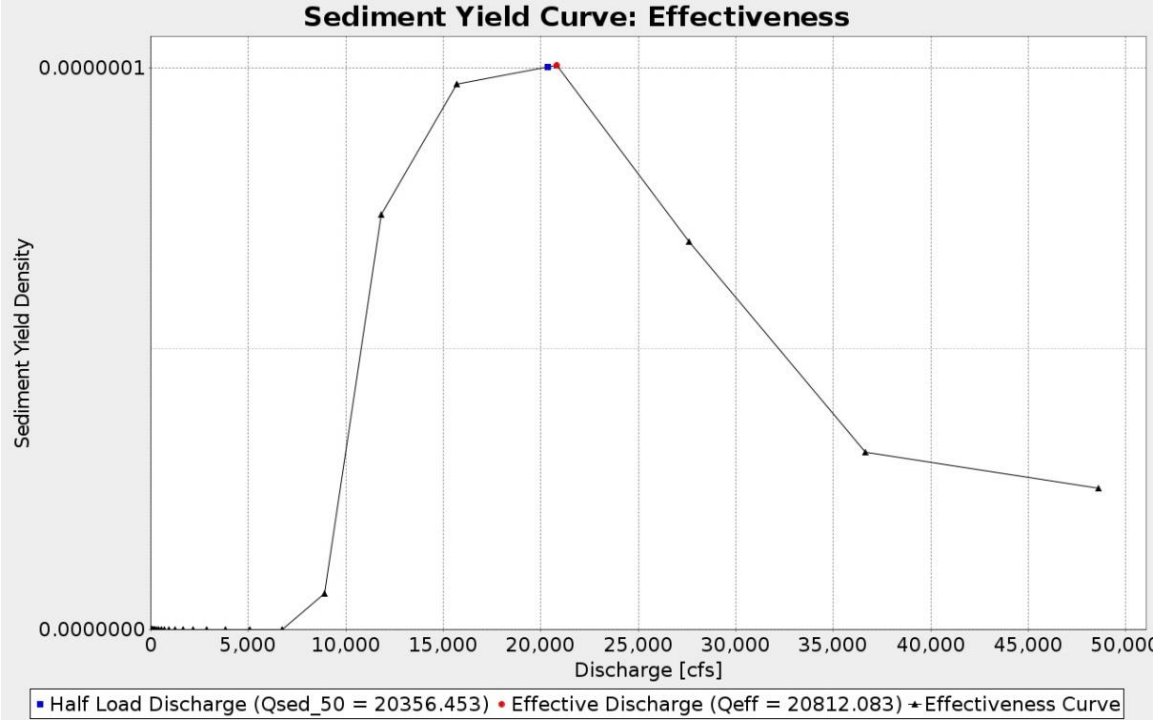

Figure 3.17. Sediment transport effectiveness for the Current Period (1993-2016).

One function of eRams is to calculate half-load (also referred to as half yield discharge) simultaneously with Q_{eff}. Half load discharge (Q_{sed50}) is described as a discharge associated with transport of half of the cumulative sediment yield for a given flow record (Sholtes and Bledsoe, 2016). Q_{sed50} is often larger than Q_{eff} for suspended load dominated streams, and is considered to be better at constraining total sediment load than effective discharge (Sholtes et al., 2014) Effective discharges (Q_{eff}) and half-load discharges were determined for the three time periods (Table 3.6) to identify potential changes to flow effectiveness over time.

Table 3.6. Effective discharge and half-load flows for the NBR initial (1960-1990), intermediate (1991-1992), and Current (1993-2019) Periods. These data were used to calculate the frequency of effective sediment transport.

Time Period	Q_{eff} (m^3/s)	Halfload (m^3/s)
Initial Period (1960-1990)	515	533
Intermediate Period (1991-1992)	1044	1397
Current Period (1993-2019)	589	576

A slight increase in effective discharge and half-load is noted between the Initial and Current Periods. Effective discharge data for the North Bosque River at Valley Mills (USGS gage 08095200) were discretized for the three time periods noted along the mass curve profile. Plotting individual exceedance flows per year for each time period serves to show both the ranges of flows associated with each period, and to show hydrological variation in magnitude and frequency over time. In addition, the effective discharges determined from the above method were plotted along the PFA to show the frequency of effective sediment transport for the NBR (Figure 3.18).

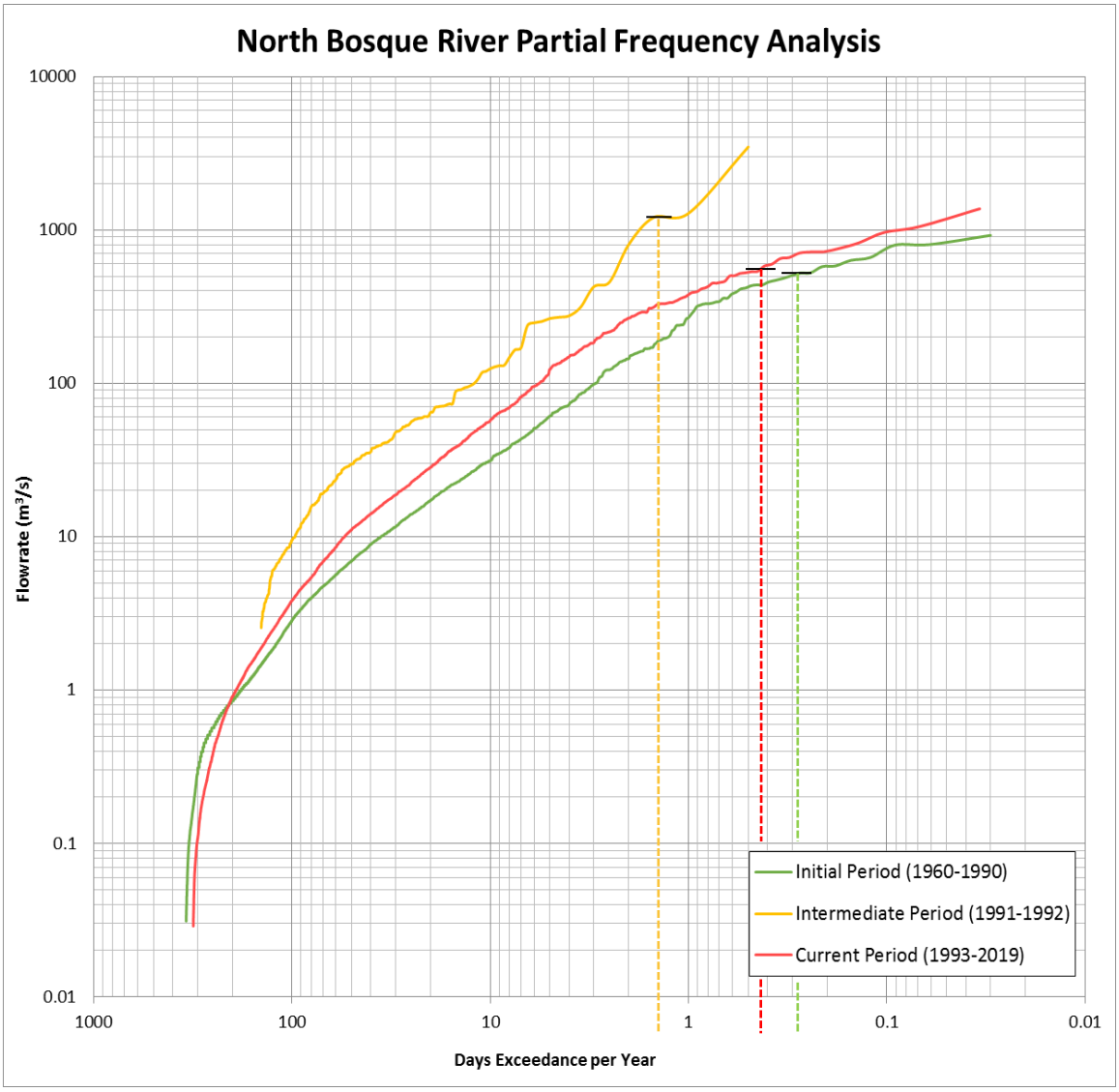

Figure 3.18. Partial frequency analysis of the NBR for various temporal extents. Effective discharges are noted for each period as a reference to determine the average annual hours the NBR is at or above critically effective flow.

This PFA shows several trends: 1) The flows for the initial period versus the current period show an increase in overall flowrate for similar exceedance probabilities - this is seen in the mass curve analysis and indicates that slight flow increase has occurred. 2) The intermediate period shows increased flow conditions associated with the 1991 flood, further emphasizing the massive flow rates that lead to permanent channel

changes. 3) Lastly, the frequency of effective flows has increased between the initial and current periods, as indicated by the drop-down lines for each pre-determined Q_{eff} value.

Both sediments and hydrological data are now combined to comprehensively analyze the NBR via the CSR Tool; this model allows researchers establish a relationship between sediment supply and the entire flow duration curve to show how the channel is impacted by upstream water and sediment. A stability profile (representative functional curve of bottom widths and channel slopes) is developed by inputting known sedimentary and hydrological data into The CSR tool. . Stable slopes are described as those that can continue to route sediment and water through the channel without altering the slope of the river. Increasing or decreasing the stable slope along the same bottom width will lead to either channel erosion or deposition. Slope values at Valley Mills range between 0.0012 and 0.0008 (Section 3.4.1); a decrease in slope to 0.0007 would be required to achieve channel stability (Figure 3.19).

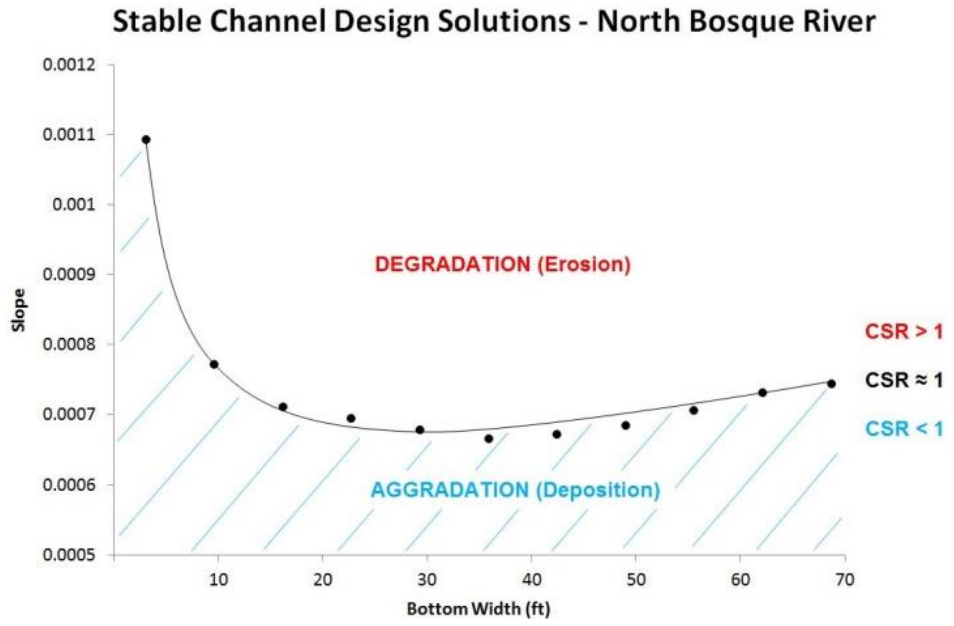

Figure 3.19. CSR Stable regime for the North Bosque River. An effective slope of .0007 was determined.

The CSR indicates that the NBR is unstable, and is likely to exhibit erosion as a result of this instability. Changes to channel geometry affect the hydraulic ability of sediment and water to route through the channel. These data suggest that the incoming sediment and water from the supply reach are leading to instability of the NBR; in particular this instability is observed in the form of channel cutbank shearing. Additional CSR Tool data for the NBR are provided in Appendix E.

[3.3] Boundary Conditions / Resisting Factors

There are three major resisting forces in a river channel; (1) river bed material, (2) river bank materials, and (3) vegetation. Identifying the properties of these components is crucial to characterize channel geometry changes as a result of sedimentary/hydrological interactions. Therefore it is essential to classify the soils, geologic formations, slope profiles, vegetative cover, and the channel geometries that comprise the boundaries of the North Bosque River.

[3.3.1] Soil Classifications and Distributions

Soil erosion occurs as a result of several processes; 1) river bank soils are subjected to surficial shear stress that acts on interface between soils and water. 2) Uplifting forces caused by river discharge 'pull' sediments loose from their cohesive interface. 3) The occurrence of cyclic turbulence pulses against the bank and bed surface, this velocity oscillation leads to soil erosion (Croad, 1981). There are several soil properties that resist these erosional forces. In particular, bulk density, a measure of the compaction of soils that similarly represents the percentage of fine materials within the soil, is described as the most notable variable correlated to erosional resistance (Wynn et al., 2004). Soil erosion rates are assessed via several techniques, including the Jet Erosion

Test (JET), which is implemented to determine critical thresholds of erosion for bank soils of the NBR reach (Hanson and Cook, 2004; Daly et al., 2013) (Section 3.3.2).

Data from the Web Soil Survey was gathered as a baseline for describing the dominant soils located within the watershed. These banks are the sedimentary source for fine sediments. The five most abundant soils were identified along the NBR between the Clifton and Valley Mills USGS gage stations. Physical properties of these soils are available in Table 3.7, which includes properties associated with erosional resistance.

Table 3.7. Primary soil units of the NBR watershed (modified from Proctor 1969 with supporting RGA derived observations). K-factor, plasticity, bulk density, K-sat (um/s for 0.5 meter soil profiles), liquid limits (%), and surface texture data from Web Soil Survey.

Soil Unit Name	USDA Soil Texture	K-Saturation (μm/s)	K-Factor Rating	Bulk Density (g/cm^3)
Frio Silty Clay Loam	Silty Clay Loam	2.7	.20	1.35
Bosque Loam	Loam	9.0	.24	1.30
Cranfill Gravelly Clay Loam	Gravelly Clay Loam	9.0	.10	1.40
Sunev Clay Loam	Clay Loam	9.0	.28	1.40
Brackett Eckrant Association	Gravelly Clay Loam	8.5	.15	1.41

These soils represent the most commonly observed soil profiles within the NBR reach, according to estimates from the Web Soil Survey [2020], these soils are illustrated for the NBR reach in Figure 3.20.

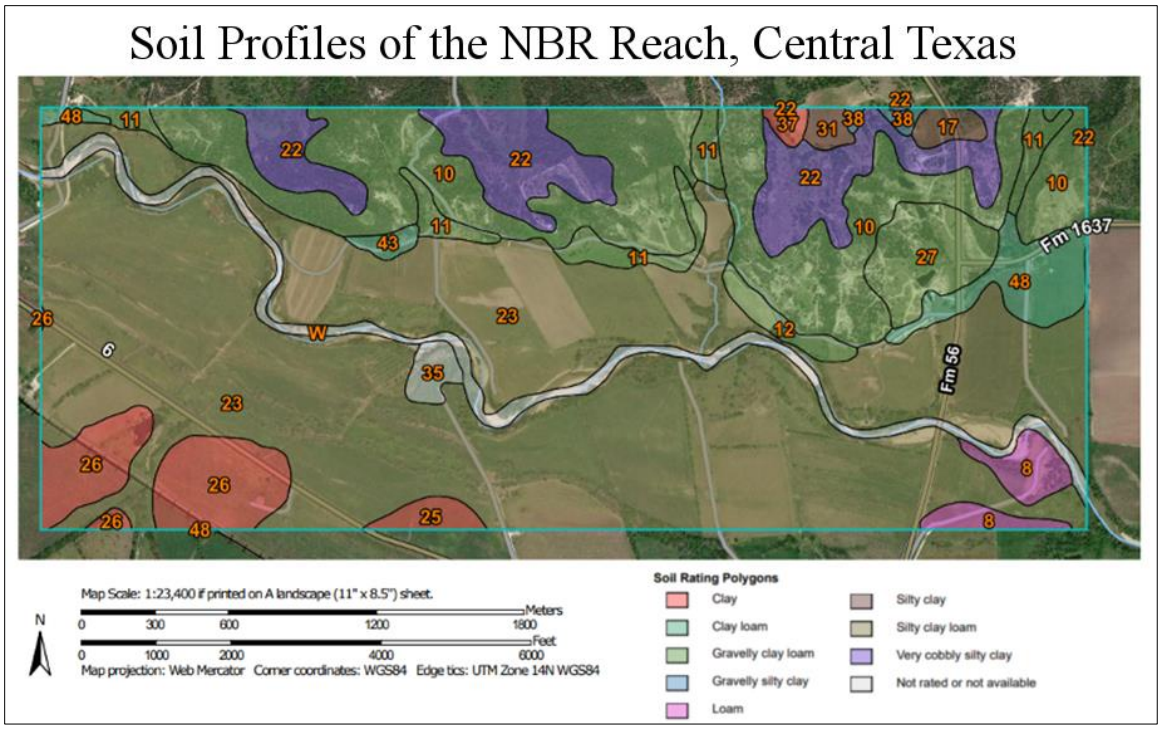

Figure 3.20. North Bosque River Soils according to Web Soil Survey, with primary soil textures labelled for the surrounding soils.

The K-factor associated with these soils is an indicator soil susceptibility to sheet and rill erosion. Higher K values indicate that the soil is more likely to erode due to these water-driven processes. This indicates that the Sunev Clay Loam and the Bosque Loams are the most likely to erode via sheet and rill erosion. In general, soils with higher bulk densities have higher clay compositions, which are associated with increased cohesive strength (resulting in higher resistance to erosional processes). The Cranfill Gravelly Clay Loam and Brackett Eckrant Association represent the most resistant soils in this regard.

Soil composition assemblages were determined via Mastersizer 2000 Analyses. Nine soil samples were collected in the same locations as the root samples; the alphanumeric ID represents the location of these samples within the NBR reach (Refer to Figure 2.4).

Soils collected along the NBR reach range in composition, though most samples are classified as variants of loamy soils similar to the top 5 soils identified from the Web Soil Survey (Figure 3.21).

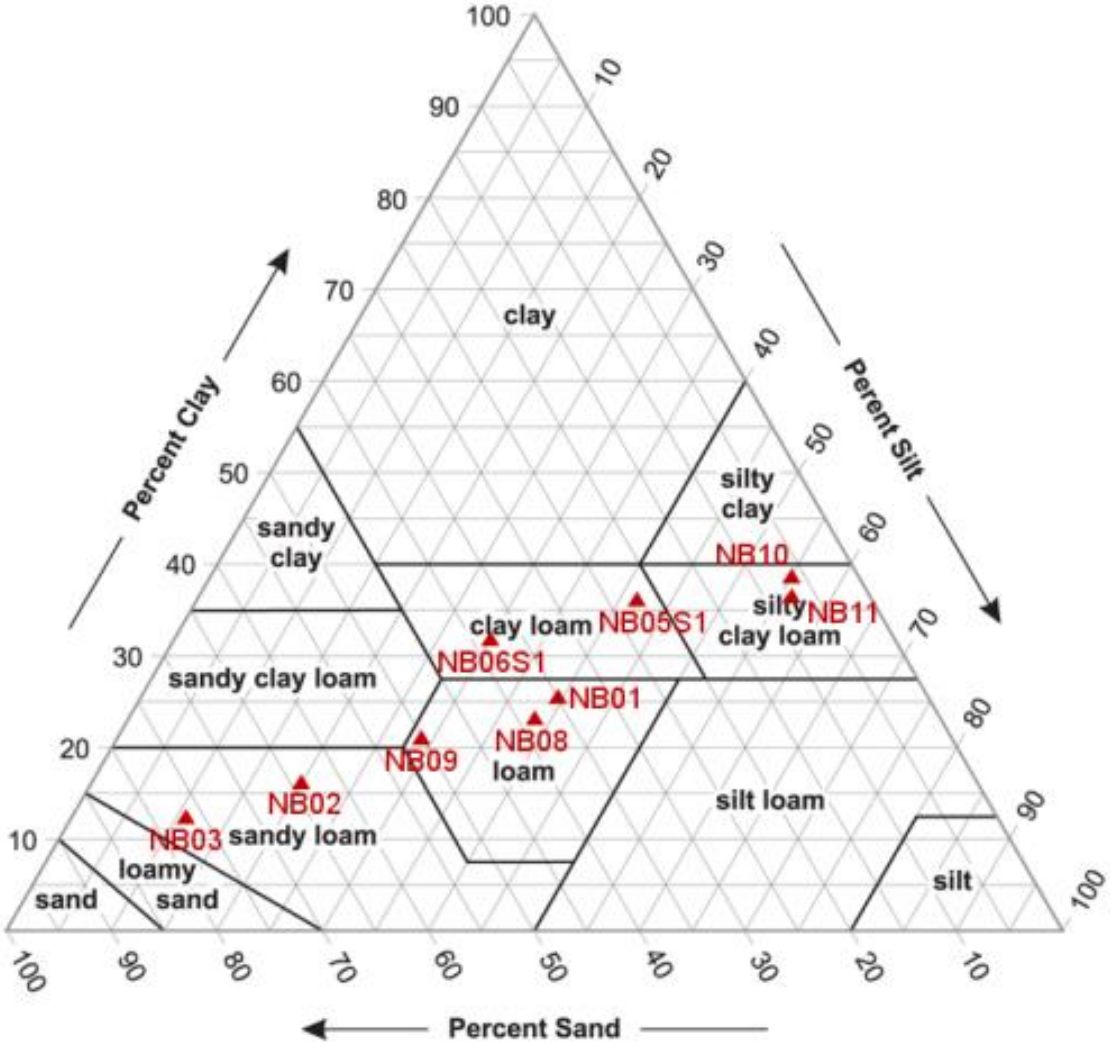

Figure 3.21. NRCS soil classification ternary diagram with corresponding sediment sample Sand-Silt-Clay ratios and identifications, samples were collected and labeled with the same notation as the root samples.

Based on the USDA classifications and the WSS profiles, sediments classified as loam via Mastersizer 2000 can be described as the Bosque Loam (NB09, NB08, and NB01). Two of the observed soils shared physical characteristics to the Frio Silty Clay

Loam (NB10 and NB11). An additional 2 soil samples match properties of the Sunev Clay Loam (NB06S1 and NB05S1). Average mean grain size of sediment samples ranged between 7 to 138μm, with some samples exhibiting a higher clay and silt composition compared to the sand-dominated samples. These soils represent the most common bank materials within the NBR reach. Detailed data from the Mastersizer2000 are available in Appendix F.

The erodibility of these soils was determined by identifying the relationship between soil type and the threshold of critical velocity required to erode these soils, previously described by Briaud [2014]. The nine NBR reach soils were classified according to the Unified Soil Classification System (Table 3.8), which is referenced in Briaud's erodibility index.

Table 3.8. USCS and USDA soil classifications for the 9 NBR reach sediment samples. USCS classifications were determined based on the physical properties (liquid limit, K-factor, plasticity, etc.) of the soils in conjunction with USDA/USCS identification frequencies described by Garcia-Gaines and Frankenstein [2015].

Sample ID	USDA	USCS
NB01	Loam	ML
NB02	Sandy Loam	SM
NB03	Sandy Loam	SM
NB05S1	Clay Loam	CL
NB06S1	Clay Loam	CL
NB08	Loam	ML
NB09	Loam	ML
NB10	Silty Clay Loam	CL
NB11	Silty Clay Loam	CL

These soils were then characterized based on their average critical velocities to determine the mean erodibility of the dominant soils of the NBR reach, the following erosion classifications were determined for the NBR reach soils (Figure 3.22).

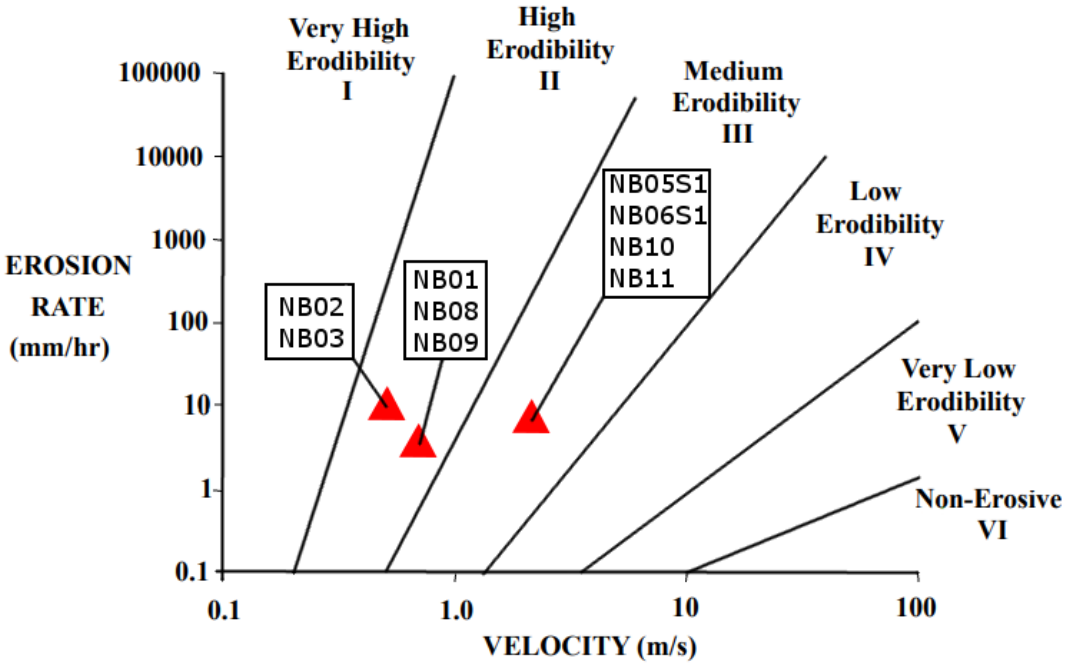

Figure 3.22. Soil erodibility regime, adapted from Briaud [2014]. Soil erosion rates above bankfull conditions range between 5-10 mm per hour. Sample erosion rates are averaged based on their grouped USCS soil classifications. Detailed descriptions of each Erodibility index are available in Appendix G.

Soils with higher clay composition and higher bulk densities such as NB11 and NB10 exhibit more resistance than the samples with higher sand composition. The NBR experiences roughly 70 bankfull hours per year based on the 1.5 year flood exceedance probabilities. At maximum erosion rates of 5-10 mm/hr (from Briaud's erosional index) the banks of the NBR could are estimated to erode at a rate of 0.35-0.7m per year. These estimates closely reflect the erosion rates determined from the air photo analysis, predictive erosion, and root dendrology methods.

[3.3.2] Bank Erodibility (Mini-Jet Erosion Assessment)

The JET method, which subjects soil samples to a measured hydraulic stress to interpolate an erosion rate, was implemented for two NBR samples. These soil samples were collected along the banks of the NBR reach with the same alphanumeric IDs as the loose soil and root samples. Shelby tube soil plugs were collected at NB01S1 (the drop off location for the NBR reach) and NB07S1 representing the half-way point of the NBR reach. These soils were attached to the jet apparatus to measure changes in soil depth over time when subjected to a known pressure head and jet velocity.

This method produces both τ_c and K_d values according to methodology outlined by Daly, Al-Madhhachi, and Miller [2013] and are developed into an erosional curve in the Jet Erosion Test Spreadsheet Tool v 2.1.1 (Daly, 2014). The two soil samples were taken from the lower third of the channel cutbanks to represent soils that are regularly submerged, where they are more frequently subjected to shear stress and erosional processes. The lower third of the NBR banks also represent bank heights that are submerged during the 1.5 year flood and Q_{eff} discharges (Barberá et al., 2007; Wu et al., 2008). The surface of the two samples is shown in Figures 3.23 and 3.24. Average K_d and Tc values for the two samples were plotted alongside a compilation of jet data from Perera and Wu [2016] for comparison to other samples processed and tested with similar methodologies (Figure 3.25).

Figure 3.23. Soil Sample Test 1, this sample was located from the same location as Root Sample NB07S1 (see methodology locator map for root samples). 10cm Shelby tube plugs were collected for use in the Mini Jet Apparatus.

Figure 3.24. Soil Sample Test 2, this sample was located at the beginning of the NBR Reach alongside root sample NB01S1.

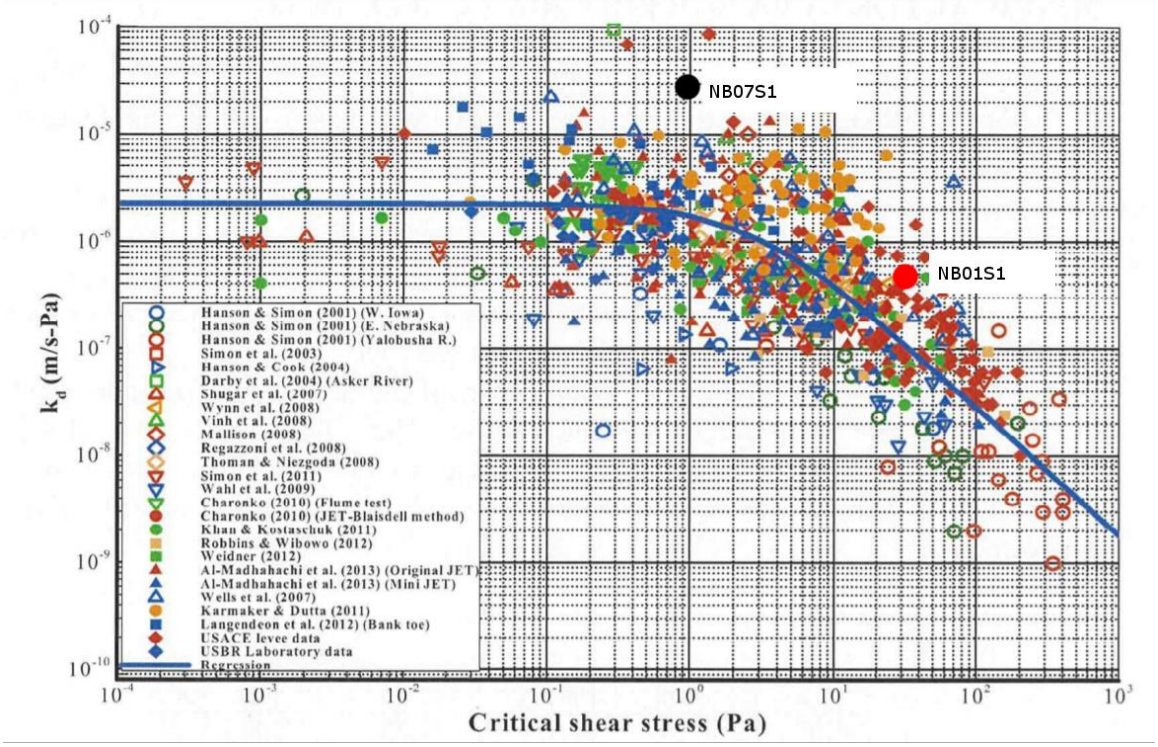

Figure 3.25. K_d vs τ_c (Pa) for the NBR soil samples derived from the Mini Jet Apparatus. Sample NB07S1 has notably anomalous K_d values, while sample NB01S1 is closer to the mean trend line.

K_d is described as the interparticular bond (shear strength) of soils, and expresses the detachment rate of the soil; simply put, high K_d values represent soils that are more likely to erode. The following table from the USBR [2019] describes the general relationship between soil erodibility and K_d (table 3.9)

Table 3.9. K_d vs. general soil erodibility (adapted from the US BR, 2019)

Erodibility	K_d (cm^3/N-s)
Very Erodible	1 to 5 (or more)
Moderately Resistant	0.05 to 2
Resistant	0.01 to 0.4
Very Resistant	0.0005 (or less) to 0.1

This relationship implies that NBR sample NB07S1 is more erodible than NB01S1 based on K_d values alone. The critical stress associated with eroding these samples supports this claim, as higher τ_c values are required to erode the more resistant NB01S1 sample. Sample NB07S1 had a higher density than NB01S1. This would normally imply that NB07S1 would be more resistant based on bulk density and clay content, however the presence of dense root mats was observed in NB01S1, which could be attributed to this increased resistivity.

[3.3.3] Assessment of Geological Physical Properties

The North Bosque River is classified as a threshold channel. Threshold channels are described as systems that have one or more of the following features; 1) erosion resistant bedrock, 2) coarse bed material, and/or 3) clay rich soils (Fripp and Goertz, 2004). The presence of these features directly influences river morphology. It is important to identify variations in channel materials to identify potential "weak that are more susceptible to erosional forces.

The erosional processes of bedrock-bound rivers have been described by Whipple and DiBiase [2013]. Whipple noted that bedload abrasion - the process of erosion resulting from impacting sediments - is a driving force that results in incision. Other processes such as plucking, cavitation, and corrosion are processes that can cause erosion, however the degree of their impacting contribution is understudied compared to abrasion studies (Whipple and DiBiase, 2013).

One test that is used to determine rocks resistance to abrasion is the Slake-Durability test. The following slake durability data were provided from a provisionary

thesis in order to characterize the resistance of the NBR watershed geologies (Crawford, 2000) (Table 3.10).

Higher retention values indicate that the sample is losing little mass, which indicates more resistance to abrasion forces. Observations made during the RGA support these data; outcrops of the Walnut Clay were notably more eroded in the field when compared to the highly resistive Edwards Limestone.

Table 3.10. Slake durability data results and thresholds for the NBR geologies. The Walnut Clay is the most likely erode, losing up to 30% of sample weight on a 2-cycle slake durability test. Both the Comanche Peak Limestone and Edwards Limestone are highly resistant, retaining more than 99% of initial sample indicating that they are unlikely to erode quickly.

Formation	2-cycle wt. Retention (%)	ASTM D4644 Class	Material Loss Threshold
Walnut Clay	70.80	Medium Slake Durability	15-40%
Comanche Peak Limestone	99.39	High Slake Durability	<15%
Edwards Limestone	99.66	High Slake Durability	<15%

To quantitatively support these observed trends, an estimation of channel degradation was implemented. Using the methodology described by Dickenson and Baillie [1999], the annual cumulative stream power for the NBR is computed in part by the following equation:

$$62.4 * Q * S / w \qquad \text{(Equation 4)}$$

Where Q is Average flow, S is the slope of the channel, and w is the average channel width. This equation yields a single stream power for the NBR. Flow records for the NBR USGS Valley Mills [Gage 09805200; 60 years] were used to calculate the

annual stream power. An estimated cumulative stream power of 61 kN/mm was determined for the NBR Reach. Implementing known abrasion data completed by Crawford [2000], an abrasion number for the NBR Reach was calculated as the slope of the weight loss percentage/elapsed time relationship for the continuous abrasion test (slake durability). The determined integrated stream power and abrasion numbers were plotted in the following Erosion/Stream Power diagram to determine an estimated erosion rate (Figure 3.26).

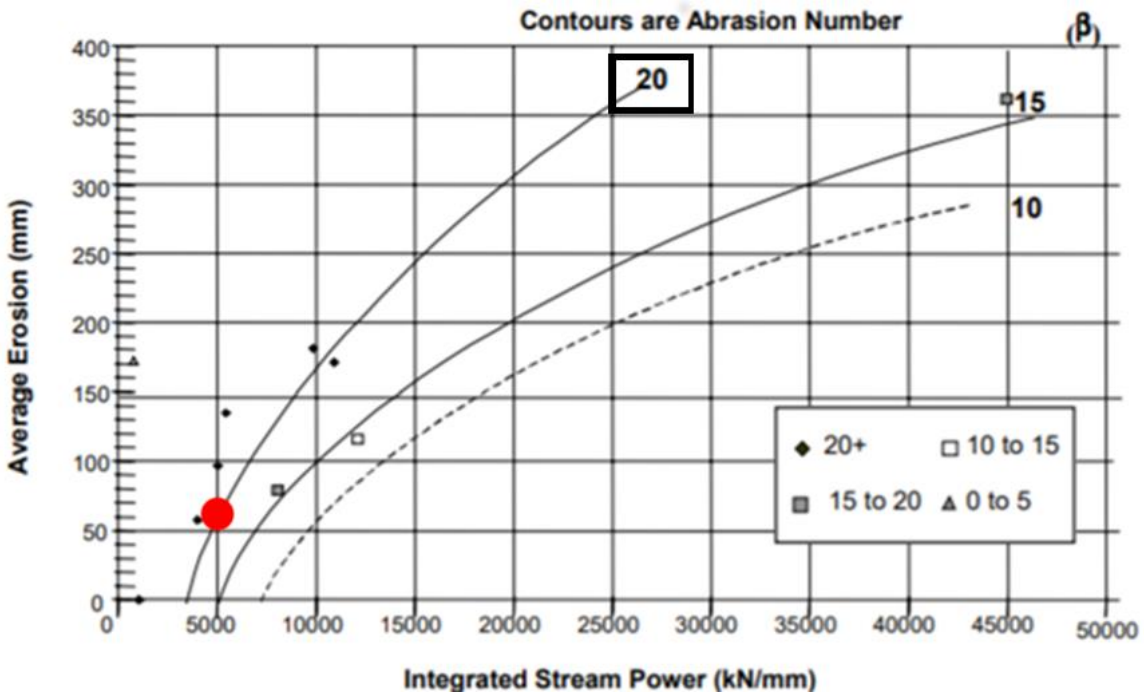

Figure 3.26. Integrated stream power / erosion rating curved for various abrasion numbers from Dickenson and Baillie (1999). An abrasion number of 20 was selected for the Walnut Clay, which represents an abrasion value close to the Taylor Marl (Adapted from Dickenson and Baillie, 1999).

The bed of the NBR reach is located along the Walnut Clay; this formation is assumed to have similar strength to the Taylor Marl, which has an abrasion value of roughly 20 according to Crawford's results [2000]. Integrating the average stream power derived from HEC-RAS and average flow records for the NBR, it would take roughly 82

years to reach an integrated stream power of 5000 kN/mm. According to the graphic developed by Dickenson and Baille [1999], an integrated stream power of 5000 equates to roughly 60 mm of erosion. The potential degradation rate of the NBR reach is determined by dividing the average erosion rate of the reach by the time it would take to achieve an integrated stream power of 5000 kN/mm (82 years). This calculation provides an average erosion rate of 0.73 mm/year, which is consistent with the estimated rates computed for regionally similar channel cross sections in the Austin Chalk at Dallas (0.31 mm per year) (Allen, 2020 pc). These estimates suggest that the NBR is more likely to widen than down-cut, as observed erosion rates from the lateral migration assessments are significantly higher than the calculated rates of degradation.

[3.3.4] Vegetation Profiles of the NBR

Vegetation is another boundary condition that reduces a rivers susceptibility to erosion. The presence of dense root mats along river channels is particularly effective at reducing lateral migration (Smith, 1976). Another study performed by Ouyang et al. [2010] describes the relationship between soil erosion and sedimentary transport in the presence of vegetation, this study determined that the presence of dense vegetation significantly alters the rate at which sediments move and erode. Other studies support this claim of vegetative buffering. Luna [2016] describes vegetation as an acting force that both enhances flood plain development and reduces bank erosion rates. Densely vegetated portions of rivers are often protected, and are less likely to erode in comparison to sparsely vegetated locations. In 2000, Millar discussed the abundance of riverine vegetation studies, but noted a lack of conclusive evidence that shows to what degree a rivers' geometry is controlled by vegetation. Millar determined that rivers, in particular

alluvium streams, show a strong correlation between channel form and riparian vegetation. While evidence shows that riparian vegetation does strengthen the riparian zone, work performed by Eaton and Giles [2008] determined that riparian vegetation does very little to control the geometry of larger rivers.

The North Bosque River is characterized by 2 primary vegetative profiles; (1) the first profile is noted along the cutbank portions of the NBR, which account for roughly half of the NBR corridor (Figure 3.27).

Figure 3.27. Overhead view of a NBR cutbank. The cutbank side is highly susceptible to erosion due to the position of vegetation along the upper portions of the bank. Lack of in-channel vegetation causes lateral migration-based undercutting of the upper vegetation in addition to lateral shearing of the cutbank. The root zones for most plants on the NBR cutbanks were observed at the top 1.5m; however some sides of the channel are more than meters tall.

The lower two-thirds of the NBR cutbanks are exposed with little to no vegetation [Class I Vegetation], while the upper portions are lightly vegetated [Class II - III Vegetation] with root zones present in the upper third of the cutbank. (2) The second NBR vegetative profile is the passive channel portion (point bars and inside of the meandering channel) (Figure 3.28).

Figure 3.28. Vegetated bank of the NBR. This vegetated bank is located in the headwaters of the NBR watershed. Many of the vegetated banks of the NBR have large gravel bar deposits. The presence of thicker vegetation acts as a buffer to erosion, with roots effectively strengthening the soils.

These portions of the NBR are more densely vegetated [Class III-IV Vegetation] with abundant vegetative cover to the waters' edge. Based on these observations the following regression parameters (associated with erodibility susceptibility) were determined for the two NBR vegetative profiles (Table 3.11), these data are used to determine the hypothetical effect that vegetation has on channel width.

Table 3.11. Gravel-bedded streams vegetation regression factors from various authors described by Anderson et al., 2004. 48% of the NBR was classified as a cutbank, while the remaining 52 was described as a point bar with dense vegetative cover. These particular regression factors are used to determine channel width along channels of a known significant flow.

Data Source	Densely Vegetated Point-Bars		Sparsely Vegetated Cutbanks	
	α	β	α	β
Andrews (1984), Gravel Bed (dimensionless form)	3.91	0.48	4.94	0.48
Charlton et al. (1978), Gravel Bed, Negligible Sediment Load	3.37	0.45	4.11	0.45
Hey and Thorne (1986), Gravel Bed	2.34	0.50	4.33	0.50
Huang and Nanson (1997), Gravel Bed	1.80	0.50	2.90	0.50

The regression factors were used to quantitatively describe the impact that vegetation has on the NBR channel. A hydrologically significant flow = 293 m^3/s (representing flows associated with RI = 1.5) was selected for this calculation. The following widths were determined from the regression factors according to methods described by Anderson [2004] (Table 3.12).

Table 3.12. Determined widths calculated with the above regression factors. Dense vegetation is associated with smaller channel widths.

Data Source:	Vegetated NBR Channel Width (m)	Weak Vegetation NBR Channel Width (m)
Andrew, 1984	59.7	75.5
Charlton et al., 1978	43.4	53.0
Hey and Thorne, 1986	40.1	74.1
Huang and Nanson, 1997	30.8	49.6

The North Bosque River reach is characterized by channel widths ranging from 50 to 70 meters wide. This technique shows the distinct pattern related to the presence of channel vegetation. More erosion is likely to occur in sparsely vegetated banks resulting in a wider channel, while dense vegetation acts as a buffer to erosion that prevents the channel from rapidly widening.

[3.4] Changes to Channel Form

Interactions between hydrologic and sedimentary forces lead to geomorphic shifts along the North Bosque River. The following results describe changes to the NBR's channel geometry, longitudinal profile, and planform resulting from these interactions.

[3.4.1] HEC-RAS Derivations of the NBR's Longitudinal Profile

The longitudinal profile of the NBR was determined from the USACE HEC-RAS model. Minimum channel elevations from 97 cross-sections were plotted against their horizontal position in the river to represent the bottom slope of the channel. This method was completed to identify changes to the NBRs channel length, which in turn can be used as a way to better describe changes to the sinuosity of a river (Section 3.4.2). Buffington [2012] described the spatial and temporal relationship between changes to the channel with the following figure (Figure 3.29).

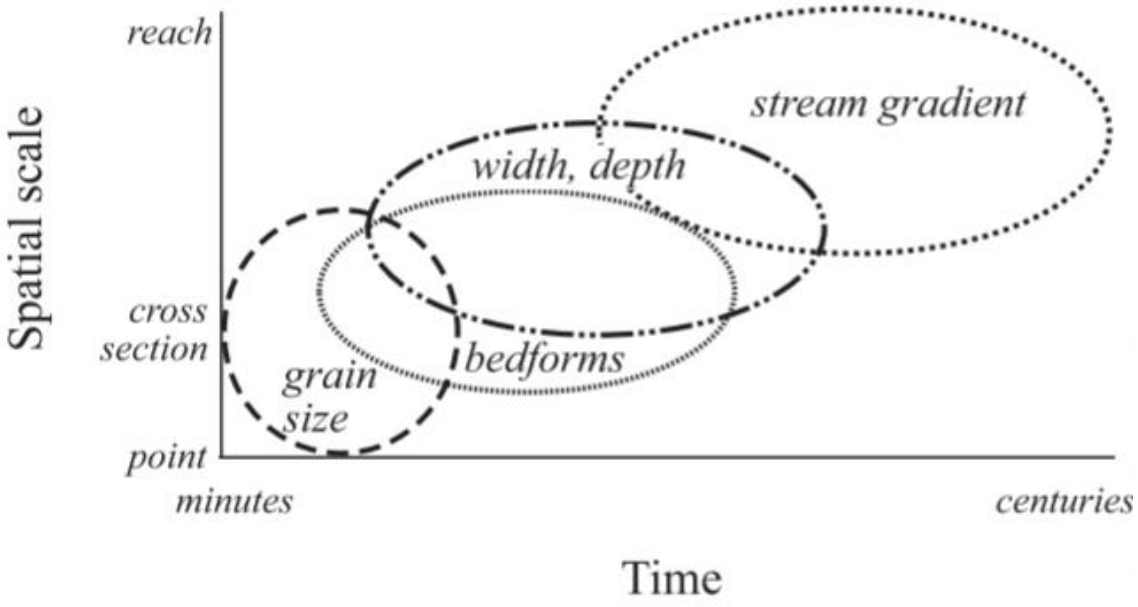

Figure 3.29. Buffington describes the relationship between time and spatial scale for alluvial rivers like the North Bosque River. Among the described variables, stream gradient (slope) is among one of the slowest to change over time, while changes to grain size and channel width occurs more rapidly. Adapted from Knighton (1998).

This figure is useful to describe the general trends in observable change to various aspects of a river, which implies that stream gradient changes are likely to be small if at all notable. Though changes to the longitudinal profile may be observed, it should be noted that the relative change to this variable is best regarded over longer periods of time (multiple years or centuries) rather than short scale temporal ranges (days and months). General observations of the NBR longitudinal profile were observed using pre-existing modeled data provided by the USACE DFW District. Utilizing the hydraulic dataset, minimum channel elevations were plotted to first identify any major changes to the base profile of the NBR. Figure 3.30 shows the three slope profiles that were identified from the minimum channel elevations in HEC-RAS.

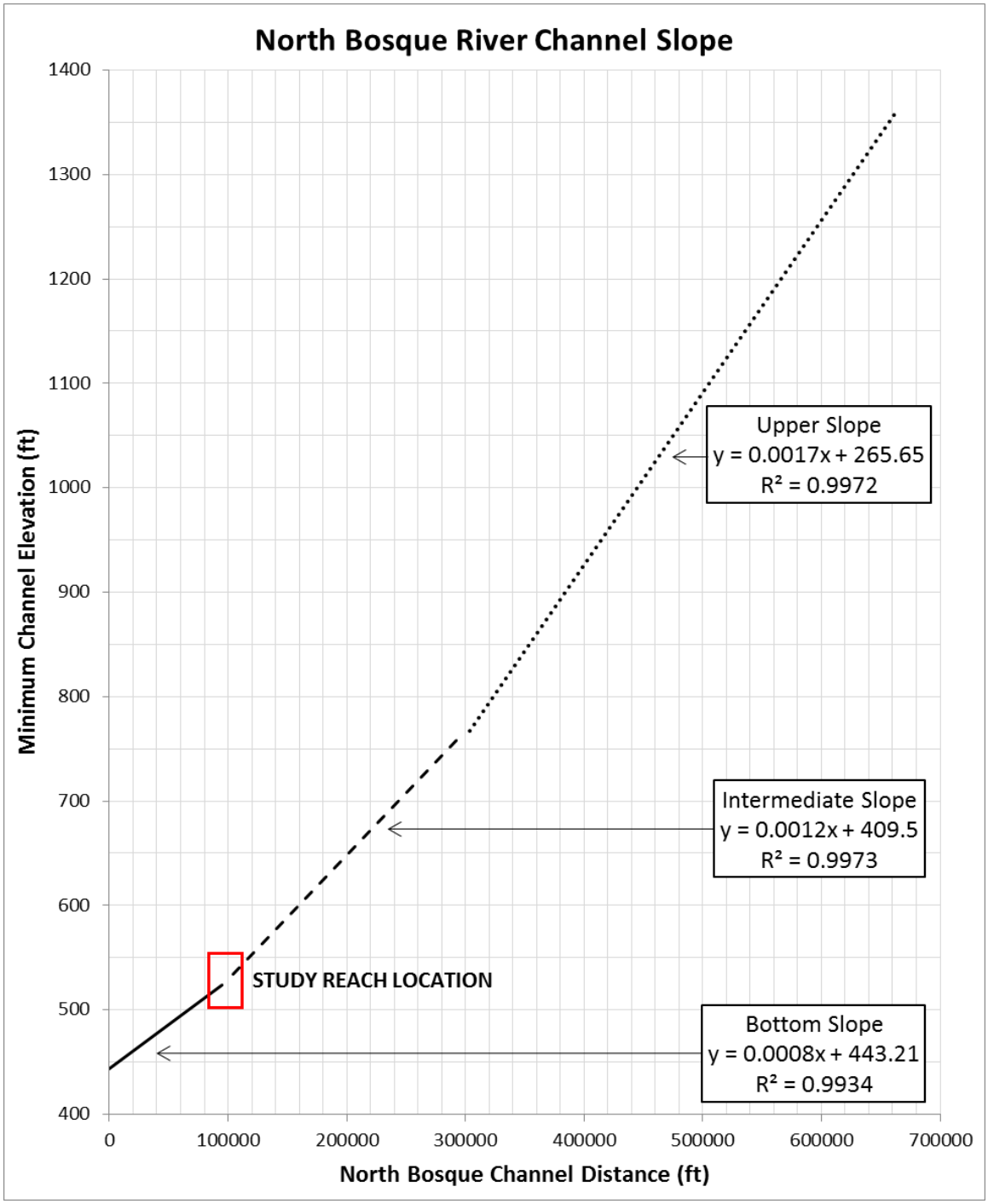

Figure 3.30. Three thalweg slopes were identified along the longitudinal plot; (1) the upper slope associated with the upper portions of the watershed has an average slope of 0.0017 m/m. (2) The intermediate slope is located from Iredell, TX to Clifton, TX and has an average slope of 0.0012 m/m. (3) The bottom slope associated with the NBR approaching Lake Waco begins south of Valley Mills, TX, and has an average slope of 0.0008 m/m.

Geological data was gathered from Proctor [1969] in effort to better substantiate the decreases in slope. According to Proctors' measurements of the geological outcrops of the NBR, it appears that the USACE derived NBR slope profile reflects the underlying geology within the watershed as seen in Figure 3.31.

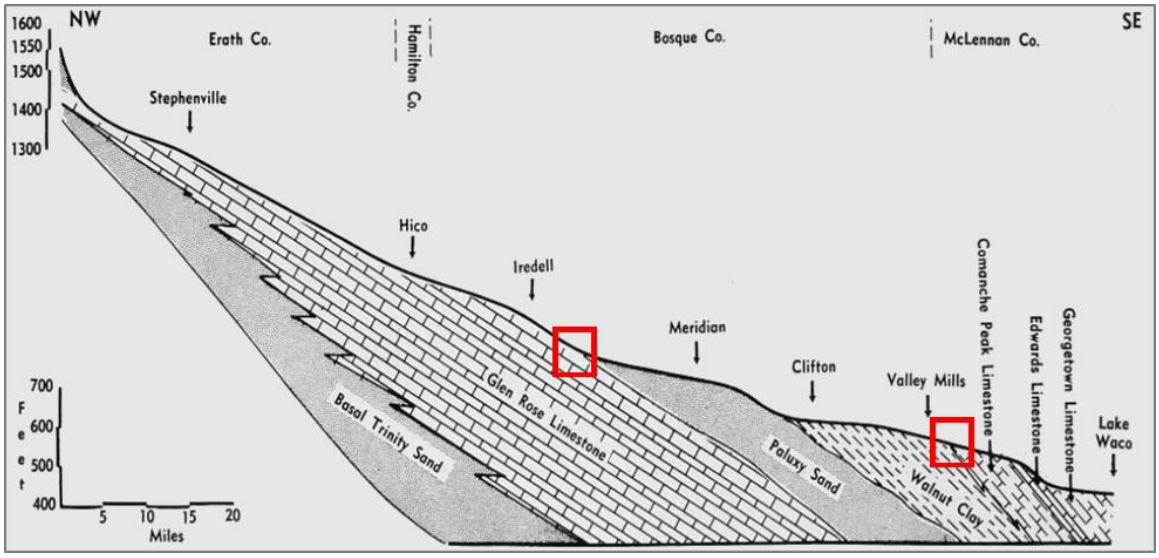

Figure 3.31. Geological longitudinal profile from Proctor's 1969 study of the NBR watershed. Approximate slope decreases (indicated by red squares) were plotted and correspond to geological contacts. Modified from Proctor, 1969.

Understanding the relationships between measured slope profiles and observed geological formations is critical when identifying the potential changes to the slope of the NBR. The following section describes the results of the techniques used to identify and describe changes to the slope of the NBR.

[3.4.2] Historical Sinuosity and Channel Centerline Analyses

Slope changes closely mirror changes to channel length and sinuosity. Sinuosity increases are synonymous with decreases in the longitudinal slope profile, while the same is true for the relationship between slope increases and decreases to channel length.

Threshold Rivers bound by large sediments and/or resistive geological formations often experience changes to the slope profile as a result of lateral erosion (i.e. cutbank shearing). Changes to channel bottom compositions and the erosion of resistive beds can also be linked to shifts in sinuosity. According to the HEC-RAS slope profile, the NBR reach is located along a geological contact between the Walnut Clay and Comanche Peak Limestone. Considering that the resistivity of bed material is one factor that drives channel form, geomorphological changes are expected as the NBR transitions from the Walnut Clay to the Comanche Peak Limestone.

Historical centerline analyses and sinuosity values were calculated for the NBR reach in order to assess variations in the slope along transitional zone. Aerial photos from 1955 to 2016 were observed for changes in centerline length. Increases in centerline length would indicate a decrease in the NBR slope. Inversely, decreases in the centerline length over time imply that the channel slope is steepening. Centerline analyses in Figure 3.32 reveal an initial increase in channel sinuosity and centerline length from 1955 to 1995, followed by a decrease for the remaining period of record (1995-2016). The trend from 1955 to 1995 indicates that the NBR is becoming more sinuous, while the range between 1995 and 2016 show a notable decrease in slope. This indicates that the NBR is straightening, which indicative of the channel slope is becoming steeper.

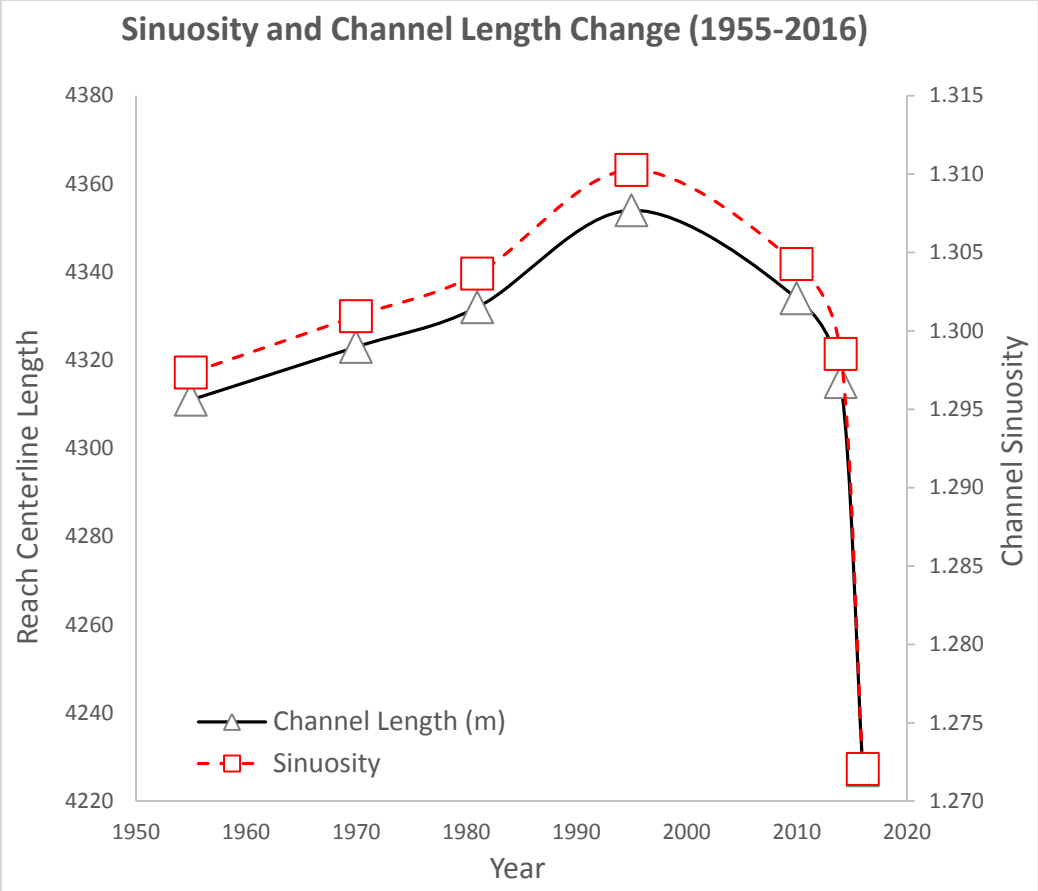

Figure 3.32. Channel length and Sinuosity change over time along the NBR Reach. A notable increasing trend between 1950 and 1995 was observed, with a simultaneous decrease in sinuosity/channel length between 1995 and 2016.

[3.5] Channel Form - Planform and Lateral Migration Assessments

Planform change along the North Bosque River is observed as bank shearing and lateral migration. Three approaches to assess lateral migration rates were completed. The following section details the resulting migration rates determined along the NBR reach.

[3.5.1] Historic Aerial Imagery Analysis

The aerial imagery analysis provides historical context to erosion along the NBR channel. Cutbank shearing along the NBR reach via photograph analysis yielded an average erosion rate of 0.50 ± 0.28 m/yr for the 20 cells. Variations in erosion rates were

recorded for each reach cutbank. Figure 3.33 details the individual erosion rates associated with each cutbank.

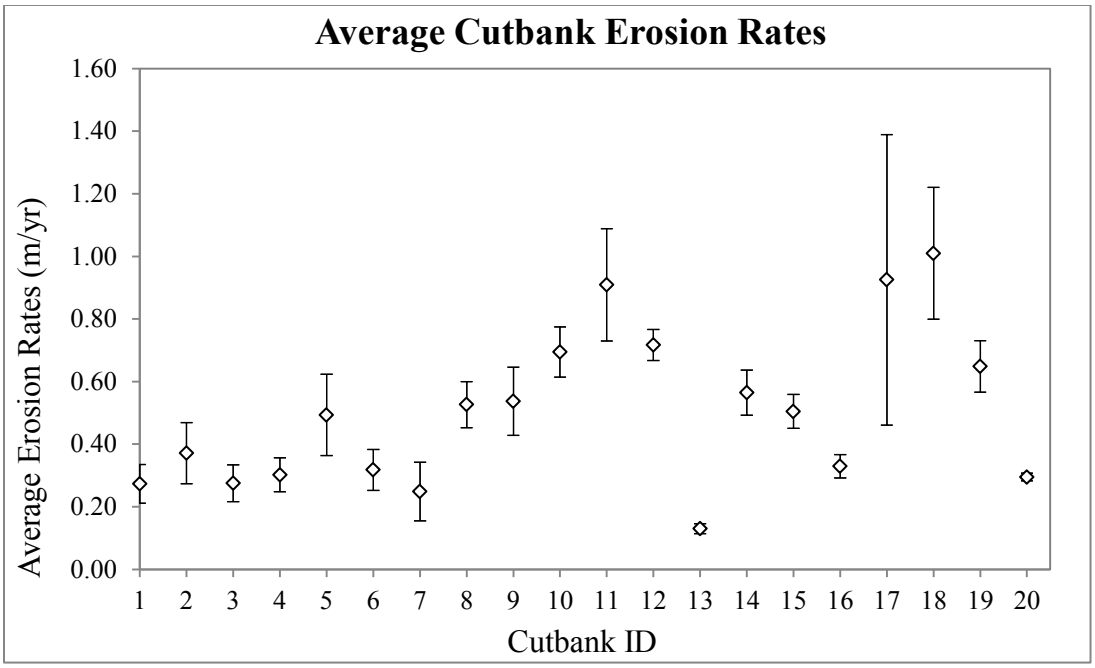

Figure 3.33. Mean cutbank erosion rates observed from 1955 to 2016 determined from the digitized aerial imagery analyses. Larger standard deviations are associated with cell size, and in some cases are related to positioning within the channel.

18 of the 20 cutbanks have standard deviations below ±0.18 m/y. Small standard deviations are associated with stable year-to-year channel erosion rates and smaller cell sizes. Cutbanks 17 and 18 have the largest standard deviations (0.46 and ±0.21 m/y respectively), indicating a high degree of variation in erosion rates along the year-to-year erosion profiles. No distinct increasing trend in erosion from the upstream to downstream cutbanks was identified (r^2 = 0.20). This erosion rate accounts for the steady cutbank shearing along the North Bosque River reach. Aerial photos along the NBR reach from 1995, 2010, and 2019 revealed an increasing channel meander width at roughly 0.3 to

0.06 m per year. Another erosion rate was determined for the NBR reach via linear regression, presented in Figure 3.34.

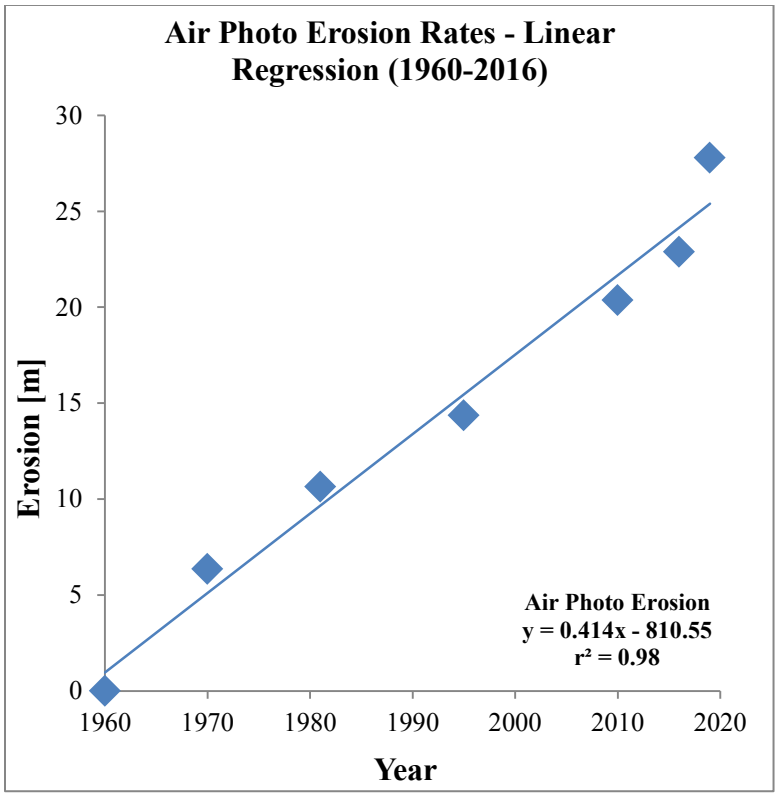

Figure 3. 34. Linear regression of assumed cumulative erosion rates for the NBR Reach. An increase in erosion rate is noted from 1995 to 2016

This linear regression assumes that the average erosion rates determined for each photo period (i.e. from 1970 to 1980) remain stable. Average erosion rates for this regression show a lower erosion rate equal to 0.41 m/yr. A smaller portion of this regression is used in Briaud's predictive method; data from 1995 to 2016 is used to calibrate the model.

[3.5.2] Briaud's Predictive Method

Briaud's Observational Method was implemented as a comparative measure of lateral migration, as it incorporates remotely measured lateral migration rates as a calibration for predicting erosion. This method allows users to determine and predict

future channel migration rates based on known soil properties and channel velocities. A useful aspect of this method is the feasibility of incorporating hypothetical hydrologic data to predict future erosion along a channel. This method can also be used to associate erosional events of known RI to estimate the magnitude of erosion. The following erosion rates from 1995 to 2016 were incorporated into Briaud's model (Table 3.14).

Table 3.13. The erosion rates determined from 1995 to 2016 via Historical Imagery Analysis are used as a calibration factor for the Observation Method. A linear regression is calculated to determine an alpha factor used in the time series erosion function.

Meander Position Over Time	
Year	Cumulative Erosion (m)
1995	0
2010	6
2014	8.52
2016	13.44

Several coefficients were calculated and determined for use in Briaud's erosion equation: (1) a beta factor (β) of 3.43 was chosen to represent soils with moderate erodibility, this value aligns with the erodibility data determined from the JET and the USCS erosion class for NBR sediments (for more information about these variables see Briaud's Erodibility Indices and V_c determination in appendix H), (2) A critical velocity (V_c) of 0.61 m/s was implemented as a velocity that begins to erode cohesive loamy soils commonly found along the NBR banks, and (3) alpha prime (α') was determined by calculating a linear regression between the observed erosion rates from 1995 to 2016 (from the Air Photo Analyses). The predicted erosion rates for this period yielded an α' of $4.45e^{-8}$ which is used in the following equation to produce time-series erosion rates in the following equation:

$$M = \alpha' \left(\frac{v}{v_c}\right)^{\beta} \times v_c \times \Delta T \qquad \text{(Equation 5)}$$

Where M is the magnitude of erosion, v is velocity of flows in m/s, v_c is the critical velocity of soils within the channel in m/s, and ΔT represents daily time steps in seconds. Utilizing this equation resulted in the following erosion profile for the NBR reach, which represents time series step-wise erosion based on daily flow averages (Figure 3.35).

A remotely observed erosion rate (1995-2016) of 0.54 m/y was established from the air photo analysis regression - this data was used to calibrate the model. Briaud's predictive method produced an erosion rate of 0.63 m/y from 1960 to 2019. This method is useful for quantifying and estimating the magnitude of erosion in relation to flood magnitude. For example, a 100 year flood was recorded between 1991 and 1992; this flood interval is presented in Figure 3.36 to show the degree of predicted erosion associated with this historical flood.

Briaud's model allows users to estimate erosion rates resulting from hypothetical flow events. Time-series flood data can be discretized into a unique dataset that provides erosional estimates for any river, as long as physical properties of the channel are identified beforehand.

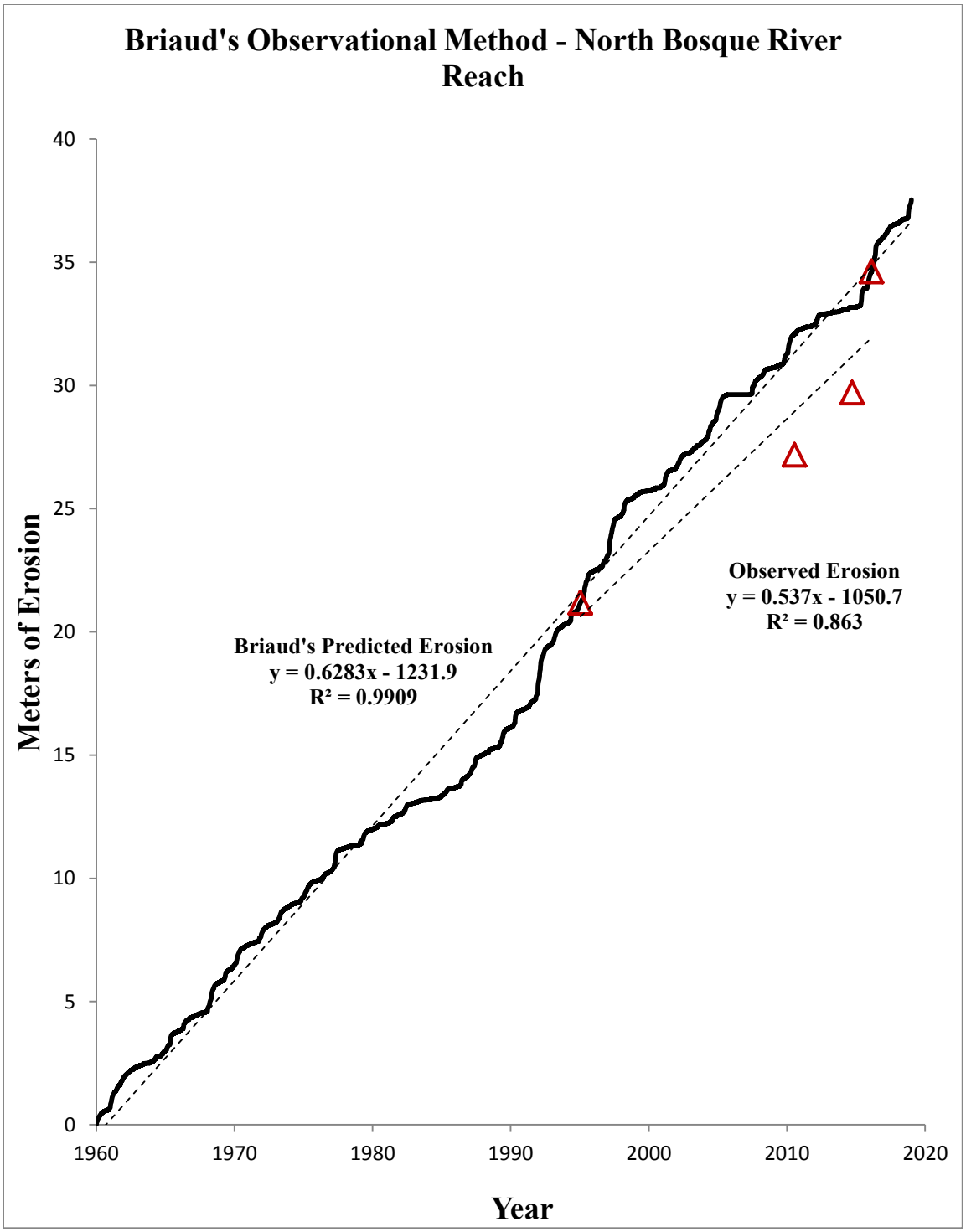

Figure 3.35. Briaud's predictive method from 1960-2019, calibrated with the 1995-2016 remotely observed erosion rates. Shallow slopes denote dry periods and droughts, while steep portions of the curve indicate high erosion rates resulting from flooding.

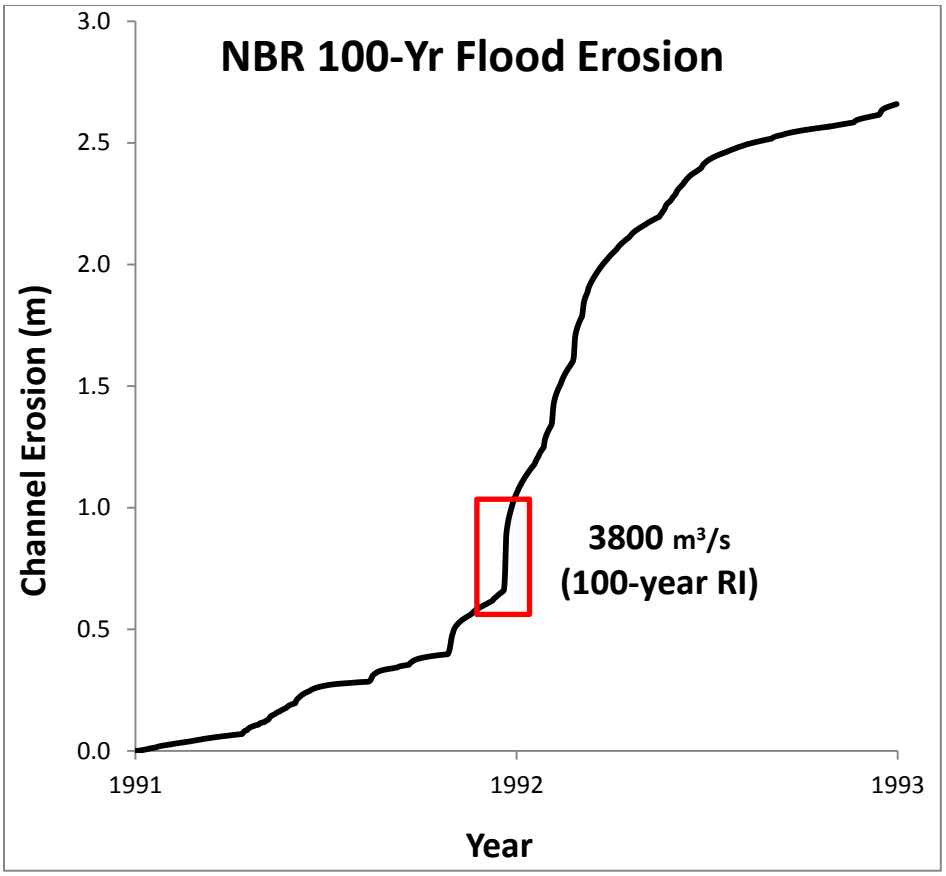

Figure 3.36. Erosional extent associated with the 100-year flood in 1991. Roughly 0.45 meters of erosion are estimated according to Briaud's model. This suggests that the 100-year flood can cause up to one years' worth of erosion (according to the remotely observed erosion rates) in a single week.

[3.5.3] Root Dendrology Migration Rates

The final method utilized to assess lateral migration rates is the Root Dendrology assessment (RD Method); this experimental method uses morphological exposure anatomy in roots to identify an exposure date with field-measured erosion. Root dendrology derived erosion rates were higher than the observed and predicted erosion rates. An average of 0.87 m/y was determined from the entire sample group (n=20). Removal of extraneous outliers yields an erosion rate of 0.98 meters per year (n=16), excluded samples are discussed in section 4.4.3. The exposure dates of each sample were

observed to identify frequency trends in the collected sample group; the following frequency diagram details the temporal extent of collected root samples (Figure 3.37).

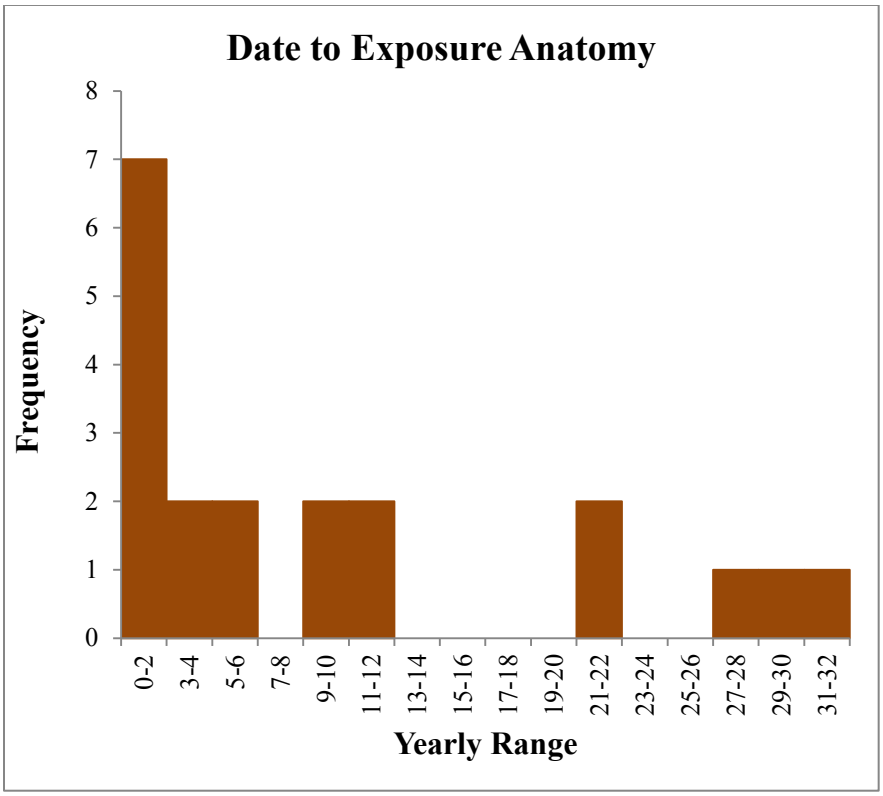

Figure 3.37. 2-year interval frequency diagram of root exposure dates. An initial peak in frequency is notable in the [0:2] interval, with fewer sample counts towards the tail of the x-axis. This attenuation in frequency is attributed to low sample rate and sample decomposition/removal. The 2-year interval was selected to best discretize sample date ranges.

Similarly, the extent of erosion associated with each sample was plotted by exposure year in Figure 3.38, this figure shows an increasing rate or erosion with more recently exposed samples.

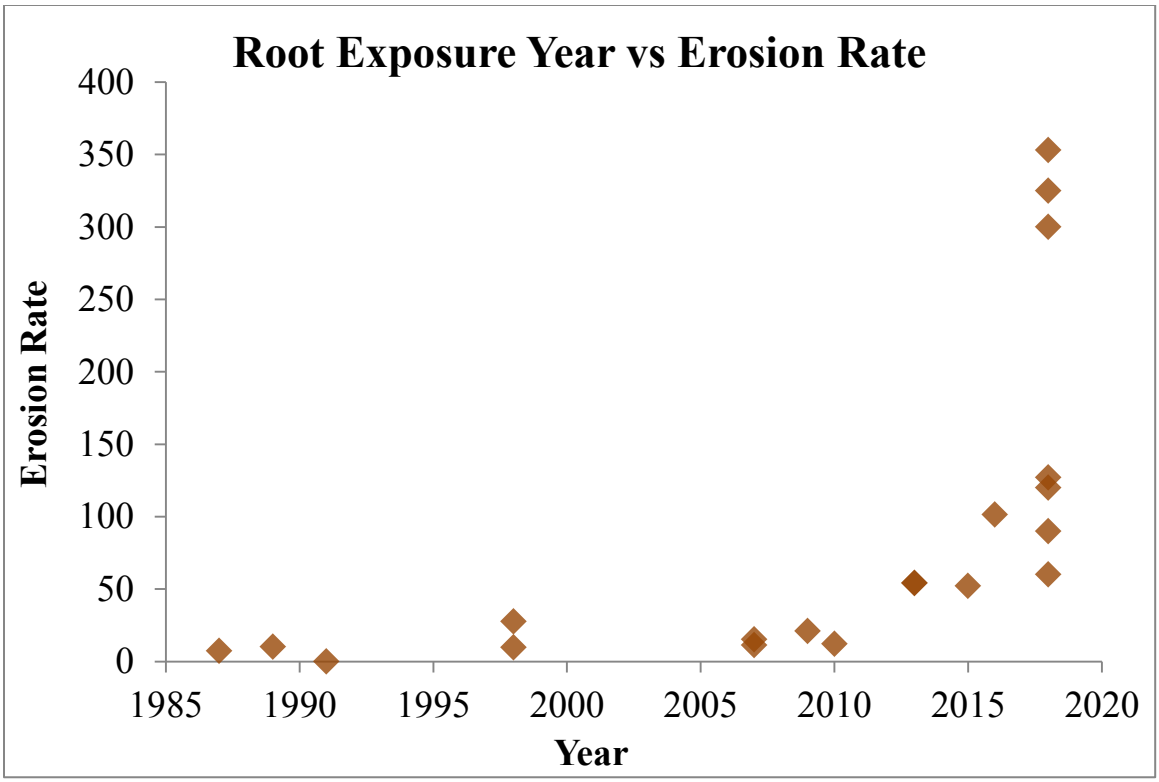

Figure 3.38. Exposure year vs. determined erosion rate for the 20 NBR reach samples. A larger range of erosion rates are attributed to more recent samples.

This plot shows several trends; 1) the range of erosion rates associated with the more recently exposed samples is higher than the older samples. 2) The only sample located in the 1991 range is NB04S1, which was taken from a large (approximately 0.75m diameter) Green Ash located in the main NBR channel. No erosion rate is associated with this sample since it was not in situ. 3) The frequency of samples is dominated by samples 0-6 year range, this is shown best in Figure 3.38. Averages for each year were determined, and were plotted into a cumulative linear regression using the methodology described for the Air Photo Analysis, this technique provides a different approach to assess erosion rates from 1987 to 2019 (Figure 3.39).

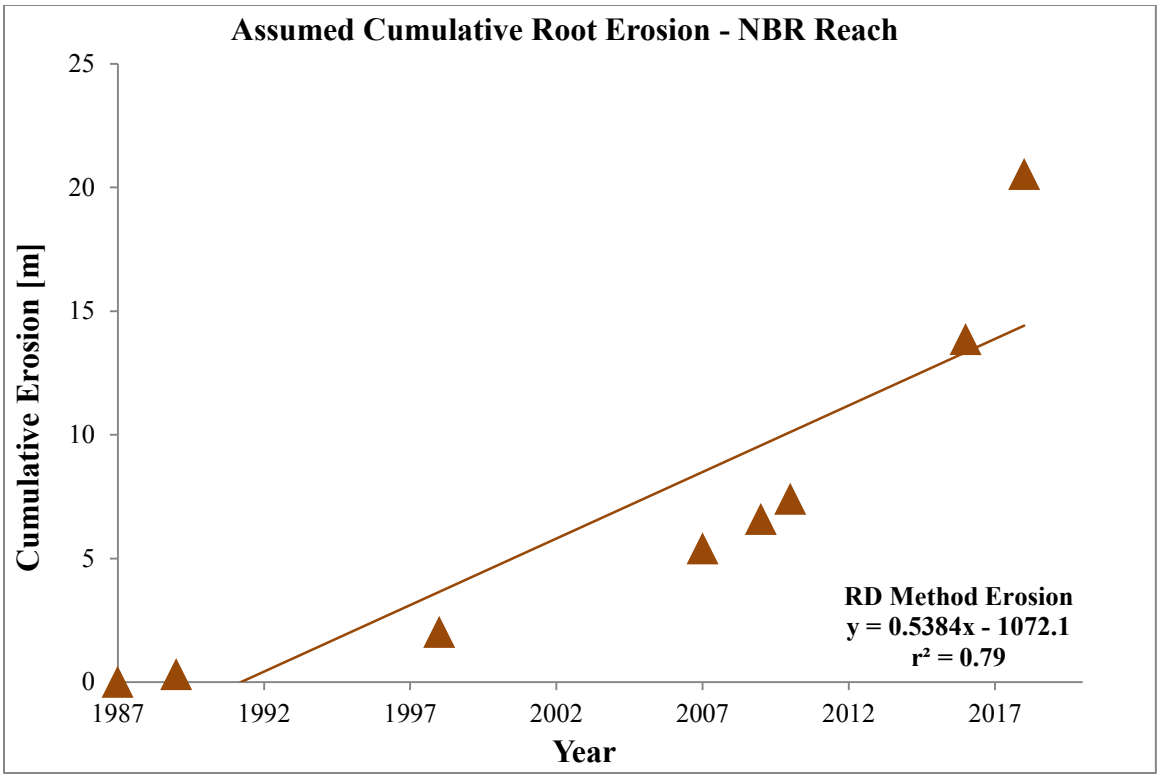

Figure 3. 39. Cumulative erosion rate estimated from 1987 to 2019. Averages for each year were summed for each subsequent year until a new erosion rate was established via root analysis. This erosional assessment assumes consistent erosion rates between data gaps. An increasing trend in erosion is noted.

This erosional assessment provides an erosion rate of 0.53 m/y (r^2 = 0.79), which still falls in range of the other erosional estimates. Once more the increasing trend in erosion is observed.

Several exposure anatomies were identified from the root cross-sections; the most significant morphological shift was the transition from ring-porous structures to diffuse-porous. These transitional zones were identified as the primary boundary that denotes a shift from initial burial to exposure. The age of each root sample was determined by counting the rings from the root exterior to this boundary. The following diagram displays several samples of note that were used to classify the date-to-structure morphologies (Figure 3.4).

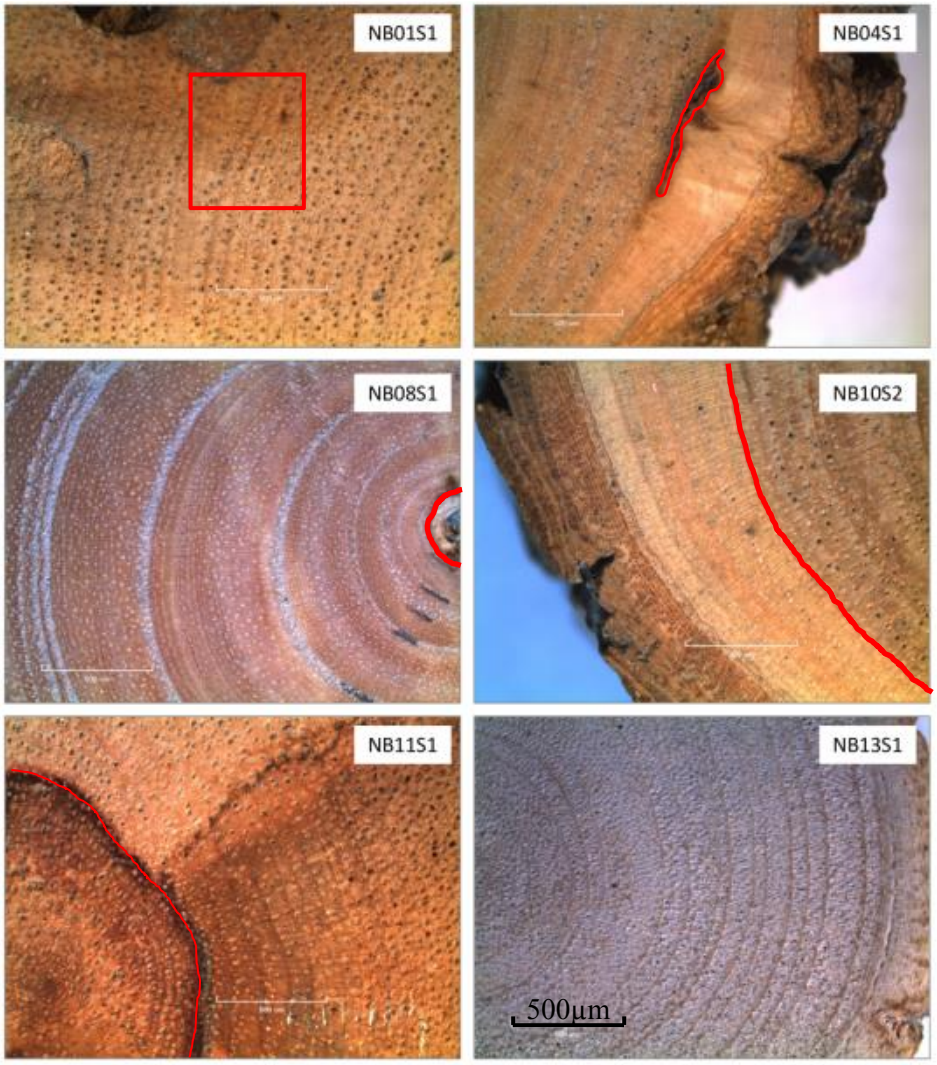

Figure 3.40. Notable root morphologies. Sample NB01S1 exhibits scarification as a result of sanding; the polishing process requires fine care in order to preserve samples. NB04S1: Scar tissues are outlined resulting from abrasion/exposure. NB08S1: Box elder with internal damage to root structure, this sample exhibits stem-like morphology. NB10S2: Transition from diffuse-porous to ring-porous indicating exposure. NB11S1: Staining and morphology shift is denoted by the red line. NB13S1: Softwood Hackbery sample exhibiting no change in morphology. Each sample uses the scale indicated on Sample NB13S1.

The Root Dendrology technique provides a unique take on erosion rate assessments, but provides only a small temporal window of erosional history and relies on sample availability. Additional RD Method data are available in Appendix I.

CHAPTER FOUR

Discussion of Results

[4.1] Key Hydrologic Factors of the NBR

River flashiness is a hydrological factor that can be used to explain the fluvial regime of the North Bosque River. Compared to other regional locations, the NBR is distinguishably flashy, as indicated by the high RBFI values. These data suggest hydrologic events - specifically flood events - will cause rapid increases in flow along the NBR corridor that are tied to erosional processes and sediment transport. Simply put, the RBFI effectively shows that the NBR is vulnerable to floods. A study performed by Baker [1975] assessed regionally similar streams for their susceptibility to flood events. His study, performed along the Balcones Escarpment in lower Central Texas (shown in Figure 4.1), indicated that the intensity of flood events in this region relate to orographic influences and the occurrence Gulf storms moving inland. A subsequent study performed by Baker et al. [1977] continued this claim that Texas streams are controlled by flood events. In this study, they found that rivers bound by Cretaceous bedrock (similar to those within the North Bosque River watershed) are dominantly controlled by flood flow. However, the NBR is located just north of the Balcones Escarpment, and may not experience hydrological influences from the Gulf; rather, the large storms are likely a result of strong atmospheric winds commonly attributed to large summer storms, similar to those often reported near Dallas-Fort Worth, Texas (NWS, 2019).

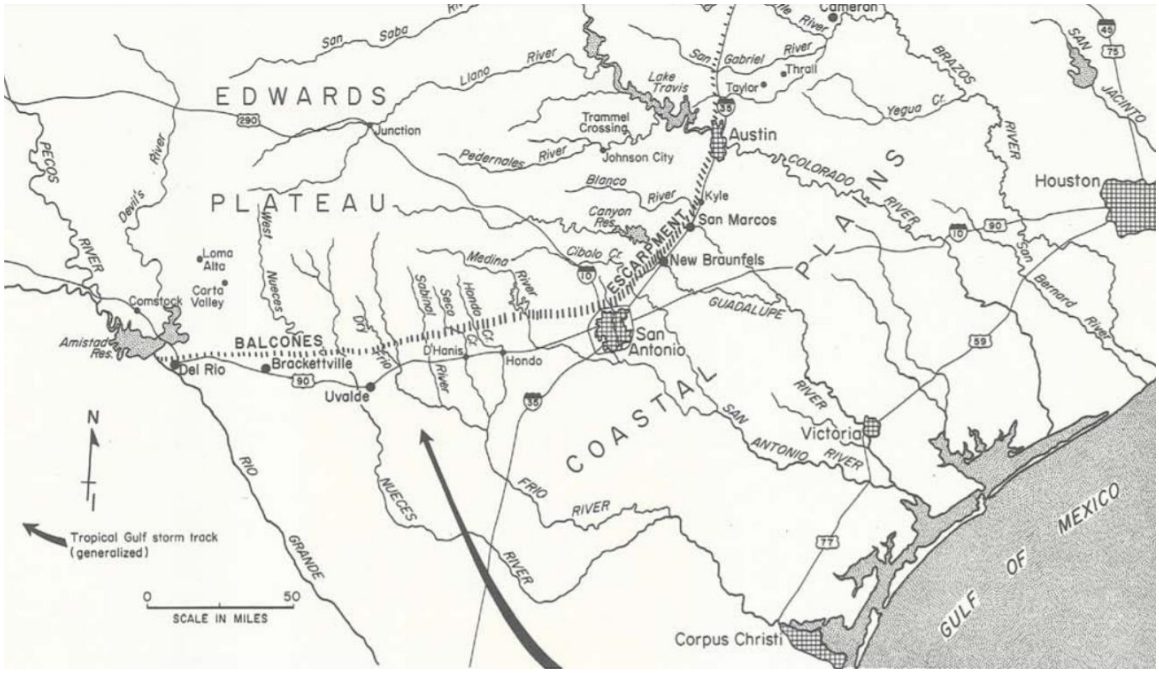

Figure 4.1. Location of the Balcones Escarpment, Central TX. From Baker, 1975.

Regardless of storm source, the geomorphic observations made by Baker hold true for the NBR, as the geomorphic setting of the Balcones Escarpment is similar to the NBR watershed. Of particular note are his observations of meander scours along rivers after a large flood in 1972, which lead to the destruction of vegetation and soil cover along the riparian zone. Baker observed vertical degradation of the channel to bedrock, with the most notable flood effects taking place along meander loops in larger order streams. Considering these trends, along with the inherent flashiness of the NBR, it can be assumed that larger floods are more likely to influence the geomorphic shape of the NBR, and should be considered a major factor that drives the NBR channel to change. Therefore, long-term hydrological changes along the NBR are attributed to the historical 100-year flood in 1991.

The geomorphic impacts of high magnitude events similar in scale to the recorded 1991 100-year flood have been further researched in New Zealand (Fuller, 2007). Fuller

implemented historical aerial imagery analyses along a 30 km reach of Kiwitea Stream (NZ) to observe hydrologically driven channel evolution. He attributed a high magnitude / low frequency storm event to elevated rates of vertical degradation and cutbank shearing. These observations support the idea that the 1991 storm and the increases in hydrologic discharge are intrinsically linked. In terms of hydrological shift, an increase to the daily average discharge was noted after the 1991 flood. Prior, daily flow rates averaged 5.6 m^3/s. This flow increased to 8.4 m^3/s after the hydrologic pulse from the 1991 storm attenuated, indicating that long term changes to the flow regime have occurred since 1991. Increases to the hydrologic flow regime are also observable along the Partial Frequency Analysis, which suggests that higher magnitude flows are more common for similar flow exceedance percentiles. This alludes to the fact that higher magnitude flows have become more frequent in the NBR watershed since the occurrence of the 1991 flood.

[4.2] NBR Sedimentary Supply, Transport, and Channel Interactions

Sediment travel distance data paired with the RGA sediment assessments suggest that the sands are moving though the NBR watershed, and are not being deposited within the main channel. Sands are sourced from a combination of bank alluvium and the Paluxy sand, which is notably more erodible than the other lithologies in the NBR watershed.

In contrast, the travel time of gravel suggest that they are locally sourced within the channel. Gravels along the NBR reach are estimated to move at approximately 0.3 km per year, indicating that - under normal yearly flow conditions - the gravels will not move far from their origin before they are deposited as point bars and channel bottom alluvium. The source of the NBR reach gravels is therefore likely a combination of the Walnut Clay

and bank alluvium, which is comprised of moderately erodible soils and gravel beds. These results reflect the findings of a study in the Wind River, WY (Smalley, Emmett and Wacker, 1994). They determined gravel transport rates of 1.6 km per year (note that gravels only account for 20 percent of the bedload in Wind River; additionally average gravel distributions were noted to be smaller than those calculated for the NBR). They also noted that sand was much more likely to move through the mixed-alluvial system. This explains why very little sand is observed in the NBR. The hydrological flow regime of the NBR is much more likely to route finer sediments through, while much larger flows are required to move NBR gravels.

A study performed by Pfeiffer, Finegan and Willenbring [2017] indicated that sediment size in threshold channels may be an important component that leads to shifts in channel geometry. They argue that the commonly cited relationship between bankfull discharge and the transport of sediment may not fully describe the complicated processes that define a channels' geometry. Rather, they suggest that there is evidence that links sediments supplied from the upstream portions of the watershed to channel geometry. In particular, they suggest that threshold streams, much like the North Bosque River, may express morphologies similar to regions with low sediment supply. However, trends in the NBRs' geometry closely mirror those observed in Central Texas, many of which are also classified as threshold systems.

[4.3] Role of Critical Thresholds along the NBR

The presence of rigid and erosionally resistant channel-beds is another primary driver of the NBRs geomorphic form. Calculated vertical degradation rates of less than 1 cm per year are notably lower than the determined lateral migration rates of the NBR

banks. This disparity in erosional magnitude suggests that the NBR will continue to migrate laterally, as the protection along the banks is null in comparison to the strength of the channel bottom. The influences of bedrock bound streams, often referred to as threshold streams, has been well-researched in Central Texas. Threshold rivers, which best describe the form of the NBR, are defined by the presence of resistant beds. The geological boundaries of the channel bottom mitigate erosional processes, and divert energy to the less resistant banks.

Work performed by Shepard [1985] in Austin, Texas indicated that the presence of bedrock in central Texas streams is a dominant influence that drives the geometry of a river. His work showed the degree of impact to the banks that result from differences in erosional resistance. The NBR bed is shown to be notably more effective at resisting erosion in contrast to the banks. Data from the slake durability test indicates that the NBR beds, particularly along the reach portion, only degrade at a rate of 0.73 mm per year. In contrast, the banks of the NBR are subject to erosional pressures and are comparatively much more likely to erode. Estimates of soil erosion rates based on Briaud's 2004 study indicate erosion rates ranging from 0.35 to 0.7 meters per year. The lower end estimates of bank erosion are significantly higher than the upper estimates of vertical downcutting. The jet data further support the comparative erodibility, and suggest that even cohesive soils with dense roots are still more likely to erode faster than the beds of the NBR reach.

Erosional dynamics in confined river channels was described by Yochum [2013], who studied 531 river reaches in Colorado to identify the relationship between stream power and geomorphic change. The NBR is vertically confined, as a result of the presence of rigid channel bottoms. Yochum noted that confined rivers often experience

increased erosion along the channel margins. This 'channel margin' erosion is primarily observed in the form of cutbank channel shearing in the NBR.

Heitmuller, Hudson and Asquith [2015] studied lithologic and hydrologic controls of mixed alluvium streams in Central Texas. The NBR shares similarities with those studied by Heitmuller et al. [2015], as it has an abundance of channel gravels that could jointly classify this stream as alluvial. This study noted the tendency of Texas streams to exhibit high variations in peak flows, a trend that is also associated with the NBR. In particular, the flashiness of the NBR agrees with this assumption, as a high RBFI indicates that a river is likely to experience a rapid increase in discharge due to incoming runoff. Furthermore, Heitmuller surmised the geometry influences of these streams into three dominant controls: 1) The most important control is the presence of resistant beds - in this case the presence alluvial gravels and rigid geological beds along the thalweg of the NBR support this morphological concept. 2) Variations in flow regime are described as another (lesser) factor that alters these threshold streams. Once again, these trends are observed in the PFA and mass curve profile. Finally, 3) Heitmuller notes that alluvial deposits play a role in the geometry of a river, however it should be noted the streams in his study are dominated by sand rather than gravels. Regardless, this aspect is of the lowest impact to channel geometry, and is in effect outweighed by the presence of resilient beds and hydrological variance.

Variation in channel-bottom bedrock erodibility was further explored by Shobe et al. [2017], who focused on the processes of channel form via weathering processes. Shobe noted that bedrock located along the thalweg (channel bottom) is actually more resistant to erosion than bedrock exposed along the banks of the river, this is due to

constant weathering cycles associated with exposure (i.e. freeze / thaw cycles). A majority of the watershed outcrops are fully buried by alluvial gravels, in most instances within the NBR reach the bedrock is protected by this alluvium. Regardless, the variation in geomaterials along the bed vs. the bank is described as a yet another major proponent that leads to channel instability (Shobe et al., 2017).

More recently, channel width has been considered a variable that reacts according to the threshold fluvial entrainment stress of the most resistant material; this relationship has been extensively described by Dunne and Jerolmack [2020]. If this is the case, the primary driver of channel width is the presence of the geological boundaries lining the channel bed of the North Bosque River. Dunne and Jerolmack also propose the idea that a relationship exists between incoming sediment supply and changes to longitudinal slope profile. One aspect of this thesis that touches on this idea is Stroth's CSR Tool, which effectively implements sedimentary supply data (in conjunction with hydrologically effective flows) to assess trends in downstream stability. The results of the CSR Tool for the NBR 'design' reach indicate that the supply from Clifton does in fact lead to instability in the channel. This trend is observable in the form of channel shearing that is most extensive along the cutbank portions of the NBR reach.

Regarding slope, changes in slope along the NBR profile are attributed to the geologic boundaries along the channel thalweg. Proctor [1969] described the notably shallow southeastward dip of the Cretaceous strata, which averages 12 to 27 feet per mile (0.002 to 0.005). The presence of the rigid channel bottom prevents significant short term vertical change to occur, particularly in the upstream portions of the NBR watershed located along the Glen Rose Limestone. Therefore, the three NBR slopes observed from

the USACE HEC-RAS model are a product of the geological boundaries, and transitions between the boundaries (refer to figure 3.32 and 3.33). Coincidentally, the downstream changes in slope are closely linked to geological contacts between formations of the NBR watershed. The steep upper boundaries of the watershed are characterized by the Glen Rose Limestone, which drives the form of the NBR. A decrease is observed spatially near the contact between the Glen Rose Limestone (K_{gr}) and the Paluxy Sand, which is notably more likely to erode than the K_{gr}. The position of the Walnut Clay / Comanche Peak contact described by Proctor's longitudinal profile [1969] closely mirrors the break in slope recorded along the HEC-RAS model, indicating yet again that the trends in slope are geologically driven.

[4.4] Lateral Erosional Assessments and Their Implications

[4.4.1] Air Photo Analyses - A Temporal Look to the Past of Erosion

The erosional response of the NBR was assessed via three methods. Remotely observed air photo analyses have been implemented in many erosional studies due to their common availability, spatial extent, and temporal variance which allows researchers to get a glimpse at past conditions (De Rose and Basher, 2011; Ning et al., 2006; Langat, Kumar, and Koech, 2019). Studies by Langat et al. [2007] focused primarily on channel erosion and accretion along the Tana River in Kenya - they linked channel change to a combination of hydrological flow regime changes, land-use changes, and the presence or absence of riparian vegetation. In a similar fashion, the NBR reach was assessed for erosional processes along meandering cutbanks. Air photo analyses from 1955 to 2016 indicate the North Bosque River is experiencing channel shearing at a rate of 0.41 meters per year ($r^2 = 0.98$). It should be noted that the magnitude of erosion appears to be

increasing since 1995. The remotely observed air photos used for calibrating Briaud's predictive model (data from 1995 to 2016) yielded an erosion rate of 0.54 meters per year (r^2 = 0.86). It should be noted that some degree of error is associated with air photo remote sensing techniques. In particular, the manual orthorectification of older aerial imagery datasets (1955 and 1970) are subject to scaling issues. In addition, the spatial resolution of these images ranges from 1 to 0.5 meters, which should be considered when comparing these erosion rates to other methodologies. Some variations cutbank erosion rates were observed, particularly downstream from the bridge located in Valley Mills. This erosional variance is attributed to the presence of the bridge; similar erosional studies have also linked riverine construction (in particular, bridges and dams) as potential sources for channel instability that can lead to increased degradation rates during flood events (Kondolf and Curry, 1986).

Work by Giradino [2011] discusses the erosion of the Brazos River in central Texas, which has similar lithological boundaries to the NBR. Giradino noted erosion rates ranging from 1.09 to 5 m/yr along the Brazos, though it should be noted the drainage area of the Brazos is significantly larger than the North Bosque River, with channel widths several times larger than the NBR. In addition, the spatial extent of this study was much larger than the NBR's - a total of 203 river kilometers were assessed for the Brazos study. However, some trends in data do align with those observed along the NBR. In particular, Giradino noted that the rate of erosional migration along the Brazos generally aligned with increases in hydrological flow. Inversely, decreases in long-term flow showed some relation to decreases in channel migration rates. Therefore, it could be inferred that the increases to hydrological flow associated with the Mass Curve Profile

and the PFA observations may explain the increased lateral migration rates of NBR reach cutbanks. This shows long term implications of the 1991 flood, which not only increases the rate of flow along the NBR, but increases the magnitude of erosion as well.

[4.4.2] Briaud's Observational Method - Predictive and Historical Analyses

Remotely obtained air photo erosion rates are a useful tool to estimate the past rates of erosion within a channel, but serve little to no insight on predicting erosion relating to certain magnitudes and frequencies of flow conditions. A recent development in river scour development was made by Briaud [2018], who implemented remotely observed erosion data into a predictive model to assess erosion resulting from bridge scour. Fortunately the observational method in Briaud's predictive model was completed via Air Photo Analysis. These data were input into Briaud's model to act as a check for the erosion rates that were measured through the air photo analyses, and provides useful context to predicting erosion events of known frequency and magnitude (Briaud, 2018). This model was limited to remotely observed calibration from 1995 to 2016, due to issues associated with gaps in flow data. An estimated average rate of 0.63 meters of erosion per year was determined from Briaud's model. While this is higher than the remotely observed rate, it is still within a reasonable range and closely represents both the 1955-2016 and 1995-2016 air photo erosion rates.

Briaud's model is not only a useful erosional assessment, but can also provide predictive context to the magnitude of erosion for certain flow events. For example, Figure 3.37 shows a useful application of this technique - proper calibration of the model allows a detailed look at erosion that can be linked to various flood conditions. Characterizing the various frequency (RIs) and magnitudes (Peak Q) of hydrological

events for the NBR can be described in terms of erosion. In the instance of the historical 100-year flood, peak flows of 3,800 m^3/s results in 0.5 meters of erosion within a week. This is the equivalent of a single average year of erosion as indicated by the average of Air Photo, Briaud model, and RD Method erosion rates (mean = 0.53 m/year). Thus, the 100-year flood is effectively equivalent to 1 years' worth of erosion. This is a useful application from a predictive standpoint, as it can directly link known RIs and flow regimes with erosional extents within a watershed.

These predictive analyses can be simply implemented with Briaud's' predictive model, but is best supported with air photo imagery or in field time series data (i.e. pin erosion measurements); as the model relies on known/measured erosion rates, which are key to gauging the relative accuracy of the model (in addition such data is required to calibrate the model). With growing concerns of climate change and their influence on storm frequency and magnitude, it becomes more crucial to begin the development of models that will effectively predict erosion. For example, some studies have suggested that increases in atmospheric greenhouse gas could lead to increases in tropical cyclone magnitude by 2-11% in the next 80 years (Knutson et al., 2010).

[4.4.3] RD Method - A Vegetative Erosional Proxy

In many cases riparian vegetation is assessed for its' tendency to protect a river from erosion. Vegetation is widely accepted as a primary factor that resists erosion and strengthens the riparian zone; an assessment completed by Smith [1976] indicated that the presence of riparian vegetation had increased the cohesion of banks by several orders of magnitude. Additionally, the presence of vegetation has been linked to reductions in soil loss along channels in several studies (Kalliola and Puhakka, 1988; Miao et al., 2010;

Hickin, 1984). However, despite the abundant research associated with riverine vegetation buffering, very few (if any) studies have actually implemented vegetation as a proxy to determine erosion rates. The RD method provides a unique approach to assess riverbank erosion rates, but is limited in scope due to the unavailability of accessible and biologically applicable root samples; regardless, the associated root erosion rates that were determined do fall in line with the averages determined from the aerial imagery analysis and predictive method.

An average erosion rate of 0.54 m/yr was determined from the RD Method, which represents a middle-ground erosion rate for the three assessments. This average was determined from 16 samples; Samples NB04S1, NB13S1, NB14S1 and NB14S2 were removed as they were not representative samples. Sample NB04S1 was located along the channel bottom. Interestingly, this is the only sample that was dated within range of the 1991 flood event (±2 years). It is likely that this large specimen was removed from the banks during the 1991 flood, and is being transported downstream. The lack of additional samples from this period indicate one of two scenarios: 1) Not enough roots were sampled for this analysis, or 2) samples in the 1991 exposure age range were transported through the channel. Sample NB13S1 was removed as a duplicate sample, and samples NB14S1/NB14S2 were also located in the main channel.

Frequency assessments of the root samples indicate that the most common erosion rates range from 0 to 50 cm per year. Of note is the plot of erosion rate by sample exposure year (Figure 3.40). This figure shows an increasing trend in erosion rate over time. This observation was made with the air photo analysis, and a slight spike in erosion rate is denoted along Briaud's predictive model post-2014. This could be attributed to the

large frequency of samples from 2013 to 2018, though average erosion rates for each single year seem to imply an increasing rate or erosion.

Roots along the meandering portions of the NBR were scarce, and when they were present they were located in the upper third of the river channel. From kayak these samples were unobtainable, and access to various personal properties was unfeasible for such a large study area. Therefore the decision to select samples upon availability was made. For future studies it may consider best practice to only collect samples from similar locations within the watershed, in fact this method is likely to prove more useful for channels with abundant root samples from both a quality and quantity aspect. In addition, the samples require intensive preparation for microscopic analyses. Harder woods often provided more detail due to their inherent ability to achieve a finer polish in the sanding process. For this reason, the density of the root samples collected should be taken into consideration - soft woods lack the cellular structure and rigidity required to make fine observations of morphological changes.

[4.4.4] Vegetation as a Lateral Erosion Mitigator

While the presence of riparian vegetation is linked to increases in erosional resistance, the location of vegetation in the upper-third of the NBR channel prevents it from providing stable protection to the active portions of the channel (within the 1.5 year flood stage). Rather, this vegetation is often undercut via channel shearing, particularly along the outside meanders of the NBR - even if it provides cohesive strength to the soils in the upper third of the bank.

[4.5] Describing the NBR's Response to High Magnitude, Low Frequency Events

The NBR is experiencing lateral change as a result of the relationship between bed and bank materials. This change is compounded as a result of the hydrological increases to magnitude and frequency of flows resulting from the historical 100-year flood that occurred in 1991. Constant exposures to critically effective flows for prolonged periods of time permanently altered the geometry of the NBR, resulting in increased erosion and more sedimentary inputs to the river. This channel change can be observed in Lane's Balance by referencing changes made to the four variables (L, D, Q, and S). In effect the stable slopes associated with the low degradative rates and rigid geological beds keep the slope variable relatively locked in, though the slight increase in slope (described as the decrease in sinuosity) indicates an increase in hydrologic flow and an increase in degradation. In this regard, Lane's Balance does hold true, as both increases to flow and a continuation of lateral migration are observed within the NBR reach. The slow transport of gravels (indicated by the travel time assessments paired with the lack of downstream gradation noted via Wolman Pebble Count) indicate that sediment size distributions is one factor that is unlikely to change significantly during the temporal scale of this study. Discharge is among the most volatile changing variable with the NBR, in addition to load change associated with the 1991 flood. Stroth's CSR Tool comprehensively assesses these variables, and shows trends that mirror Lane's conceptual model. These results comprehensively suggest that the NBR is likely to continue to erode, but more importantly indicate that it is susceptible to high magnitude flood events that will permanently alter the hydrological processes of the watershed.

CHAPTER FIVE

Conclusion

The North Bosque River is a dynamic fluvial system influenced by a multitude of variables; though many of the NBR's channel responses are associated with the historical flood in 1991, which permanently altered the NBR's morphology and flow regime. Several key conclusions can be made about the North Bosque River: 1) High magnitude, low frequency events play a critical role in the geomorphic form of the NBR; erosional events, sediment transport, and long-term flow rates increases are associated with infrequent flood events. This response is observed via RBFI analyses, hydrological increases to flow conditions, and is linked to the frequency of higher magnitude flows from the initial (1955-1990) to current (1993-2019) flow periods. 2) Bedrock along the channel bottom of the NBR acts as an erosionally resistant boundary that both mitigates vertical degradation and expedites channel shearing along cutbanks of the NBR. Erosional assessments of both bank soils and channel bed indicate that the banks are notably less resistant to erosional forces, and are thus more likely to erode. 3) The dominant erosional process within the NBR channel is cutbank shearing, which occurs at a rate of 0.41 to 0.98 meters per year. 4) Vegetation reduces erosion along the upper 1/3 of the bank profile, but is infrequently associated with reducing streamflow driven erosion. 5) The slope of the NBR, despite minor changes noted via centerline analyses, has remained relatively stable over time. This stability is likely due to the fact that the NBR is a threshold stream with bedrock lining the channel bottom throughout the watershed. In addition, changes to the slope profile in riverine systems generally occur

over large temporal scales. However, a slight straightening of the NBR is observed after 1995, which can be attributed to the 1991 storm altering the equilibrium of the NBR. This slope change is likely a process of the NBR adjusting form in response to the increased flow conditions. Finally, 6) the NBR is best described as unstable. The susceptibility to flooding, paired with the imbalance in sedimentary inputs observed via CSR analysis, indicate that the NBR will continue to erode in the future as it approaches a new equilibrium. This study shows the impacts to channel form that result from a significant hydrologic event, and provides a comprehensive look at the factors that resist and control erosional processes along the North Bosque River.

APPENDICES

APPENDIX A.

Aerial Imagery Analysis Photo Metadata for 1955, 1970, 1981, 1995, 2010, 2014, 2016, and 2019.

Year	Month	Day	Entity ID	Imagery Type	Resolution	Water Level at Valley Mills (Ft)	Discharge (cfs)	Spatial Extent
1955	March	22	AR1VGC000010011	Aerial Photo Single Frames	N/A	ND	ND	Full Study Reach
1970	March	26	AR1VCKE00010210	Aerial Photo Single Frames	N/A	ND	ND	Full Study Reach
1981	Nov.	1	NC1NHAP810221047	NHAP	N/A	ND	ND	Full Study Reach
1995	January	19	DI00000000730375	DOQ	1 foot	ND	55	Full Study Reach
			DI00000000730332	DOQ	1 foot	ND	55	Full Study Reach
2010	August	10	M_3109721_SW_14_1_20100801	NAIP	1 foot	5.8	35	Full Study Reach
			M_3109720_SE_14_1_20100801	NAIP	1 foot	5.8	35	Full Study Reach
2014	October	14	3888387_319721320150214	High Resolution Orthoimagery	1/2 foot	4.9	12	Full Study Reach
			3888384_319720420150214	High Resolution Orthoimagery	1/2 foot	4.9	12	Full Study Reach
2016	March	5	N/A	DigitalGlobe	1/2 meter	6.85	330	Partial - Cells 4 to end
2019	January	4	N/A	DigitalGlobe	1/2 meter	10.7	3000	Partial - First 3 Cells

APPENDIX B.

Root Sample Field Data, Species Identification, and Erosion Rate Values.

Sample ID	Description - Location	Latitude	Longitude	NRS Tree Species Code	Tree ID	Bank V. Erosion (cm)	Bank Hzn. Erosion (cm)	Channel Width (m)	Date To Structure (y)	*Erosion Rate (cm/y)*	Stg Ht
NB01S1	Alluvium channel bottom - Northern bank - Bullion Property	31.67830	-97.50416	FRTE	Texas Ash - *Fraxinus texensis*	366	236	56.4	32	7.38	3.7
NB01S2	Alluvium channel bottom - Northern bank - Bullion Property	31.67830	-97.50409	FRTE	Texas Ash - *Fraxinus texensis*	365	353	56.4	1	353.00	1.7
NB02S1	Threshold channel - Northern bank - Upstream Cell 1	31.67888	-97.50111	ULAM	American Elm - *Ulmus americana*	168	134	64.6	12	11.17	1.3
NB02S2	Threshold channel - Northern bank - Upstream Cell 1	31.67891	-97.50107	ULAM	American Elm - *Ulmus americana*	133	110	64.6	9	12.22	0.8
NB03S1	Threshold channel - Southern bank - Central Cell 1	31.67726	-97.49995	ULAM	American Elm - *Ulmus americana*	81	182	59.4	12	15.17	0.0
NB04S1	Threshold channel - Southern bank - Central Cell 1 - Special Case Channel Sample	31.67764	-97.50008	FRTE	Green Ash - *Fraxinus pennsylvanica*	1	1	62.0	28	0.04	2.0
NB05S1	Threshold channel - Southern bank - Downstream Cell 1	31.67703	-97.49942	ULAM	American Elm - *Ulmus americana*	200	304	46.9	3	101.33	1.0
NB06S1	Threshold channel - Southern bank - Downstream Cell 1	31.67304	-97.49583	FRTE	Texas Ash - *Fraxinus texensis*	100	325	42.7	*1*	325.00	1.5

NB07S1	Threshold channel - Northern bank - Upstream Cell 2	31.67304	-97.49574	FRTE	Texas Ash - *Fraxinus texensis*	147	204	45.6	21	9.71	2.9
NB08S1	Threshold channel - Southern bank - Central Cell 2	31.67272	-97.49303	ACNE2	Boxelder - *Acer negundo*	289	579	50.1	21	27.57	1.1
NB09S1	Transitional channel bottom - Southern bank - Downstream Cell 2	31.67266	-97.49045	FRTE	Texas Ash - *Fraxinus texensis*	109	127	50.9	1	127.00	1.5
NB09S2	Transitional channel bottom - Southern bank - Downstream Cell 2	31.67266	-97.49045	FRTE	Texas Ash - *Fraxinus texensis*	150	209	50.9	4	52.25	2.9
NB10S1	Alluvium channel bottom - Southern bank - Upstream Cell 3	31.67298	-97.49014	FRTE	Texas Ash - *Fraxinus texensis*	290	120	41.8	*1*	120.00	1.3
NB10S2	Alluvium channel bottom - Southern bank - Upstream Cell 3	31.67299	-97.49012	FRTE	Texas Ash - *Fraxinus texensis*	127	210	45.9	10	21.00	1.3
NB11S1	Alluvium channel bottom - Southern bank - Upstream Cell 3	31.67002	-97.48725	CAIL2	Pecan - *Carya illinoinensis*	128	304	50.3	30	10.13	1.4
NB12S1	Alluvium channel bottom - Southern bank - Upstream Cell 3	31.67007	-97.48713	PODE3	Eastern Cottonwood - *Populus deltoides*	138	300	72.2	1	300.00	3.3
NB13S1	Alluvium channel bottom - Southern bank - Upstream Cell 3	31.67014	-97.48697	CEOC	Hackberry - *Celtis occidentalis*	326	60	71.5	*1*	60.00	2.8
NB13S2	Alluvium channel bottom - Southern bank - Upstream Cell 3	31.67018	-97.48697	CEOC	Hackberry - *Celtis occidentalis*	278	90	71.5	*1*	90.00	1.0

NB14S1	Alluvium channel bottom - Southern bank - Downstream Cell 3 - Special Case Point Bar Sample	31.67240	-97.48208	FRTE	Texas Ash - *Fraxinus texensis*	98	325	39.9	6	54.17	0.9
NB14S2	Alluvium channel bottom - Southern bank - Downstream Cell 3 - "…"	31.67240	-97.48208	FRTE	Texas Ash - *Fraxinus texensis*	90	325	39.9	6	54.17	3.7

APPENDIX C 1.

Rapid Geomorphic Assessment River Crossing Locations, River Names, and Underlying Geological Formation.

#	Address	Latitude	Longitude	River Name	Geologic Unit (USGS)
1	FM 219, Stephenville, TX 76401	32°19'34.3"N	98°18'13.5" W	North Fork North Bosque River	Paluxy Formation
2	29511 FM 219, Stephenville, TX 76401	32°16'54.7"N	98°20'24.7" W	South Fork North Bosque River	Paluxy Formation
3	TX-108, Stephenville, TX 76401	32°18'12.4"N	98°15'32.4" W	North Fork North Bosque River	Glen Rose Formation
4	FM 8, Stephenville, TX 76401	32°14'45.4"N	98°21'04.5" W	Goose Branch	Glen Rose Formation
5	Co Rd 563, Stephenville, TX 76401	32°15'25.6"N	98°17'28.7" W	South Fork North Bosque River	Glen Rose Formation
6	TX-108, Stephenville, TX 76401	32°15'45.2"N	98°13'47.9" W	North Fork North Bosque River	Glen Rose Formation
7	7288 Co Rd 373, Dublin, TX 76446	32°10'33.2"N	98°20'50.6" W	Green Creek	Alluvium/Paluxy Formation
8	Co Rd 387, Stephenville, TX 76401	32°12'41.6"N	98°17'24.2" W	South Fork North Bosque River	Alluvium/Paluxy Formation
9	219-253 FM 8, Stephenville, TX 76401	32°14'06.0"N	98°12'14.9" W	North Bosque River	Alluvium/Glen Rose Formation
10	328 Lower Granbury Rd, Stephenville, TX 76401	32°13'40.5"N	98°09'38.9" W	Pole Hollow Branch	Paluxy Formation
11	Co Rd 256, Stephenville, TX 76401	32°11'51.0"N	98°12'59.6" W	North Bosque River	Glen Rose Formation
12	Co Rd 454, Stephenville, TX 76401	32°11'35.4"N	98°11'02.7" W	North Bosque River	Alluvium/Glen Rose Formation
13	US-377, Dublin, TX 76446	32°08'43.1"N	98°17'54.3" W	Green Creek	Alluvium/Glen Rose Formation
14	Co Rd 258, Dublin, TX 76446	32°09'41.1"N	98°15'00.4" W	Alarm Creek	Alluvium/Paluxy Formation
15	US-67, Stephenville, TX 76401	32°10'47.3"N	98°05'20.6" W	Duffau Creek	Walnut Formation

16	Unnamed Road, Glen Rose, TX 76043	32°09'09.6"N	97°53'03.4" W	Rough Creek	Walnut Formation
17	Co Rd 277, Dublin, TX 76446	32°06'19.1"N	98°14'35.8" W	Duffa Creek	Glen Rose Formation
18	14899 FM914, Stephenville, TX 76401	32°07'02.8"N	98°11'42.4" W	Live Oak Creek	Glen Rose Formation
19	Unnamed Road, Hico, TX 76457	32°07'35.3"N	98°09'33.9" W	North Bosque River	Alluvium/Glen Rose Formation
20	3773 FM913, Stephenville, TX 76401	32°08'39.5"N	98°06'27.9" W	Sims Creek	Alluvium/Paluxy Formation
21	Rj Ranch, 45109 FM 2481, Hico, TX 76457	32°06'53.2"N	98°01'23.0" W	Duffa Creek	Alluvium/Paluxy Formation
22	TX-220, Iredell, TX 76649	32°05'25.8"N	97°58'18.5" W	Camp Branch	Walnut Formation
23	Unnamed Road, Glen Rose, TX 76043	32°07'18.6"N	97°54'01.0" W	East Bosque River	Walnut Formation
24	County Rd 2660, Glen Rose, TX 76043	32°05'54.4"N	97°47'54.8" W	Mustang Creek	Comanche Peak Limestone/Walnut Formation
25	Co Rd 246, Hico, TX 76457	32°06'02.4"N	98°09'19.3" W	North Bosque River	Alluvium/Glen Rose Formation
26	US-281, Hico, TX 76457	32°05'28.2"N	98°06'17.4" W	Round Hole Branch	Paluxy Formation
27	Co Rd 229, Hico, TX 76457	32°05'21.4"N	98°03'23.1" W	Little Duffau Creek	Alluvium/Paluxy Formation
28	Blackwell Ln, Iredell, TX 76649	32°04'00.6"N	97°52'06.0" W	Flag Branch	Walnut Formation
29	Unnamed Road, Walnut Springs, TX 76690	32°04'18.7"N	97°49'08.9" W	Rough Creek	Paluxy Formation
30	Co Rd 307, Dublin, TX 76446	32°03'15.7"N	98°17'14.6" W	North Fork Little Green Creek	Alluvium/Paluxy Formation
31	FM914, Dublin, TX 76446	32°03'14.6"N	98°12'26.4" W	Green Creek	Alluvium/Glen Rose Formation
32	Co Rd 248, Dublin, TX 76446	32°02'25.6"N	98°06'41.9" W	North Bosque River	Alluvium/Glen Rose Formation

33	Co Rd 244, Hico, TX 76457	32°02'32.3"N	98°03'21.0" W	Little Duffau Creek	Paluxy Formation
34	TX-220, Hico, TX 76457	32°02'46.3"N	98°00'11.8" W	Duffau Creek	Alluvium/Glen Rose Formation
35	Co Rd 2435, Iredell, TX 76649	32°02'18.5"N	97°56'07.0" W	Rocky Creek	Paluxy Formation
36	28362 FM914, Dublin, TX 76446	32°01'46.4"N	98°12'21.8" W	Little Green Creek	Paluxy Formation
37	535 Co Rd 269, Dublin, TX 76446	32°02'12.3"N	98°07'34.4" W	Green Creek	Alluvium/Glen Rose Formation
38	Co Rd 270, Hico, TX 76457	32°00'04.3"N	98°04'53.2" W	North Bosque River	Alluvium/Glen Rose Formation
39	Co Rd 2435, Hico, TX 76457	32°01'02.0"N	97°58'08.4" W	Duffau Creek	Glen Rose Formation
40	Unnamed Road, Hico, TX 76457	32°00'34.0"N	97°55'30.5" W	Duffau Creek	Glen Rose Formation
41	FM 927, Walnut Springs, TX 76690	32°01'06.6"N	97°46'57.5" W	East Bosque River	Alluvium/Walnut Formation
42	FM 927, Iredell, TX 76649	31°59'57.2"N	97°49'53.8" W	Hester Branch	Alluvium/Glen Rose Formation
43	Co Rd 293, Dublin, TX 76446	31°58'43.9"N	98°08'49.0" W	Gilmore Creek	Alluvium/Glen Rose Formation
44	County Rd 133, Hico, TX 76457	31°58'13.0"N	98°05'38.3" W	Little Gilmore Creek	Alluvium/Glen Rose Formation
45	Walnut St, Hico, TX 76457	31°58'38.0"N	98°02'06.8" W	North Bosque River	Alluvium/Glen Rose Formation
46	Hwy 6, Iredell, TX 76649	31°58'39.6"N	97°53'42.9" W	North Bosque River	Alluvium/Glen Rose Formation
47	FM 927, Iredell, TX 76649	31°59'12.3"N	97°52'22.1" W	North Bosque River	Alluvium/Glen Rose Formation
48	County Rd 2370, Meridian, TX 76665	31°59'25.0"N	97°45'28.4" W	North Bosque River	Alluvium/Paluxy Formation
49	Co Rd 122, Hico, TX 76457	31°55'17.1"N	98°07'30.7" W	Honey Creek	Alluvium/Paluxy Formation

50	Co Rd 121, Hico, TX 76457	31°55'22.4"N	98°04'45.6" W	Honey Creek	Alluvium/Glen Rose Formation
51	1956 Co Rd 237, Hico, TX 76457	31°56'45.4"N	97°59'20.1" W	North Bosque River	Alluvium/Glen Rose Formation
52	Co Rd 2215, Iredell, TX 76649	31°57'19.3"N	97°56'04.6" W	North Bosque River	Alluvium/Glen Rose Formation
53	14046 Hwy 6, Iredell, TX 76649	31°58'44.7"N	97°50'43.6" W	North Bosque River	Glen Rose Formation
54	Hwy 6, Meridian, TX 76665	31°57'20.4"N	97°46'33.5" W	North Bosque River	Walnut Formation
55	County Rd 2540, Meridian, TX 76665	31°57'42.1"N	97°40'37.0" W	North Bosque River	Walnut Formation
56	Hwy 6, Meridian, TX 76665	31°56'31.4"N	97°42'49.2" W	North Bosque River	Walnut Formation
57	406-414 TX-22, Meridian, TX 76665	31°55'08.2"N	97°39'44.9" W	North Bosque River	Alluvium/Walnut Formation
58	TX-22, Meridian, TX 76665	31°55'27.7"N	97°37'13.2" W	North Bosque River	Comanche Peak Limestone/Walnut Formation
59	Co Rd 207, Hico, TX 76457	31°52'46.0"N	98°01'29.7" W	Long Branch	Walnut Formation
60	Co Rd 233, Hico, TX 76457	31°53'36.3"N	97°56'37.1" W	Fall Creek	Walnut Formation
61	Co Rd 2130, Iredell, TX 76649	31°53'50.1"N	97°50'29.9" W	Spring Creek	Alluvium/Walnut Formation
62	Farm Rd 1473, Meridian, TX 76665	31°52'43.6"N	97°45'52.7" W	Spring Creek	Alluvium/Walnut Formation
63	Hwy 6, Clifton, TX 76634	31°52'49.1"N	97°38'37.3" W	Dyes Branch	Walnut Formation
64	Farm Rd 1991, Clifton, TX 76634	31°51'55.4"N	97°36'10.6" W	North Bosque River	Alluvium/Walnut Formation
65	FM 219, Hico, TX 76457	31°50'23.9"N	97°57'04.2" W	Meridian Creek	Walnut Formation
66	FM1238, Iredell, TX 76649	31°52'44.8"N	97°53'27.0" W	Spring Creek	Comanche Peak Limestone

67	TX-22, Meridian, TX 76665	31°50'47.3"N	97°44'23.8" W	Spring Creek	Alluvium/Walnut Formation
68	County Rd 4170, Clifton, TX 76634	31°51'13.8"N	97°40'55.5" W	Bee Creek	Walnut Formation
69	Hwy 6, Clifton, TX 76634	31°51'07.9"N	97°37'30.7" W	Schumacher Creek	Walnut Formation
70	Co Rd 227, Hico, TX 76457	31°48'40.8"N	97°55'49.6" W	Meridian Creek	Alluvium/Walnut Formation
71	Co Rd 229, Hico, TX 76457	31°48'55.7"N	97°51'33.3" W	North Prong Meridian Creek	Alluvium/Walnut Formation
72	Co Rd 225, Hico, TX 76457	31°46'56.2"N	97°52'44.3" W	South Prong Meridian Creek	Comanche Peak Limestone
73	TX-22, Cranfills Gap, TX 76637	31°47'38.1"N	97°48'39.4" W	Meridian Creek	Alluvium/Walnut Formation
74	451 County Rd 4180, Cranfills Gap, TX 76637	31°48'09.1"N	97°43'43.2" W	Meridian Creek	Alluvium/Walnut Formation
75	Hwy 6, Clifton, TX 76634	31°48'42.3"N	97°36'42.1" W	Meridian Creek	Alluvium/Walnut Formation
76	Farm Rd 1991, Clifton, TX 76634	31°47'35.4"N	97°34'20.4" W	North Bosque River	Alluvium/Walnut Formation
77	Farm Rd 708, Clifton, TX 76634	31°47'18.2"N	97°32'10.3" W	North Bosque River	Comanche Peak Limestone
78	Co Rd 313, Cranfills Gap, TX 76637	31°44'12.6"N	97°48'57.3" W	North Fork Neils Creek	Alluvium/Walnut Formation
79	928 Co Rd 4185, Cranfills Gap, TX 76637	31°45'19.5"N	97°46'04.1" W	Boggy Branch	Comanche Peak Limestone
80	County Rd 4195, Clifton, TX 76634	31°45'17.9"N	97°40'51.4" W	Gary Creek	Walnut Formation
81	279 County Rd 4150, Clifton, TX 76634	31°45'50.1"N	97°37'53.1" W	Turkey Creek	Walnut Formation
82	Co Rd 312, Jonesboro, TX 76538	31°41'41.8"N	97°49'23.2" W	South Fork Neils Creek	Walnut Formation
83	8321 FM 219, Gatesville, TX 76528	31°43'42.7"N	97°43'17.6" W	Neils Creek	Walnut Formation

84	FM 182, Valley Mills, TX 76689	31°42'11.5"N	97°39'56.9" W	Neils Creek	Alluvium/Walnut Formation
85	County Rd 4250, Clifton, TX 76634	31°42'45.9"N	97°37'58.0" W	Neils Creek	Alluvium/Walnut Formation
86	County Rd 4245, Clifton, TX 76634	31°43'29.0"N	97°34'43.6" W	Neils Creek	Walnut Formation
87	1972 Co Rd 4100, Iredell, TX 76649	31°49'54.0"N	97°48'00.8" W	Camfield Branch	Walnut Formation
88	County Rd 3137, Valley Mills, TX 76689	31°40'47.5"N	97°34'11.6" W	Shoal Creek	Comanche Peak Limestone
89	Hwy 6, Valley Mills, TX 76689	31°41'36.6"N	97°32'07.1" W	Neils Creek	Alluvium/Walnut Formation
90	217 River Rd, Valley Mills, TX 76689	31°40'43.8"N	97°30'26.0" W	North Bosque River	Alluvium/Walnut Formation
91	FM 56, Valley Mills, TX 76689	31°40'11.7"N	97°28'10.3" W	North Bosque River	Alluvium/Walnut Formation
92	20470 China Spring Rd, Valley Mills, TX 76689	31°40'54.7"N	97°23'43.3" W	North Bosque River	Denton Clay, Fort Worth Limestone, Duck Creek Limestone
93	263 County Rd 3194, Valley Mills, TX 76689	31°38'59.2"N	97°29'19.7" W	North Bosque River	Walnut Formation
94	15287-14863 Hwy 6, Valley Mills, TX 76689	31°37'43.8"N	97°24'53.3" W	Bass Lake	Pawpaw Formation Weno Limestone
95	200-298 Shiloh Trail, China Spring, TX 76633	31°39'06.3"N	97°20'13.9" W	North Bosque River	Main Street Limestone
96	100-528 Canyon Oaks Rd, Crawford, TX 76638	31°35'48.3"N	97°20'32.1" W	Davis Branch	Pawpaw Formation Weno Limestone
97	3801-3849 Baylor Camp Rd, China Spring, TX 76633	31°36'59.8"N	97°18'26.9" W	North Bosque River	Alluvium/Denton Clay, Fort Worth Limestone, Duck Creek Limestone
98	Yankie Rd, Waco, TX	31°36'38.2"N	97°16'03.4" W	North Bosque River	Fluviatile Terrace Deposits/Main Street Limestone
99	276-610 Dosher Ln, Woodway, TX 76712	31°34'38.9"N	97°17'30.6" W	Tennant Branch	Main Street Limestone
100	6285 N State Hwy 6, Waco, TX 76712	31°33'51.4"N	97°16'57.5" W	Tennant Branch	Grayson Marl

APPENDIX C-2.

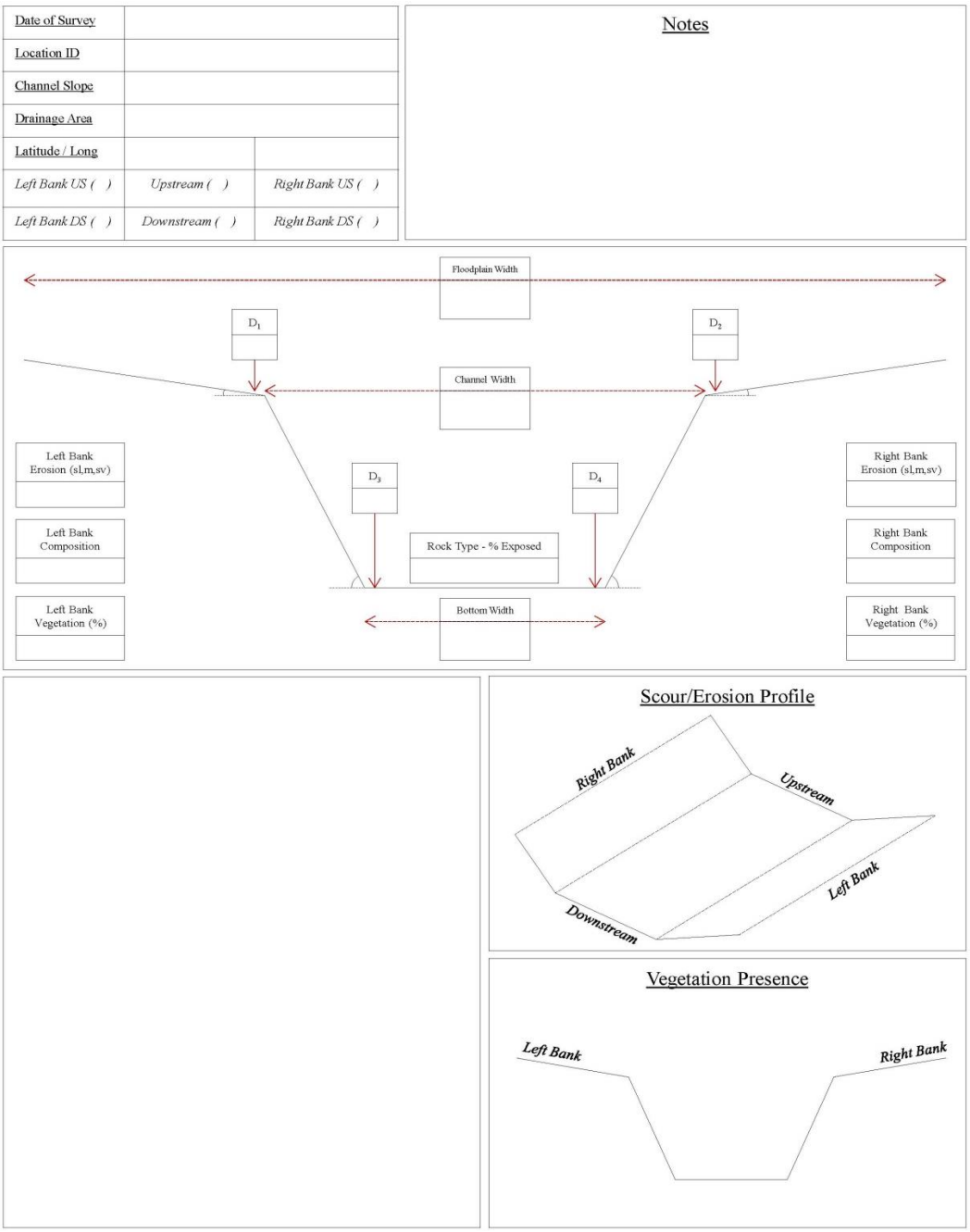

Figure C.1. Metrics and parameters recorded at each river crossing. Survey date, crossing location, slope, drainage area, and latitude/longitude are recorded prior to the visit. Up to six pictures are taken at different angles for post-referencing and metric verification. Notes of the survey including features of interest are recorded. Bank composition, erosion severity, and vegetation presence are recoded for both banks. Depth profiles are recorded using a laser rangefinder - note that most surveys were completed from bridges; Bridge height must be subtracted from depth profiles in order to properly note channel geometry. Estimates of bottom sediments are made and recorded.

APPENDIX D-1

Wolman Pebble Count Raw Data.

Kayak Drop Off (Location 1)	
31.677845, -97.503375	
Gravel Size (mm)	Count
>128	1
128	0
90	2
64	7
45	25
32	23
22.6	22
16	22
11	8
8	5
5.6	7
4	1
2.8	0
2	0
TOTAL	123

	Percent	mm
d_{16}	16.01563	10.86
d_{50}	50.01293	21.72
d_{84}	84.00545	40.54

Location 2	
31.675439, -97.498055	
Gravel Size (mm)	Count
>128	0
128	1
90	3
64	11
45	19
32	28
22.6	24
16	13
11	8
8	6
5.6	7
4	2
2.8	1
2	4
TOTAL	127

	Percent	mm
d_{16}	16.00542	8.159
d_{50}	50.01533	22.27
d_{84}	84.01374	41.83

APPENDIX D-2.

Wolman Pebble Count Data Continued.

Location 3	
31.672719, -97.492927	
Gravel Size (mm)	Count
>128	0
128	1
90	5
64	24
45	21
32	27
22.6	12
16	11
11	8
8	2
5.6	0
4	0
2.8	0
2	0
TOTAL	111

	Percent	mm
d_{16}	16.0389	14.94
d_{50}	50.0026	30.775
d_{84}	84.01092	55.45

Location 4	
31.670044, -97.488957	
Gravel Size (mm)	Count
>128	0
128	0
90	0
64	7
45	11
32	21
22.6	27
16	17
11	10
8	14
5.6	3
4	1
2.8	0
2	0
TOTAL	111

	Percent	mm
d_{16}	16.01432	7.98
d_{50}	50.09626	19
d_{84}	84.00238	32.31

APPENDIX D-3.

Wolman Pebble Count Data Continued.

Location 5	
31.671350, -97.485607	
Gravel Size (mm)	Count
>128	0
128	0
90	2
64	12
45	29
32	20
22.6	19
16	14
11	5
8	6
5.6	1
4	0
2.8	0
2	0
TOTAL	108

	Percent	mm
d_{16}	16.00397	13.518
d_{50}	50.03794	27.28
d_{84}	84.0011	44.02

Neils Creek	
31.693844, -97.537376	
Gravel Size (mm)	Count
>128	0
128	8
90	12
64	15
45	24
32	9
22.6	9
16	8
11	7
8	4
5.6	2
4	1
2.8	2
2	1
TOTAL	102

	Percent	mm
d_{16}	16.00997	11.05
d_{50}	50.00521	37.12
d_{84}	84.00085	72.52

APPENDIX E.

Capacity/Supply Ratio Tool Statistics for the North Bosque River.

Supply Reach Summary	
Discharge (cfs)	Supply Effectiveness
566.00	.00
1698.00	.00
2830.00	.04
3962.00	.09
5094.00	.22
6226.00	.10
7358.00	.50
8490.00	.76
9622.00	1.26
10754.00	1.28
11886.00	.39
13018.00	.46
14150.00	2.69
15282.00	4.92

Width (ft)	Slope	CSR	
3	.00109	1.000	
Depth (ft)	tau*	Bed n	Design Effectiveness
8.62	.01	.036	.00
13.83	.00	.039	.00
.00	.01	.000	.00
17.06	.16	.028	1.90
18.43	.17	.028	1.98
19.40	.18	.028	.53
20.15	.19	.028	.80
20.79	.20	.028	.87
21.33	.20	.028	1.18
21.82	.21	.028	1.00
22.26	.21	.028	.27
22.66	.21	.028	.28
23.03	.22	.028	1.46
23.39	.22	.028	2.44

Width (ft)	Slope	CSR	
10	.00077	1.001	
Depth (ft)	tau*	Bed n	Design Effectiveness
6.88	.02	.030	.05
11.67	.01	.031	.00
14.93	.01	.032	.00
16.32	.11	.028	1.41
17.95	.12	.028	1.70
19.11	.13	.028	.50
19.97	.13	.028	.79
20.69	.14	.028	.89
21.32	.14	.028	1.24
21.85	.15	.028	1.08
22.34	.15	.028	.29
22.79	.15	.028	.31
23.19	.16	.028	1.66
23.58	.16	.028	2.80

Width (ft)	Slope	CSR	
16	.00071	.998	
Depth (ft)	tau*	Bed n	Design Effectiveness
5.85	.02	.029	.12
10.13	.03	.029	.00
12.97	.02	.029	.00
15.25	.02	.030	.00
16.77	.10	.028	1.53
18.18	.11	.028	.50
19.20	.12	.028	.83
20.04	.12	.028	.98
20.71	.13	.028	1.40
21.32	.13	.028	1.25
21.85	.13	.028	.34
22.33	.14	.028	.37
22.78	.14	.028	1.98
23.19	.14	.028	3.38

Width (ft)	Slope	CSR	
23	.00070	.999	
Depth (ft)	tau*	Bed n	Design Effectiveness
5.13	.03	.029	.17
9.06	.04	.029	.01
11.69	.04	.029	.01
13.81	.04	.029	.00
15.63	.04	.029	.00
17.03	.10	.028	.48
18.24	.11	.028	.86
19.17	.12	.028	1.06
19.94	.12	.028	1.55
20.61	.12	.028	1.41
21.21	.13	.028	.39
21.74	.13	.028	.43
22.20	.13	.028	2.33
22.63	.14	.028	4.01

Width (ft)	Slope	CSR	
29	.00068	1.001	
Depth (ft)	tau*	Bed n	Design Effectiveness
4.56	.02	.029	.20
8.25	.04	.029	.01
10.75	.04	.029	.02
12.75	.04	.028	.02
14.44	.05	.028	.02
15.97	.05	.028	.00
17.22	.10	.028	.78
18.31	.11	.028	1.02
19.17	.11	.028	1.54
19.91	.12	.028	1.44
20.55	.12	.028	.41
21.13	.12	.028	.46
21.64	.13	.028	2.50
22.09	.13	.028	4.32

Width (ft)	Slope	CSR	
36	.00067	.999	
Depth (ft)	tau*	Bed n	Design Effectiveness
4.19	.02	.029	.22
7.56	.04	.029	.01
9.94	.04	.029	.03
11.88	.05	.028	.04
13.50	.05	.028	.05
14.94	.05	.028	.02
16.26	.09	.028	.69
17.41	.10	.028	.92
18.37	.11	.028	1.46
19.17	.11	.028	1.40
19.88	.11	.028	.41
20.49	.12	.028	.46
21.03	.12	.028	2.54
21.54	.12	.028	4.47

Width (ft)	Slope	CSR	
42	.00067	1.000	
Depth (ft)	tau*	Bed n	Design Effectiveness
3.81	.02	.029	.24
7.00	.03	.029	.01
9.25	.04	.029	.04
11.06	.05	.028	.06
12.63	.05	.028	.09
14.00	.06	.028	.03
15.25	.06	.028	.06
16.38	.10	.028	.87
17.44	.10	.028	1.43
18.31	.11	.028	1.41
19.08	.11	.028	.42
19.75	.11	.028	.48
20.36	.12	.028	2.74
20.87	.12	.028	4.84

Width (ft)	Slope	CSR	
49	.00068	1.001	
Depth (ft)	tau*	Bed n	Design Effectiveness
3.50	.02	.029	.26
6.50	.03	.029	.02
8.63	.04	.029	.04
10.31	.05	.028	.07
11.81	.05	.028	.13
13.13	.06	.028	.05
14.38	.06	.028	.10
15.47	.06	.028	.13
16.51	.10	.028	1.41
17.41	.10	.028	1.42
18.24	.11	.028	.43
18.95	.11	.028	.51
19.59	.12	.028	2.92
20.17	.12	.028	5.25

Width (ft)	Slope	CSR	
55	.00071	1.002	
Depth (ft)	tau*	Bed n	Design Effectiveness
3.25	.02	.030	.28
6.06	.03	.029	.02
8.00	.04	.029	.04
9.66	.05	.028	.08
11.06	.06	.028	.16
12.31	.06	.028	.06
13.50	.06	.028	.14
14.56	.07	.028	.19
15.56	.07	.028	.31
16.51	.10	.028	1.48
17.35	.11	.028	.46
18.11	.11	.028	.55
18.79	.12	.028	3.19
19.40	.12	.028	5.80

Width (ft)	Slope	CSR	
62	.00073	1.000	
Depth (ft)	tau*	Bed n	Design Effectiveness
3.07	.02	.030	.31
5.69	.03	.029	.02
7.50	.04	.029	.04
9.06	.05	.028	.10
10.44	.06	.028	.20
11.63	.06	.028	.08
12.75	.07	.028	.18
13.75	.07	.028	.25
14.69	.07	.028	.41
15.63	.08	.028	.43
16.45	.10	.028	.47
17.22	.11	.028	.57
17.95	.11	.028	3.40
18.60	.12	.028	6.27

Width (ft)	Slope	CSR	
69	.00075	.998	
Depth (ft)	tau*	Bed n	Design Effectiveness
2.88	.02	.030	.32
5.35	.03	.029	.02
7.13	.04	.029	.04
8.56	.05	.028	.09
9.88	.06	.028	.20
11.03	.06	.028	.09
12.06	.06	.028	.19
13.06	.07	.028	.28
14.00	.07	.028	.49
14.88	.08	.028	.50
15.69	.08	.028	.15
16.45	.11	.028	.56
17.22	.11	.028	3.41
17.86	.12	.028	6.35

APPENDIX F-1

Statistical Analysis of Soil Sample NB01S1.

Result Analysis Report

Sample Name: SB - NB01	**SOP Name:** lame clay	**Measured:** Tuesday, November 19, 2019 2:03:30 PM	
Sample Source & type:	**Measured by:** Samuel T. Barber	**Analysed:** Tuesday, November 19, 2019 2:03:31 PM	
Sample bulk lot ref:	**Result Source:** Measurement		
Particle Name: Kaolinite high	**Accessory Name:** Hydro 2000MU (A)	**Analysis model:** General purpose	**Sensitivity:** Enhanced
Particle RI: 1.570	**Absorption:** 0.1	**Size range:** 0.020 to 2000.000 um	**Obscuration:** 16.90 %
Dispersant Name: Sodium Hexametaphosphate	**Dispersant RI:** 1.482	**Weighted Residual:** 1.239 %	**Result Emulation:** Off
Concentration: 0.0155 %Vol	**Span :** 4.308	**Uniformity:** 1.43	**Result units:** Volume
Specific Surface Area: 1.79 m^2/g	**Surface Weighted Mean D[3,2]:** 3.345 um	**Vol. Weighted Mean D[4,3]:** 50.937 um	

d(0.1): 0.963 um **d(0.5):** 30.499 um **d(0.9):** 132.361 um

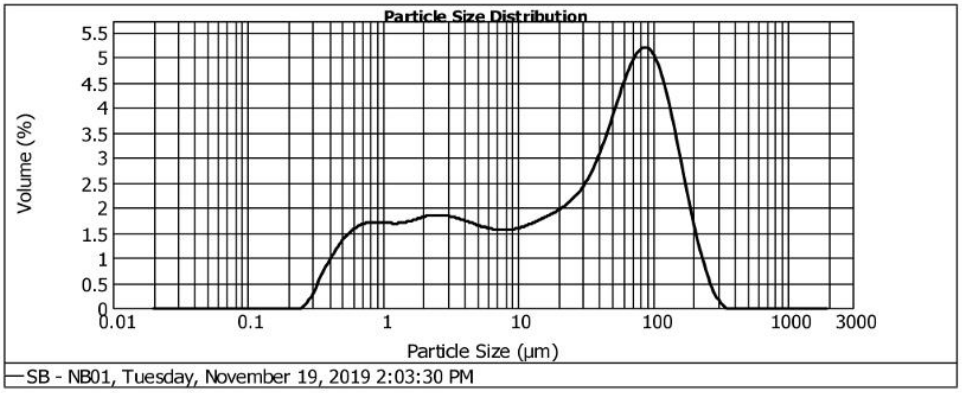

Size (µm)	Volume In %	Size (µm)	Volume In %	Size (µm)	Volume In %	Size (µm)	Volume In %	Size (µm)	Volume In %	Size (µm)	Volume In %
0.040	0.00	0.252	0.06	1.584	1.24	9.966	1.14	62.713	3.37	394.625	0.00
0.045	0.00	0.280	0.17	1.765	1.27	11.105	1.17	69.879	3.56	439.718	0.00
0.050	0.00	0.313	0.38	1.966	1.29	12.374	1.20	77.864	3.67	489.964	0.00
0.055	0.00	0.348	0.56	2.191	1.31	13.788	1.24	86.762	3.67	545.951	0.00
0.062	0.00	0.388	0.71	2.442	1.31	15.364	1.29	96.676	3.56	608.336	0.00
0.069	0.00	0.432	0.86	2.721	1.30	17.119	1.33	107.723	3.34	677.849	0.00
0.077	0.00	0.482	0.98	3.031	1.29	19.075	1.39	120.032	3.02	755.306	0.00
0.085	0.00	0.537	1.07	3.378	1.26	21.255	1.45	133.748	2.62	841.613	0.00
0.095	0.00	0.598	1.14	3.764	1.23	23.684	1.52	149.031	2.17	937.782	0.00
0.106	0.00	0.666	1.18	4.194	1.20	26.390	1.62	166.061	1.72	1044.941	0.00
0.118	0.00	0.743	1.21	4.673	1.17	29.406	1.74	185.036	1.28	1164.344	0.00
0.132	0.00	0.828	1.21	5.207	1.14	32.766	1.90	206.180	0.89	1297.392	0.00
0.147	0.00	0.922	1.20	5.802	1.12	36.510	2.10	229.740	0.59	1445.642	0.00
0.163	0.00	1.027	1.20	6.465	1.10	40.682	2.33	255.992	0.30	1610.833	0.00
0.182	0.00	1.145	1.19	7.204	1.10	45.330	2.59	285.243	0.14	1794.900	0.00
0.203	0.00	1.276	1.20	8.027	1.10	50.510	2.86	317.837	0.02	2000.000	
0.226	0.00	1.421	1.21	8.944	1.11	56.282	3.13	354.156	0.00		
0.252		1.584		9.966		62.713		394.625			

APPENDIX F-2

Statistical Analysis of Soil Sample NB02S1.

Result Analysis Report

Sample Name: SB - NB02	**SOP Name:** lame clay	**Measured:** Tuesday, November 19, 2019 2:11:09 PM
Sample Source & type:	**Measured by:** Samuel T. Barber	**Analysed:** Tuesday, November 19, 2019 2:11:10 PM
Sample bulk lot ref:	**Result Source:** Measurement	

Particle Name: Kaolinite high	**Accessory Name:** Hydro 2000MU (A)	**Analysis model:** General purpose	**Sensitivity:** Enhanced
Particle RI: 1.570	**Absorption:** 0.1	**Size range:** 0.020 to 2000.000 um	**Obscuration:** 15.76 %
Dispersant Name: Sodium Hexametaphosphate	**Dispersant RI:** 1.482	**Weighted Residual:** 0.824 %	**Result Emulation:** Off

Concentration: 0.0233 %Vol	**Span :** 2.203	**Uniformity:** 0.682	**Result units:** Volume
Specific Surface Area: 1.15 m²/g	**Surface Weighted Mean D[3,2]:** 5.221 um	**Vol. Weighted Mean D[4,3]:** 95.019 um	

d(0.1): 1.581 um **d(0.5):** 89.091 um **d(0.9):** 197.863 um

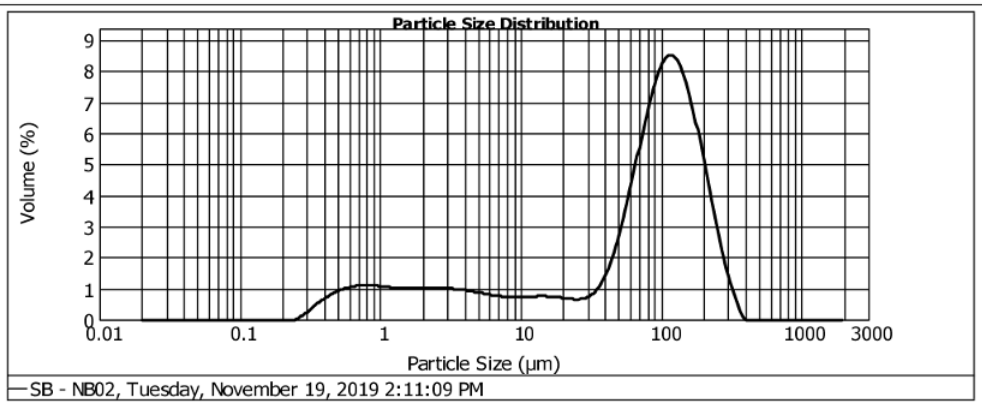

Size (µm)	Volume In %	Size (µm)	Volume In %	Size (µm)	Volume In %	Size (µm)	Volume In %	Size (µm)	Volume In %	Size (µm)	Volume In %
0.040	0.00	0.252	0.05	1.584	0.71	9.966	0.52	62.713	3.55	394.625	0.00
0.045	0.00	0.280	0.14	1.765	0.72	11.105	0.52	69.879	4.26	439.718	0.00
0.050	0.00	0.313	0.27	1.966	0.72	12.374	0.53	77.864	4.91	489.964	0.00
0.055	0.00	0.348	0.39	2.191	0.73	13.788	0.53	86.762	5.46	545.951	0.00
0.062	0.00	0.388	0.48	2.442	0.72	15.364	0.53	96.676	5.85	608.336	0.00
0.069	0.00	0.432	0.58	2.721	0.72	17.119	0.51	107.723	6.03	677.849	0.00
0.077	0.00	0.482	0.65	3.031	0.70	19.075	0.49	120.032	5.98	755.306	0.00
0.085	0.00	0.537	0.71	3.378	0.69	21.255	0.47	133.748	5.70	841.613	0.00
0.095	0.00	0.598	0.75	3.764	0.67	23.684	0.46	149.031	5.22	937.782	0.00
0.106	0.00	0.666	0.77	4.194	0.64	26.390	0.48	166.061	4.58	1044.941	0.00
0.118	0.00	0.743	0.78	4.673	0.62	29.406	0.54	185.036	3.85	1164.344	0.00
0.132	0.00	0.828	0.78	5.207	0.59	32.766	0.67	206.180	3.06	1297.392	0.00
0.147	0.00	0.922	0.76	5.802	0.56	36.510	0.89	229.740	2.30	1445.642	0.00
0.163	0.00	1.027	0.74	6.465	0.54	40.682	1.22	255.992	1.59	1610.833	0.00
0.182	0.00	1.145	0.73	7.204	0.52	45.330	1.66	285.243	1.00	1794.900	0.00
0.203	0.00	1.276	0.72	8.027	0.52	50.510	2.22	317.837	0.56	2000.000	
0.226	0.00	1.421	0.71	8.944	0.51	56.282	2.85	354.156	0.12		
0.252		1.584		9.966		62.713		394.625			

APPENDIX F-3

Statistical Analysis of Soil Sample NB03S1.

Result Analysis Report

Sample Name: SB - NB03	**SOP Name:** lame clay	**Measured:** Tuesday, November 19, 2019 2:45:23 PM	
Sample Source & type:	**Measured by:** Samuel T. Barber	**Analysed:** Tuesday, November 19, 2019 2:45:24 PM	
Sample bulk lot ref:	**Result Source:** Measurement		
Particle Name: Kaolinite high	**Accessory Name:** Hydro 2000MU (A)	**Analysis model:** General purpose	**Sensitivity:** Enhanced
Particle RI: 1.570	**Absorption:** 0.1	**Size range:** 0.020 to 2000.000 um	**Obscuration:** 15.24 %
Dispersant Name: Sodium Hexametaphosphate	**Dispersant RI:** 1.482	**Weighted Residual:** 0.626 %	**Result Emulation:** Off
Concentration: 0.0325 %Vol	**Span :** 2.833	**Uniformity:** 0.93	**Result units:** Volume
Specific Surface Area: 0.807 m²/g	**Surface Weighted Mean D[3,2]:** 7.438 um	**Vol. Weighted Mean D[4,3]:** 192.486 um	

d(0.1): 3.307 um **d(0.5):** 138.868 um **d(0.9):** 396.682 um

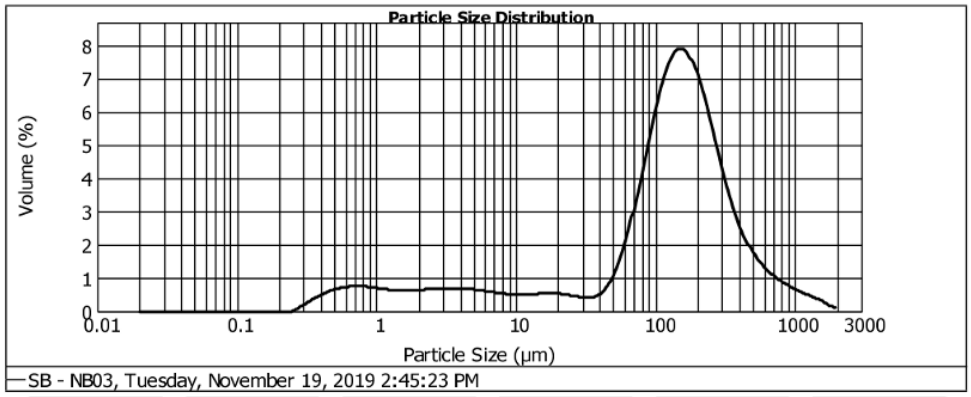

Size (µm)	Volume In %	Size (µm)	Volume In %	Size (µm)	Volume In %	Size (µm)	Volume In %	Size (µm)	Volume In %	Size (µm)	Volume In %
0.040	0.00	0.252	0.04	1.584	0.44	9.966	0.35	62.713	1.86	394.625	1.71
0.045	0.00	0.280	0.12	1.765	0.45	11.105	0.35	69.879	2.46	439.718	1.41
0.050	0.00	0.313	0.21	1.966	0.46	12.374	0.36	77.864	3.11	489.964	1.18
0.055	0.00	0.348	0.29	2.191	0.46	13.788	0.37	86.762	3.77	545.951	1.00
0.062	0.00	0.388	0.36	2.442	0.47	15.364	0.38	96.676	4.40	608.336	0.85
0.069	0.00	0.432	0.42	2.721	0.48	17.119	0.38	107.723	4.93	677.849	0.74
0.077	0.00	0.482	0.47	3.031	0.48	19.075	0.38	120.032	5.32	755.306	0.64
0.085	0.00	0.537	0.50	3.378	0.49	21.255	0.36	133.748	5.55	841.613	0.56
0.095	0.00	0.598	0.52	3.764	0.48	23.684	0.33	149.031	5.59	937.782	0.48
0.106	0.00	0.666	0.53	4.194	0.48	26.390	0.31	166.061	5.44	1044.941	0.42
0.118	0.00	0.743	0.53	4.673	0.46	29.406	0.28	185.036	5.13	1164.344	0.35
0.132	0.00	0.828	0.52	5.207	0.45	32.766	0.29	206.180	4.69	1297.392	0.29
0.147	0.00	0.922	0.50	5.802	0.43	36.510	0.33	229.740	4.16	1445.642	0.23
0.163	0.00	1.027	0.48	6.465	0.41	40.682	0.44	255.992	3.60	1610.833	0.14
0.182	0.00	1.145	0.46	7.204	0.39	45.330	0.64	285.243	3.04	1794.900	0.10
0.203	0.00	1.276	0.45	8.027	0.37	50.510	0.94	317.837	2.53	2000.000	
0.226	0.00	1.421	0.44	8.944	0.36	56.282	1.35	354.156	2.08		
0.252		1.584		9.966		62.713		394.625			

APPENDIX F-4

Statistical Analysis of Soil Sample NB05S1.

Result Analysis Report

Sample Name: SB - NB05S1	**SOP Name:** lame clay	**Measured:** Tuesday, November 19, 2019 1:54:08 PM	
Sample Source & type:	**Measured by:** Samuel T. Barber	**Analysed:** Tuesday, November 19, 2019 1:54:09 PM	
Sample bulk lot ref:	**Result Source:** Measurement		
Particle Name: Kaolinite high	**Accessory Name:** Hydro 2000MU (A)	**Analysis model:** General purpose	**Sensitivity:** Enhanced
Particle RI: 1.570	**Absorption:** 0.1	**Size range:** 0.020 to 2000.000 um	**Obscuration:** 16.36 %
Dispersant Name: Sodium Hexametaphosphate	**Dispersant RI:** 1.482	**Weighted Residual:** 1.924 %	**Result Emulation:** Off
Concentration: 0.0111 %Vol	**Span :** 18.918	**Uniformity:** 5.19	**Result units:** Volume
Specific Surface Area: 2.49 m²/g	**Surface Weighted Mean D[3,2]:** 2.412 um	**Vol. Weighted Mean D[4,3]:** 49.967 um	

d(0.1): 0.729 um **d(0.5):** 9.075 um **d(0.9):** 172.407 um

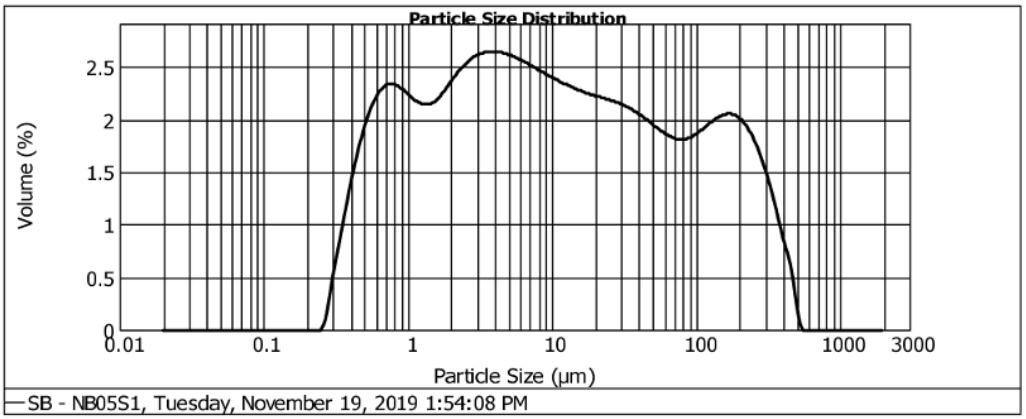

Size (µm)	Volume In %	Size (µm)	Volume In %	Size (µm)	Volume In %	Size (µm)	Volume In %	Size (µm)	Volume In %	Size (µm)	Volume In %
0.040	0.00	0.252	0.06	1.584	1.57	9.966	1.68	62.713	1.30	394.625	0.56
0.045	0.00	0.280	0.34	1.765	1.63	11.105	1.66	69.879	1.28	439.718	0.38
0.050	0.00	0.313	0.58	1.966	1.70	12.374	1.64	77.864	1.28	489.964	0.06
0.055	0.00	0.348	0.82	2.191	1.75	13.788	1.62	86.762	1.29	545.951	0.00
0.062	0.00	0.388	1.05	2.442	1.80	15.364	1.60	96.676	1.32	608.336	0.00
0.069	0.00	0.432	1.24	2.721	1.83	17.119	1.58	107.723	1.36	677.849	0.00
0.077	0.00	0.482	1.40	3.031	1.86	19.075	1.57	120.032	1.39	755.306	0.00
0.085	0.00	0.537	1.52	3.378	1.87	21.255	1.56	133.748	1.43	841.613	0.00
0.095	0.00	0.598	1.61	3.764	1.87	23.684	1.54	149.031	1.45	937.782	0.00
0.106	0.00	0.666	1.65	4.194	1.86	26.390	1.53	166.061	1.45	1044.941	0.00
0.118	0.00	0.743	1.65	4.673	1.85	29.406	1.51	185.036	1.43	1164.344	0.00
0.132	0.00	0.828	1.63	5.207	1.83	32.766	1.49	206.180	1.38	1297.392	0.00
0.147	0.00	0.922	1.59	5.802	1.81	36.510	1.46	229.740	1.31	1445.642	0.00
0.163	0.00	1.027	1.55	6.465	1.78	40.682	1.43	255.992	1.21	1610.833	0.00
0.182	0.00	1.145	1.52	7.204	1.76	45.330	1.39	285.243	1.08	1794.900	0.00
0.203	0.00	1.276	1.51	8.027	1.73	50.510	1.36	317.837	0.92	2000.000	
0.226	0.00	1.421	1.53	8.944	1.71	56.282	1.32	354.156	0.73		
0.252		1.584		9.966		62.713		394.625			

APPENDIX F-5

Statistical Analysis of Soil Sample NB06S1.

Result Analysis Report

Sample Name: SB - NB06S1	**SOP Name:** lame clay	**Measured:** Tuesday, November 19, 2019 2:39:54 PM
Sample Source & type:	**Measured by:** Samuel T. Barber	**Analysed:** Tuesday, November 19, 2019 2:39:55 PM
Sample bulk lot ref:	**Result Source:** Measurement	

Particle Name: Kaolinite high	**Accessory Name:** Hydro 2000MU (A)	**Analysis model:** General purpose	**Sensitivity:** Enhanced
Particle RI: 1.570	**Absorption:** 0.1	**Size range:** 0.020 to 2000.000 um	**Obscuration:** 16.55 %
Dispersant Name: Sodium Hexametaphosphate	**Dispersant RI:** 1.482	**Weighted Residual:** 1.550 %	**Result Emulation:** Off

Concentration: 0.0131 %Vol	**Span :** 11.914	**Uniformity:** 3.82	**Result units:** Volume
Specific Surface Area: 2.06 m²/g	**Surface Weighted Mean D[3,2]:** 2.912 um	**Vol. Weighted Mean D[4,3]:** 71.493 um	

d(0.1): 0.854 um **d(0.5):** 17.658 um **d(0.9):** 211.233 um

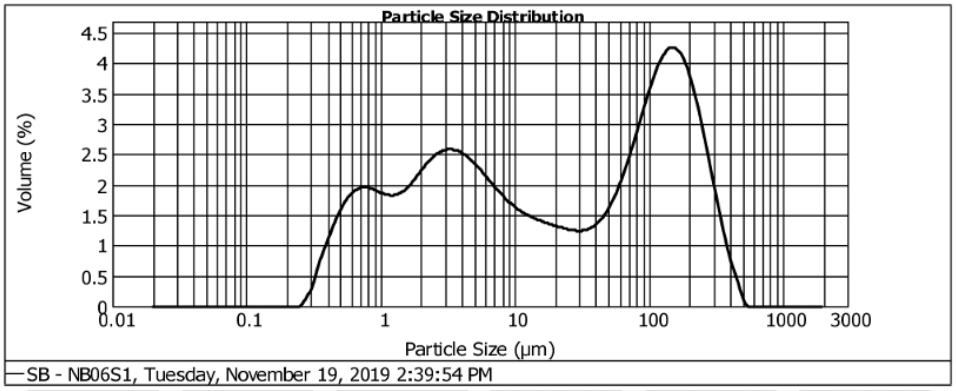

Size (µm)	Volume In %	Size (µm)	Volume In %	Size (µm)	Volume In %	Size (µm)	Volume In %	Size (µm)	Volume In %	Size (µm)	Volume In %
0.040	0.00	0.252	0.05	1.584	1.43	9.966	1.12	62.713	1.59	394.625	0.48
0.045	0.00	0.280	0.17	1.765	1.52	11.105	1.08	69.879	1.82	439.718	0.26
0.050	0.00	0.313	0.41	1.966	1.61	12.374	1.04	77.864	2.07	489.964	0.03
0.055	0.00	0.348	0.63	2.191	1.70	13.788	1.01	86.762	2.32	545.951	0.00
0.062	0.00	0.388	0.82	2.442	1.77	15.364	0.98	96.676	2.56	608.336	0.00
0.069	0.00	0.432	1.00	2.721	1.81	17.119	0.96	107.723	2.76	677.849	0.00
0.077	0.00	0.482	1.15	3.031	1.83	19.075	0.93	120.032	2.92	755.306	0.00
0.085	0.00	0.537	1.27	3.378	1.82	21.255	0.91	133.748	3.00	841.613	0.00
0.095	0.00	0.598	1.34	3.764	1.79	23.684	0.89	149.031	3.01	937.782	0.00
0.106	0.00	0.666	1.38	4.194	1.74	26.390	0.88	166.061	2.92	1044.941	0.00
0.118	0.00	0.743	1.38	4.673	1.67	29.406	0.88	185.036	2.75	1164.344	0.00
0.132	0.00	0.828	1.36	5.207	1.59	32.766	0.89	206.180	2.50	1297.392	0.00
0.147	0.00	0.922	1.33	5.802	1.50	36.510	0.93	229.740	2.18	1445.642	0.00
0.163	0.00	1.027	1.30	6.465	1.42	40.682	0.99	255.992	1.83	1610.833	0.00
0.182	0.00	1.145	1.29	7.204	1.33	45.330	1.09	285.243	1.45	1794.900	0.00
0.203	0.00	1.276	1.31	8.027	1.25	50.510	1.22	317.837	1.09	2000.000	
0.226	0.00	1.421	1.35	8.944	1.18	56.282	1.39	354.156	0.76		
0.252		1.584		9.966		62.713		394.625			

APPENDIX F-6

Statistical Analysis of Soil Sample NB08S1.

Result Analysis Report

Sample Name: SB - NB08	**SOP Name:** lame clay	**Measured:** Tuesday, November 19, 2019 3:00:10 PM	
Sample Source & type:	**Measured by:** Samuel T. Barber	**Analysed:** Tuesday, November 19, 2019 3:00:11 PM	
Sample bulk lot ref:	**Result Source:** Measurement		
Particle Name: Kaolinite high	**Accessory Name:** Hydro 2000MU (A)	**Analysis model:** General purpose	**Sensitivity:** Enhanced
Particle RI: 1.570	**Absorption:** 0.1	**Size range:** 0.020 to 2000.000 um	**Obscuration:** 19.03 %
Dispersant Name: Sodium Hexametaphosphate	**Dispersant RI:** 1.482	**Weighted Residual:** 1.220 %	**Result Emulation:** Off
Concentration: 0.0186 %Vol	**Span :** 4.401	**Uniformity:** 1.45	**Result units:** Volume
Specific Surface Area: 1.81 m²/g	**Surface Weighted Mean D[3,2]:** 3.314 um	**Vol. Weighted Mean D[4,3]:** 62.735 um	

d(0.1): 0.905 um **d(0.5):** 36.997 um **d(0.9):** 163.718 um

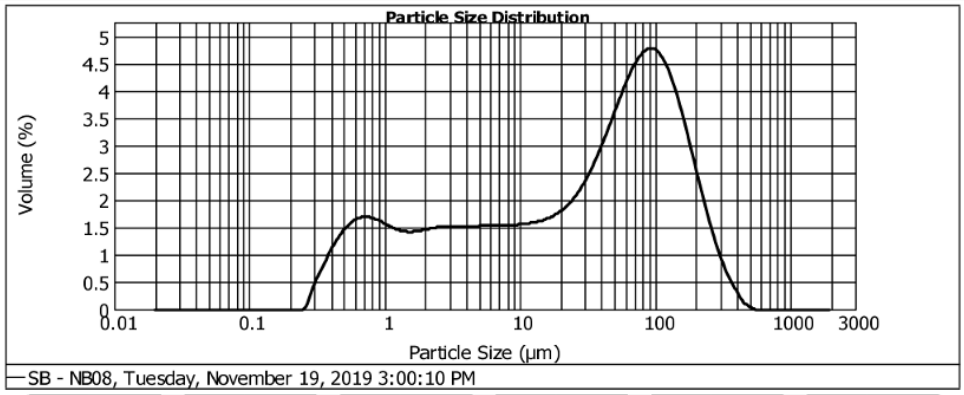

Size (µm)	Volume In %	Size (µm)	Volume In %	Size (µm)	Volume In %	Size (µm)	Volume In %	Size (µm)	Volume In %	Size (µm)	Volume In %
0.040	0.00	0.252	0.06	1.584	1.01	9.966	1.11	62.713	3.09	394.625	0.18
0.045	0.00	0.280	0.32	1.765	1.02	11.105	1.12	69.879	3.24	439.718	0.07
0.050	0.00	0.313	0.48	1.966	1.04	12.374	1.13	77.864	3.35	489.964	0.02
0.055	0.00	0.348	0.65	2.191	1.06	13.788	1.15	86.762	3.39	545.951	0.00
0.062	0.00	0.388	0.82	2.442	1.07	15.364	1.18	96.676	3.36	608.336	0.00
0.069	0.00	0.432	0.95	2.721	1.07	17.119	1.22	107.723	3.26	677.849	0.00
0.077	0.00	0.482	1.06	3.031	1.08	19.075	1.28	120.032	3.08	755.306	0.00
0.085	0.00	0.537	1.13	3.378	1.08	21.255	1.35	133.748	2.85	841.613	0.00
0.095	0.00	0.598	1.18	3.764	1.08	23.684	1.45	149.031	2.56	937.782	0.00
0.106	0.00	0.666	1.20	4.194	1.08	26.390	1.56	166.061	2.23	1044.941	0.00
0.118	0.00	0.743	1.19	4.673	1.08	29.406	1.70	185.036	1.90	1164.344	0.00
0.132	0.00	0.828	1.16	5.207	1.08	32.766	1.87	206.180	1.56	1297.392	0.00
0.147	0.00	0.922	1.12	5.802	1.08	36.510	2.05	229.740	1.25	1445.642	0.00
0.163	0.00	1.027	1.08	6.465	1.08	40.682	2.26	255.992	0.96	1610.833	0.00
0.182	0.00	1.145	1.04	7.204	1.09	45.330	2.48	285.243	0.70	1794.900	0.00
0.203	0.00	1.276	1.01	8.027	1.09	50.510	2.69	317.837	0.49	2000.000	
0.226	0.00	1.421	1.00	8.944	1.10	56.282	2.90	354.156	0.33		
0.252		1.584		9.966		62.713		394.625			

APPENDIX F-7

Statistical Analysis of Soil Sample NB09S1.

Result Analysis Report

Sample Name: SB - NB09	**SOP Name:** lame clay	**Measured:** Tuesday, November 19, 2019 2:52:12 PM
Sample Source & type:	**Measured by:** Samuel T. Barber	**Analysed:** Tuesday, November 19, 2019 2:52:13 PM
Sample bulk lot ref:	**Result Source:** Measurement	

Particle Name: Kaolinite high	**Accessory Name:** Hydro 2000MU (A)	**Analysis model:** General purpose	**Sensitivity:** Enhanced
Particle RI: 1.570	**Absorption:** 0.1	**Size range:** 0.020 to 2000.000 um	**Obscuration:** 15.46 %
Dispersant Name: Sodium Hexametaphosphate	**Dispersant RI:** 1.482	**Weighted Residual:** 1.114 %	**Result Emulation:** Off

Concentration: 0.0181 %Vol	**Span :** 2.983	**Uniformity:** 0.987	**Result units:** Volume
Specific Surface Area: 1.48 m²/g	**Surface Weighted Mean D[3,2]:** 4.058 um	**Vol. Weighted Mean D[4,3]:** 82.761 um	

d(0.1): 1.128 um **d(0.5):** 65.852 um **d(0.9):** 197.586 um

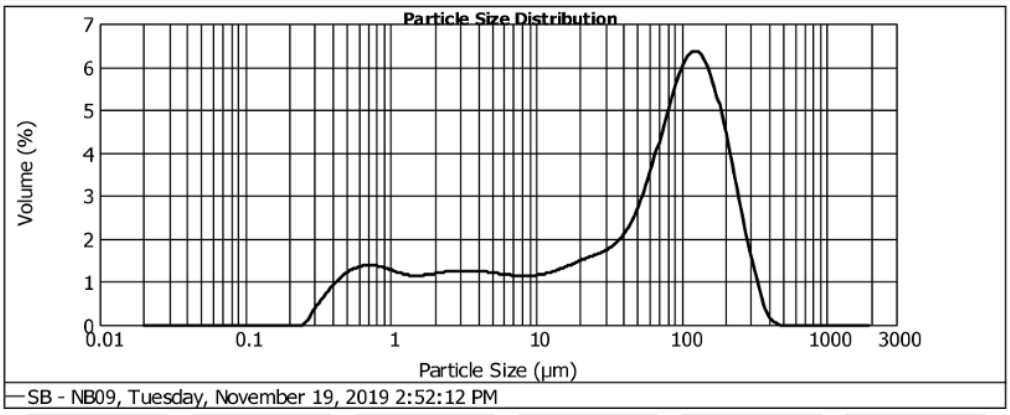

Size (µm)	Volume In %	Size (µm)	Volume In %	Size (µm)	Volume In %	Size (µm)	Volume In %	Size (µm)	Volume In %	Size (µm)	Volume In %
0.040	0.00	0.252	0.05	1.584	0.81	9.966	0.82	62.713	2.79	394.625	0.10
0.045	0.00	0.280	0.25	1.765	0.83	11.105	0.84	69.879	3.20	439.718	0.00
0.050	0.00	0.313	0.39	1.966	0.85	12.374	0.88	77.864	3.61	489.964	0.00
0.055	0.00	0.348	0.53	2.191	0.87	13.788	0.92	86.762	3.98	545.951	0.00
0.062	0.00	0.388	0.67	2.442	0.88	15.364	0.96	96.676	4.27	608.336	0.00
0.069	0.00	0.432	0.78	2.721	0.89	17.119	1.01	107.723	4.46	677.849	0.00
0.077	0.00	0.482	0.87	3.031	0.89	19.075	1.05	120.032	4.50	755.306	0.00
0.085	0.00	0.537	0.93	3.378	0.89	21.255	1.10	133.748	4.40	841.613	0.00
0.095	0.00	0.598	0.97	3.764	0.88	23.684	1.14	149.031	4.15	937.782	0.00
0.106	0.00	0.666	0.98	4.194	0.87	26.390	1.19	166.061	3.78	1044.941	0.00
0.118	0.00	0.743	0.97	4.673	0.86	29.406	1.25	185.036	3.30	1164.344	0.00
0.132	0.00	0.828	0.95	5.207	0.84	32.766	1.33	206.180	2.75	1297.392	0.00
0.147	0.00	0.922	0.91	5.802	0.83	36.510	1.44	229.740	2.18	1445.642	0.00
0.163	0.00	1.027	0.87	6.465	0.81	40.682	1.59	255.992	1.62	1610.833	0.00
0.182	0.00	1.145	0.84	7.204	0.81	45.330	1.80	285.243	1.12	1794.900	0.00
0.203	0.00	1.276	0.82	8.027	0.80	50.510	2.08	317.837	0.71	2000.000	
0.226	0.00	1.421	0.81	8.944	0.81	56.282	2.41	354.156	0.28		
0.252		1.584		9.966		62.713		394.625			

APPENDIX F-8

Statistical Analysis of Soil Sample NB10S1.

Result Analysis Report

Sample Name: SB - NB10	**SOP Name:** lame clay	**Measured:** Tuesday, November 19, 2019 2:18:30 PM	
Sample Source & type:	**Measured by:** Samuel T. Barber	**Analysed:** Tuesday, November 19, 2019 2:18:31 PM	
Sample bulk lot ref:	**Result Source:** Measurement		
Particle Name: Kaolinite high	**Accessory Name:** Hydro 2000MU (A)	**Analysis model:** General purpose	**Sensitivity:** Enhanced
Particle RI: 1.570	**Absorption:** 0.1	**Size range:** 0.020 to 2000.000 um	**Obscuration:** 16.40 %
Dispersant Name: Sodium Hexametaphosphate	**Dispersant RI:** 1.482	**Weighted Residual:** 1.834 %	**Result Emulation:** Off
Concentration: 0.0104 %Vol	**Span :** 6.764	**Uniformity:** 2.27	**Result units:** Volume
Specific Surface Area: 2.53 m²/g	**Surface Weighted Mean D[3,2]:** 2.374 um	**Vol. Weighted Mean D[4,3]:** 20.457 um	

d(0.1): 0.751 um **d(0.5):** 7.890 um **d(0.9):** 54.125 um

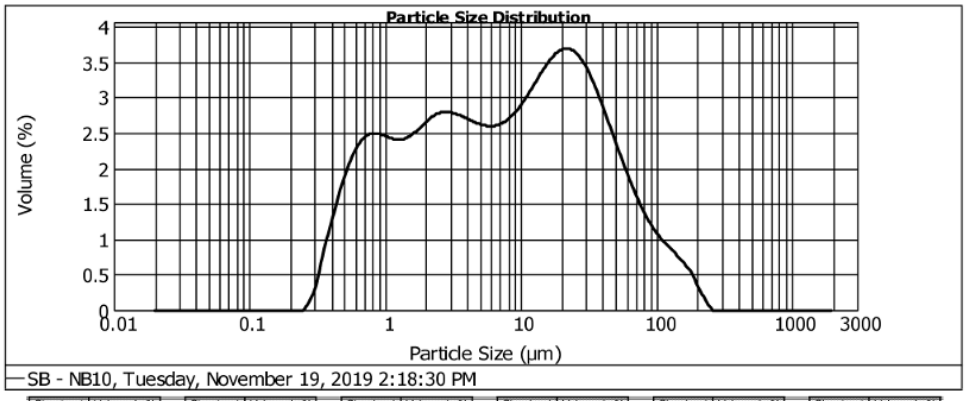

Size (µm)	Volume In %	Size (µm)	Volume In %	Size (µm)	Volume In %	Size (µm)	Volume In %	Size (µm)	Volume In %	Size (µm)	Volume In %
0.040	0.00	0.252	0.06	1.584	1.78	9.966	2.09	62.713	1.24	394.625	0.00
0.045	0.00	0.280	0.18	1.765	1.84	11.105	2.19	69.879	1.09	439.718	0.00
0.050	0.00	0.313	0.45	1.966	1.90	12.374	2.30	77.864	0.96	489.964	0.00
0.055	0.00	0.348	0.71	2.191	1.95	13.788	2.40	86.762	0.84	545.951	0.00
0.062	0.00	0.388	0.94	2.442	1.97	15.364	2.50	96.676	0.75	608.336	0.00
0.069	0.00	0.432	1.18	2.721	1.97	17.119	2.57	107.723	0.67	677.849	0.00
0.077	0.00	0.482	1.38	3.031	1.96	19.075	2.61	120.032	0.61	755.306	0.00
0.085	0.00	0.537	1.54	3.378	1.94	21.255	2.61	133.748	0.55	841.613	0.00
0.095	0.00	0.598	1.66	3.764	1.91	23.684	2.58	149.031	0.47	937.782	0.00
0.106	0.00	0.666	1.73	4.194	1.88	26.390	2.50	166.061	0.40	1044.941	0.00
0.118	0.00	0.743	1.76	4.673	1.86	29.406	2.39	185.036	0.28	1164.344	0.00
0.132	0.00	0.828	1.76	5.207	1.84	32.766	2.25	206.180	0.15	1297.392	0.00
0.147	0.00	0.922	1.74	5.802	1.84	36.510	2.09	229.740	0.04	1445.642	0.00
0.163	0.00	1.027	1.72	6.465	1.85	40.682	1.92	255.992	0.00	1610.833	0.00
0.182	0.00	1.145	1.70	7.204	1.88	45.330	1.74	285.243	0.00	1794.900	0.00
0.203	0.00	1.276	1.70	8.027	1.93	50.510	1.57	317.837	0.00	2000.000	
0.226	0.00	1.421	1.73	8.944	2.00	56.282	1.40	354.156	0.00		
0.252		1.584		9.966		62.713		394.625			

APPENDIX F-9

Statistical Analysis of Soil Sample NB11S1.

Result Analysis Report

Sample Name: SB - NB11	**SOP Name:** lame clay	**Measured:** Tuesday, November 19, 2019 1:44:08 PM	
Sample Source & type:	**Measured by:** Samuel T. Barber	**Analysed:** Tuesday, November 19, 2019 1:44:10 PM	
Sample bulk lot ref:	**Result Source:** Measurement		
Particle Name: Kaolinite high	**Accessory Name:** Hydro 2000MU (A)	**Analysis model:** General purpose	**Sensitivity:** Enhanced
Particle RI: 1.570	**Absorption:** 0.1	**Size range:** 0.020 to 2000.000 um	**Obscuration:** 19.59 %
Dispersant Name: Sodium Hexametaphosphate	**Dispersant RI:** 1.482	**Weighted Residual:** 1.874 %	**Result Emulation:** Off
Concentration: 0.0135 %Vol	**Span :** 5.848	**Uniformity:** 1.99	**Result units:** Volume
Specific Surface Area: 2.36 m²/g	**Surface Weighted Mean D[3,2]:** 2.544 um	**Vol. Weighted Mean D[4,3]:** 22.649 um	

d(0.1): 0.776 um **d(0.5):** 9.907 um **d(0.9):** 58.715 um

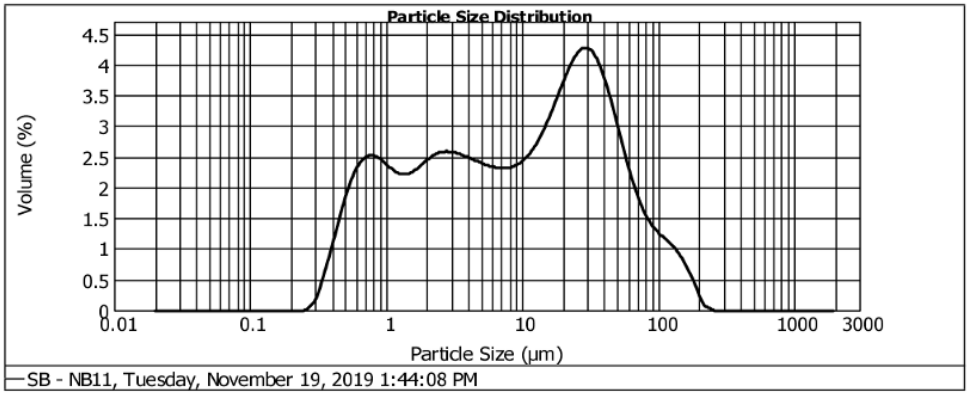

Size (µm)	Volume In %	Size (µm)	Volume In %	Size (µm)	Volume In %	Size (µm)	Volume In %	Size (µm)	Volume In %	Size (µm)	Volume In %
0.040	0.00	0.252	0.03	1.584	1.63	9.966	1.75	62.713	1.43	394.625	0.00
0.045	0.00	0.280	0.09	1.765	1.69	11.105	1.84	69.879	1.23	439.718	0.00
0.050	0.00	0.313	0.30	1.966	1.75	12.374	1.96	77.864	1.07	489.964	0.00
0.055	0.00	0.348	0.56	2.191	1.80	13.788	2.10	86.762	0.96	545.951	0.00
0.062	0.00	0.388	0.82	2.442	1.82	15.364	2.27	96.676	0.88	608.336	0.00
0.069	0.00	0.432	1.10	2.721	1.83	17.119	2.46	107.723	0.81	677.849	0.00
0.077	0.00	0.482	1.35	3.031	1.81	19.075	2.65	120.032	0.74	755.306	0.00
0.085	0.00	0.537	1.55	3.378	1.79	21.255	2.82	133.748	0.66	841.613	0.00
0.095	0.00	0.598	1.69	3.764	1.76	23.684	2.95	149.031	0.53	937.782	0.00
0.106	0.00	0.666	1.77	4.194	1.73	26.390	3.02	166.061	0.40	1044.941	0.00
0.118	0.00	0.743	1.78	4.673	1.70	29.406	3.01	185.036	0.22	1164.344	0.00
0.132	0.00	0.828	1.75	5.207	1.67	32.766	2.92	206.180	0.06	1297.392	0.00
0.147	0.00	0.922	1.69	5.802	1.65	36.510	2.75	229.740	0.01	1445.642	0.00
0.163	0.00	1.027	1.63	6.465	1.63	40.682	2.52	255.992	0.00	1610.833	0.00
0.182	0.00	1.145	1.58	7.204	1.63	45.330	2.25	285.243	0.00	1794.900	0.00
0.203	0.00	1.276	1.56	8.027	1.65	50.510	1.96	317.837	0.00	2000.000	
0.226	0.00	1.421	1.58	8.944	1.69	56.282	1.68	354.156	0.00		
0.252		1.584		9.966		62.713		394.625			

APPENDIX G.

The Erosion Function Chart (Briaud, 2004).

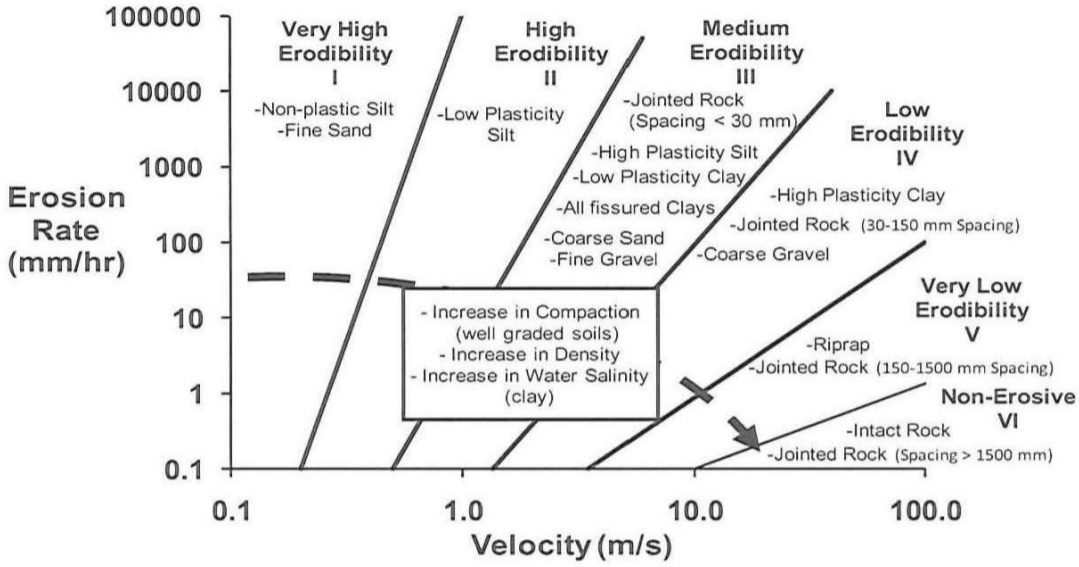

APPENDIX H.

Briaud's Critical Velocity vs. Mean Grain Size [2004]

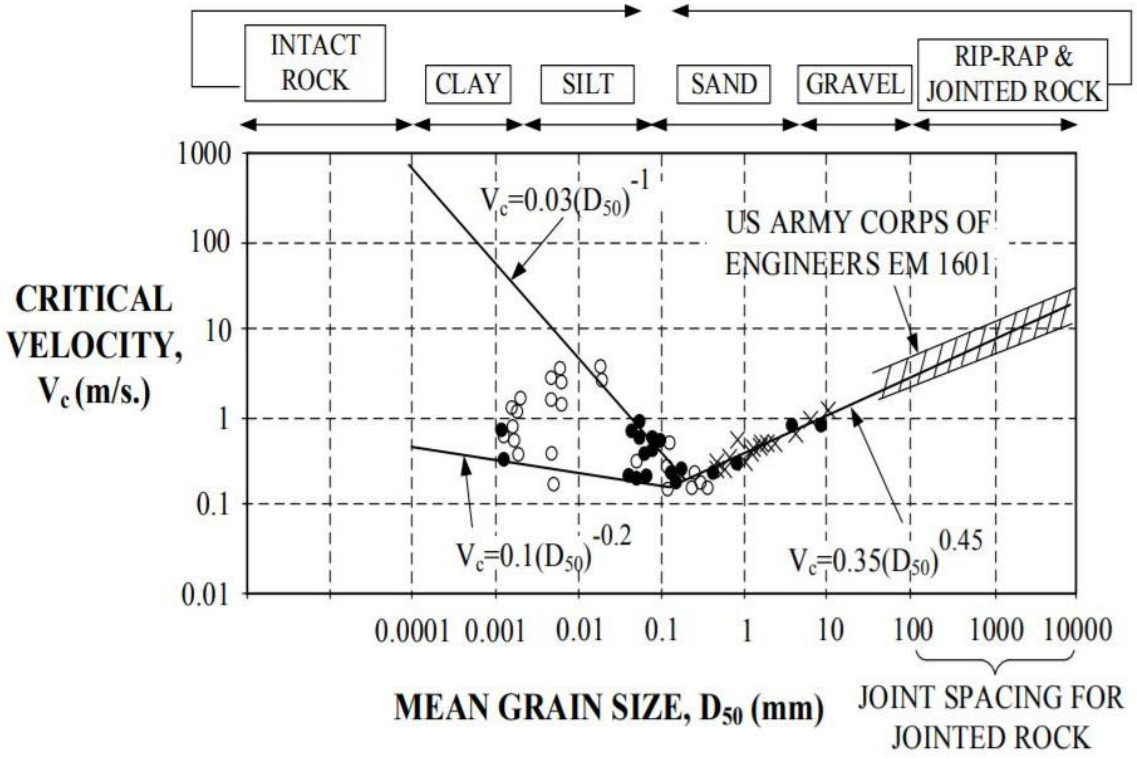

APPENDIX I.

Tabular RD Method Field Data.

ID	Bank Vertical Erosion (cm)	Bank Lateral Erosion (cm)	Channel Width (m)	Date To Structure (Years)	Erosion Rates (Cm/Yr)	Stage Height (Feet)	Stage Height (Meters)
NB01S1	366	236	56.4	32	7.38	12.0	3.7
NB01S2	365	353	56.4	1	353.00	12.0	3.7
NB02S1	168	134	64.6	12	11.17	5.5	1.7
NB02S2	133	110	64.6	9	12.22	4.4	1.3
NB03S1	81	182	59.4	12	15.17	2.7	0.8
NB04S1	1	1	62.0	28	0.04	0.0	0.0
NB05S1	200	304	46.9	3	101.33	6.6	2.0
NB06S1	100	325	42.7	1	325.00	3.3	1.0
NB07S1	147	204	45.6	21	9.71	4.8	1.5
NB08S1	289	579	50.1	21	27.57	9.5	2.9
NB09S1	109	127	50.9	1	127.00	3.6	1.1
NB09S2	150	209	50.9	4	52.25	4.9	1.5
NB10S1	290	120	41.8	1	120.00	9.5	2.9
NB10S2	127	210	45.9	10	21.00	4.2	1.3
NB11S1	128	304	50.3	30	10.13	4.2	1.3
NB12S1	138	300	72.2	1	300.00	4.5	1.4
NB13S1	326	60	71.5	1	60.00	10.7	3.3
NB13S2	278	90	71.5	1	90.00	9.1	2.8
NB14S1	98	325	39.9	6	54.17	3.2	1.0
NB14S2	90	325	39.9	6	54.17	3.0	0.9

BIBLIOGRAPHY

Abernethy, B., and Rutherfurd, I.D., 2000, The effect of riparian tree roots on the mass-stability of riverbanks: Earth Surface Processes and Landforms, v. 25, no. 9, p. 921–937.

Alfieri, L., Burek, P., Feyen, L., and Forzieri, G., 2015, Global warming increases the frequency of river floods in Europe.

Anderson, R.J., Bledsoe, B.P., and Hession, W.C., 2004, Width of Streams and Rivers in Response to Vegetation, Bank Material, and Other Factors1: JAWRA Journal of the American Water Resources Association, v. 40, no. 5, p. 1159–1172.

Andrews, E.D., 1980, Effective and bankfull discharges of streams in the Yampa River basin, Colorado and Wyoming: Journal of Hydrology, v. 46, no. 3, p. 311–330.

Annayat, W., and Sil, B.S., 2020, Assessing channel morphology and prediction of centerline channel migration of the Barak River using geospatial techniques: Bulletin of Engineering Geology and the Environment.

Aryal, Y., and Zhu, J., 2020, Effect of watershed disturbance on seasonal hydrological drought: An improved double mass curve (IDMC) technique: Journal of Hydrology, v. 585, p. 124746.

Asquith, W.H., and Roussel, M.C., 2004, Atlas of depth-duration frequency of precipitation annual maxima for Texas: Texas Department of Transportation Texas Department of Transportation Project Summary Report 5–1301–01–S, accessed March 24, 2021, at Atlas of depth-duration frequency of precipitation annual maxima for Texas at http://pubs.er.usgs.gov/publication/70176111.

Báčová, M., and Krása, J., 2016, Application of historical and recent aerial imagery in monitoring water erosion occurrences in Czech highlands: Soil and Water Research, v. 11 (2016), no. No. 4, p. 267–276.

Baker, V.R., 1984, Flood Sedimentation in Bedrock Fluvial Systems: p. 87–98.

Baker, V.R. Flood Hazards along the Balcones Escarpment in Central Texas: p. 26.

Baker, V., and Kochel, R.C., 1979, Long-term flood frequency analysis using geological data: IAHS AISH Publ., v. 128.

Baker, D.B., Richards, R.P., Loftus, T.T., and Kramer, J.W., 2004, A New Flashiness Index: Characteristics and Applications to Midwestern Rivers and Streams1: JAWRA Journal of the American Water Resources Association, v. 40, no. 2, p. 503–522.

Barbour, J.R., Stark, C.P., Lin, C.-W., Chen, H., Horng, M.-J., Ko, C.-P., Yi, T.-C., Tsai, T.-T., Chang, W.-S., Lee, S.-P., and Huang, C., 2009, Magnitude-frequency distributions of boundary shear stress along a rapidly eroding bedrock river: Geophysical Research Letters, v. 36, no. 4.

Barry, J.J., Buffington, J.M., and King, J.G., 2004, A general power equation for predicting bed load transport rates in gravel bed rivers: Water Resources Research, v. 40, no. 10.

Beechie, T., Buhle, E., Ruckelshaus, M., Fullerton, A., and Holsinger, L., 2006, Hydrologic regime and the conservation of salmon life history diversity: Biological Conservation, v. 130, no. 4, p. 560–572.

Beechie, T.J., Pollock, M.M., and Baker, S., 2008, Channel incision, evolution and potential recovery in the Walla Walla and Tucannon River basins, northwestern USA: Earth Surface Processes and Landforms, v. 33, no. 5, p. 784–800.

Bevenger, G.S., 1995, A Pebble Count Procedure for Assessing Watershed Cumulative Effects: U.S. Department of Agriculture, Forest Service, Rocky Mountain Forest and Range Experiment Station, 28 p.

Biedenharn, D.S., and Copeland, R.R., 2000, Effective Discharge Calculation: p. 10.

Biedenharn, D.S., Thorne, C.R., and Watson, C.C., 2000, Recent morphological evolution of the Lower Mississippi River: Geomorphology, v. 34, no. 3, p. 227–249.

Boix-Fayos, C., Barberá, G.G., López-Bermúdez, F., and Castillo, V.M., 2007, Effects of check dams, reforestation and land-use changes on river channel morphology: Case study of the Rogativa catchment (Murcia, Spain): Geomorphology, v. 91, no. 1, p. 103–123.

Bradley, D.N., and Tucker, G.E., 2012, Measuring gravel transport and dispersion in a mountain river using passive radio tracers: Earth Surface Processes and Landforms, v. 37, no. 10, p. 1034–1045.

Brandt, S.A., 2000, Classification of geomorphological effects downstream of dams: CATENA, v. 40, no. 4, p. 375–401.

Briaud, J.-L., and Montalvo-Bartolomei, A., 2014, Observation Method to Predict Meander Migration and Vertical Degradation of Rivers: FHWA/TX-13/0-6724-2, 108 p.

Briaud, J.-L., and Montalvo-Bartolomei, A.M., 2017, Meander migration: the observation method: Canadian Geotechnical Journal, v. 54, no. 8, p. 1104–1117.

Buffington, J.M., 2012, Changes in channel morphology over human time scales [Chapter 32]: In: Church, Michael; Biron, Pascale M.; Roy, Andre G., eds. Gravel-Bed Rivers: Processes, Tools, Environments. Chichester, UK: Wiley. p. 435-463., p. 435–463.

Burn, D.H., 1990, Evaluation of regional flood frequency analysis with a region of influence approach: Water Resources Research, v. 26, no. 10, p. 2257–2265.

Carling, P., 1988, The concept of dominant discharge applied to two gravel-bed streams in relation to channel stability thresholds: Earth Surface Processes and Landforms, v. 13, no. 4, p. 355–367.

Carrara, P.E., and Carroll, T.R., 1979, The determination of erosion rates from exposed tree roots in the piceance basin, Colorado: Earth Surface Processes, v. 4, no. 4, p. 307–317.

Carson, M.A., and Griffiths, G.A., 1989, Gravel transport in the braided Waimakariri River: Mechanisms, measurements and predictions: Journal of Hydrology, v. 109, no. 3, p. 201–220.

Cheney, M.G., 1940, Geology of North-Central Texas: AAPG Bulletin, v. 24, no. 1, p. 65–118.

Church, M., 2006, Bed Material Transport and the Morphology of Alluvial River Channels: Annual Review of Earth and Planetary Sciences, v. 34, no. 1, p. 325–354.

Claps, P., and Laio, F., 2003, Can continuous streamflow data support flood frequency analysis? An alternative to the partial duration series approach: Water Resources Research, v. 39, no. 8.

Copeland, R.R., 1994, Numerical modeling of hydraulic sorting and armoring in alluvial rivers.: p. 1

Croad, N. (1981). Physics of erosion of cohesive soils. Dissertation. Research Space at Auckland, 1981.

Daly, E., 2014, Quantifying Fluvial Resistance of Streambanks Using Jet Erosion Tests:

Daly, E., Fox, G., Miller, R., and Al-Madhhachi, A.-S., 2013, A Scour Depth Approach for Deriving Erodibility Parameters from Jet Erosion Tests: American Society of Agricultural and Biological Engineers, v. 56, no. 6, p. 1343–1351.

Das, T., 2014, River Bank Erosion Induced Human Displacement and Its Consequences: Living Reviews in Landscape Research, v. 8.

Davis, C.M., and Fox, J.F., 2009, Sediment Fingerprinting: Review of the Method and Future Improvements for Allocating Nonpoint Source Pollution: Journal of Environmental Engineering, v. 135, no. 7, p. 490–504.

De Rose, R.C., and Basher, L.R., 2011, Measurement of river bank and cliff erosion from sequential LIDAR and historical aerial photography: Geomorphology, v. 126, no. 1, p. 132–147.

Dickensen, S., and Bailie, M., 1991, Predicting Scour in Weak Rock of the Oregon Coast Range: Final Report: Oregon State University. Dept. of Civil, Construction, and Environmental Engineering.

Dolan, R., Hayden, B., and Heywood, J., 1978, A new photogrammetric method for determining shoreline erosion: Coastal Engineering, v. 2, p. 21–39.

Dumitriu, D., 2018, Sub-Bankfull Flow Frequency versus Magnitude of Flood Events in Outlining Effective Discharges. Case Study: Trotuș River (Romania): Water, v. 10, no. 10, p. 1292.

Dunne, K.B.J., and Jerolmack, D.J., 2018, Evidence of, and a proposed explanation for, bimodal transport states in alluvial rivers: Earth Surface Dynamics, v. 6, no. 3, p. 583–594.

Dunne, K.B.J., and Jerolmack, D.J., 2020, What sets river width? Science Advances, v. 6, no. 41, p. eabc1505.

Eaton, B.C., and Giles, T.R., 2009, Assessing the effect of vegetation-related bank strength on channel morphology and stability in gravel-bed streams using numerical models: Earth Surface Processes and Landforms, v. 34, no. 5, p. 712–724.

Fant, C., Srinivasan, R., Boehlert, B., Rennels, L., Chapra, S.C., Strzepek, K.M., Corona, J., Allen, A., and Martinich, J., 2017, Climate Change Impacts on US Water Quality Using Two Models: HAWQS and US Basins: Water, v. 9, no. 2, p. 118.

Fisher, G.B., Bookhagen, B., and Amos, C.B., 2013, Channel planform geometry and slopes from freely available high-spatial resolution imagery and DEM fusion: Implications for channel width scalings, erosion proxies, and fluvial signatures in tectonically active landscapes: Geomorphology, v. 194, p. 46–56.

Fuller, I.C., 2007, Geomorphic Work during a "150-Year" Storm: Contrasting Behaviors of River Channels in a New Zealand Catchment: Annals of the Association of American Geographers, v. 97, no. 4, p. 665–676.

Galay, V.J., 1983, Causes of river bed degradation: Water Resources Research, v. 19, no. 5, p. 1057–1090.

Gintz, D., Hassan, M.A., and Schmidt, K.-H., 1996, Frequency and Magnitude of Bedload Transport in a Mountain River: Earth Surface Processes and Landforms, v. 21, no. 5, p. 433–445.

Giradino, J., 2011, Rates of Channel Migration on the Brazos River: p. 128.

Goff, J.R., and Ashmore, P., 1994, Gravel transport and morphological change in braided sunwapta river, Alberta, Canada: Earth Surface Processes and Landforms, v. 19, no. 3, p. 195–212.

Gregory, K.J., 2006, The human role in changing river channels: Geomorphology, v. 79, no. 3, p. 172–191.

Guerrero, M., and Di Federico, V., 2018, Suspended sediment assessment by combining sound attenuation and backscatter measurements – analytical method and experimental validation: Advances in Water Resources, v. 113, p. 167–179.

Hamed, K., and Rao, A.R., 2019, Flood Frequency Analysis: CRC Press, 384 p.

Hamshaw, S.D., Bryce, T., Rizzo, D.M., O'Neil-Dunne, J., Frolik, J., and Dewoolkar, M.M., 2017, Quantifying streambank movement and topography using unmanned aircraft system photogrammetry with comparison to terrestrial laser scanning: River Research and Applications, v. 33, no. 8, p. 1354–1367.

Haniffa, M., 2019, Improvement of The Observation Method to Predict Meander Migration by Using A Probabilistic Analysis:

Hanson, G., and Cook, K., 2004, Apparatus, Test Procedures, and Analytical Methods to Measure Soil Erodibility In Situ: Applied Engineering in Agriculture, v. 20, no. 4, p. 455–462.

Harrelson, C.C., Rawlins, C.L., and Potyondy, J.P., 1994, Stream channel reference sites: An illustrated guide to field technique: U.S. Department of Agriculture, Forest Service, Rocky Mountain Forest and Range Experiment Station RM-GTR-245, RM-GTR-245 p., accessed August 12, 2020, at https://www.fs.usda.gov/treesearch/pubs/20753.

Heeren, D., Mittelstet, A., Fox, G., Storm, D., Al-Madhhachi, A., Midgley, S., Stunkel, K., and Tejral, R., 2012, Using Rapid Geomorphic Assessments to Assess Streambank Stability in Oklahoma Ozark Streams: American Society of Agricultural and Biological Engineers, v. 55, no. 3, p. 957–968.

Heitmuller, F.T., Hudson, P.F., and Asquith, W.H., 2015, Lithologic and hydrologic controls of mixed alluvial–bedrock channels in flood-prone fluvial systems: Bankfull and macrochannels in the Llano River watershed, central Texas, USA: Geomorphology, v. 232, p. 1–19.

Hey, R.D., 2006, Fluvial Geomorphological Methodology for Natural Stable Channel Design1: JAWRA Journal of the American Water Resources Association, v. 42, no. 2, p. 357–386.

Hey, R.D., and Thorne, C.R., 1986, Stable Channels with Mobile Gravel Beds: Journal of Hydraulic Engineering, v. 112, no. 8, p. 671–689.

Hickin, E.J., 1984, Vegetation and River Channel Dynamics: The Canadian Geographer / Le Géographe canadien, v. 28, no. 2, p. 111–126.

Hitz, O.M., Gärtner, H., Heinrich, I., and Monbaron, M., 2008, Wood anatomical changes in roots of European ash (Fraxinus excelsior L.) after exposure: Dendrochronologia, v. 25, no. 3, p. 145–152.

Hooke, J.M., 1980, Magnitude and distribution of rates of river bank erosion: Earth Surface Processes, v. 5, no. 2, p. 143–157.

Huang, H.Q., and Nanson, G.C., 1997, Vegetation and channel variation; a case study of four small streams in southeastern Australia: Geomorphology, v. 18, no. 3, p. 237–249.

Hubble, T.C.T., Docker, B.B., and Rutherfurd, I.D., 2010, The role of riparian trees in maintaining riverbank stability: A review of Australian experience and practice: Ecological Engineering, v. 36, no. 3, p. 292–304.

Jansen, J.D., 2006, Flood magnitude–frequency and lithologic control on bedrock river incision in post-orogenic terrain: Geomorphology, v. 82, no. 1, p. 39–57.

Kalliola, R., and Puhakka, M., 1988, River Dynamics and Vegetation Mosaicism: A Case Study of the River Kamajohka, Northernmost Finland: Journal of Biogeography, v. 15, no. 5/6, p. 703–719.

Kenney, M.A., Wilcock, P.R., Hobbs, B.F., Flores, N.E., and Martínez, D.C., 2012, Is Urban Stream Restoration Worth It?1: Is Urban Stream Restoration Worth It? JAWRA Journal of the American Water Resources Association, v. 48, no. 3, p. 603–615.

Klemeš, V., 1979, Storage mass-curve analysis in a systems-analytic perspective: Water Resources Research, v. 15, no. 2, p. 359–370.

Knutson, T.R., McBride, J.L., Chan, J., Emanuel, K., Holland, G., Landsea, C., Held, I., Kossin, J.P., Srivastava, A.K., and Sugi, M., 2010, Tropical cyclones and climate change: Nature Geoscience, v. 3, no. 3, p. 157–163.

Kondolf, G.M., 1997, Application of the Pebble Count Notes on Purpose, Method, and Variants1: JAWRA Journal of the American Water Resources Association, v. 33, no. 1, p. 79–87.

Kondolf, G.M., and Curry, R.R., 1986, Channel erosion along the Carmel river, Monterey county, California: Earth Surface Processes and Landforms, v. 11, no. 3, p. 307–319.

Lamb, M.P., Finnegan, N.J., Scheingross, J.S., and Sklar, L.S., 2015, New insights into the mechanics of fluvial bedrock erosion through flume experiments and theory: Geomorphology, v. 244, p. 33–55.

Lamoreaux, P.E., and Newton, J.G., 1986, Catastrophic subsidence: An environmental hazard, shelby county, Alabama: Environmental Geology and Water Sciences, v. 8, no. 1, p. 25–40.

Lane, E.W., 1955, importance of fluvial morphology in hydraulic engineering: Proceedings (American Society of Civil Engineers) ; v. 81, paper no. 745.

Langat, P.K., Kumar, L., and Koech, R., 2019, Monitoring river channel dynamics using remote sensing and GIS techniques: Geomorphology, v. 325, p. 92–102.

Leopold, L. B. (1980). Techniques and interpretation: The sediment studies of GK Gilbert. *Geological Society of America Special Papers*, *183*, 125-128.

Leopold, L.B., Wolman, M.G., and Miller, J.P., 1995, Fluvial Processes in Geomorphology: Courier Corporation, 548 p.

Li, C., Czapiga, M.J., Eke, E.C., Viparelli, E., and Parker, G., 2015, Variable Shields number model for river bankfull geometry: bankfull shear velocity is viscosity-dependent but grain size-independent: Journal of Hydraulic Research, v. 53, no. 1, p. 36–48.

Li, Y., Zhang, Q., Liu, X., and Yao, J., 2020, Water balance and flashiness for a large floodplain system: A case study of Poyang Lake, China: Science of The Total Environment, v. 710, p. 135499.

Logar, I., Brouwer, R., and Paillex, A., 2019, Do the societal benefits of river restoration outweigh their costs? A cost-benefit analysis: Journal of Environmental Management, v. 232, p. 1075–1085.

Malik, I., 2008, Dating of small gully formation and establishing erosion rates in old gullies under forest by means of anatomical changes in exposed tree roots (Southern Poland): Geomorphology, v. 93, no. 3, p. 421–436.

Malik, I., and Matyja, M., 2008, Bank erosion history of a mountain stream determined by means of anatomical changes in exposed tree roots over the last 100 years (Bílá Opava River — Czech Republic): Geomorphology, v. 98, no. 1–2, p. 126–142.

Malik, I., and Wistuba, M., 2012, Dendrochronological methods for reconstructing mass movements — An example of landslide activity analysis using tree-ring eccentricity: Geochronometria, v. 39, no. 3, p. 180–196.

Miao, C., Ni, J., and Borthwick, A.G.L., 2010, Recent changes of water discharge and sediment load in the Yellow River basin, China: Progress in Physical Geography: Earth and Environment, v. 34, no. 4, p. 541–561.

Micheli, E.R., and Larsen, E.W., 2011, River channel cutoff dynamics, Sacramento River, California, USA: River Research and Applications, v. 27, no. 3, p. 328–344.

Miller, B.A., and Schaetzl, R.J., 2012, Precision of Soil Particle Size Analysis using Laser Diffractometry: Soil Science Society of America Journal, v. 76, no. 5, p. 1719–1727.

Motta, D., Abad, J.D., Langendoen, E.J., and Garcia, M.H., 2012, A simplified 2D model for meander migration with physically-based bank evolution: Geomorphology, v. 163–164, p. 10–25.

Nash, D.B., 1994, Effective Sediment-Transporting Discharge from Magnitude-Frequency Analysis: The Journal of Geology, v. 102, no. 1, p. 79–95.

National Academies of Sciences, E., 2017, Guidance for Design Hydrology for Stream Restoration and Channel Stability:

Navratil, O., Albert, M.-B., Hérouin, E., and Gresillon, J.-M., 2006, Determination of bankfull discharge magnitude and frequency: comparison of methods on 16 gravel-bed river reaches: Earth Surface Processes and Landforms, v. 31, no. 11, p. 1345–1363.

Nelson, E.J., and Booth, D.B., 2002, Sediment sources in an urbanizing, mixed land-use watershed: Journal of Hydrology, v. 264, no. 1, p. 51–68.

Ning, S.-K., Chang, N.-B., Jeng, K.-Y., and Tseng, Y.-H., 2006, Soil erosion and non-point source pollution impacts assessment with the aid of multi-temporal remote sensing images: Journal of Environmental Management, v. 79, no. 1, p. 88–101.

Osman, A.M., and Thorne, C.R., 1988, Riverbank Stability Analysis. I: Theory: Journal of Hydraulic Engineering, v. 114, no. 2, p. 134–150.

Ouyang, W., Hao, F., Skidmore, A.K., and Toxopeus, A.G., 2010a, Soil erosion and sediment yield and their relationships with vegetation cover in upper stream of the Yellow River: Science of The Total Environment, v. 409, no. 2, p. 396–403.

Ouyang, W., Skidmore, A.K., Hao, F., and Wang, T., 2010b, Soil erosion dynamics response to landscape pattern: Science of The Total Environment, v. 408, no. 6, p. 1358–1366.

Palmer, M., Allan, D., Meyer, J., and Bernhardt, E., 2007, River Restoration in the Twenty-First Century: Data and Experiential Knowledge to Inform Future Efforts: Restoration Ecology, v. 15, no. 3, p. 472–481.

Parker, G., 1990, Surface-based bedload transport relation for gravel rivers: Journal of Hydraulic Research, v. 28, no. 4, p. 417–436.

Parker, G., Klingeman, P.C., and McLean, D.G., 1983, Bedload and size distribution in paved gravel-bed streams: Journal of Hydraulic Engineering, v. 109, no. 5, p. 793–794.

Parsons, M., Thoms, M., and Norris, R.H., 2004, Development of a Standardised Approach to River Habitat Assessment in Australia: Environmental Monitoring and Assessment, v. 98, p. 109–130.

Perera, C., and Wu, W., 2016, Erosion Coefficients of Cohesive Sediments: p. 293–302.

Pfeiffer, A.M., Finnegan, N.J., and Willenbring, J.K., 2017, Sediment supply controls equilibrium channel geometry in gravel rivers: Proceedings of the National Academy of Sciences, v. 114, no. 13, p. 3346–3351.

Pickup, G., and Warner, R.F., 1976, Effects of hydrologic regime on magnitude and frequency of dominant discharge: Journal of Hydrology, v. 29, no. 1, p. 51–75.

Pitlick, J., Cui, Y., and Wilcock, P., 2009, Manual for computing bed load transport using BAGS (Bedload Assessment for Gravel-bed Streams) Software: Gen. Tech. Rep. RMRS-GTR-223. Fort Collins, CO: U.S. Department of Agriculture, Forest Service, Rocky Mountain Research Station. 45 p., v. 223.

Potyondy, J., & Bunte, K. (2002). Analyzing pebble count data collected by size classes. *US Department of Agriculture Forest Service, MS Excel Spreadsheet, Version*, *1*.

Proctor, C., 1969, The North Bosque Watershed - Inventory of a Drainage Basin: Baylor Geological Studies, v. 16.

Rinaldi, M., and Johnson, P.A., 1997, Characterization of Stream Meanders for Stream Restoration: Journal of Hydraulic Engineering, v. 123, no. 6, p. 567–570.

Robert, E.M.R., Mencuccini, M., and Martínez-Vilalta, J., 2017, The Anatomy and Functioning of the Xylem in Oaks, *in* Gil-Pelegrín, E., Peguero-Pina, J.J., and Sancho-Knapik, D. eds., Oaks Physiological Ecology. Exploring the Functional Diversity of Genus Quercus L.: Springer International Publishing, Cham, p. 261–302.

Rosburg, T.T., Nelson, P.A., and Bledsoe, B.P., 2017, Effects of Urbanization on Flow Duration and Stream Flashiness: A Case Study of Puget Sound Streams, Western Washington, USA: JAWRA Journal of the American Water Resources Association, v. 53, no. 2, p. 493–507.

Roy, S., Emi, U., Blachly, B., Fox, E., and Gardner, K., 2018a, A multiscale approach to balance trade-offs among dam infrastructure, river restoration, and cost: PNAS.

Roy, S.G., Uchida, E., de Souza, S.P., Blachly, B., Fox, E., Gardner, K., Gold, A.J., Jansujwicz, J., Klein, S., McGreavy, B., Mo, W., Smith, S.M.C., Vogler, E., Wilson, K., and others, 2018b, A multiscale approach to balance trade-offs among dam infrastructure, river restoration, and cost: Proceedings of the National Academy of Sciences, v. 115, no. 47, p. 12069–12074.

Rutherfurd, I., and Grove, J. The Influence of Trees on Stream Bank Erosion: Evidence from Root-Plate Abutments, accessed March 31, 2020, at ResearchGate at https://www.researchgate.net/publication/289318660_The_Influence_of_Trees_on_Stream_Bank_Erosion_Evidence_from_Root-Plate_Abutments.

Saez, J.L., Corona, C., Stoffel, M., Rovéra, G., Astrade, L., and Berger, F., 2011, Mapping of erosion rates in marly badlands based on a coupling of anatomical changes in exposed roots with slope maps derived from LiDAR data: Earth Surface Processes and Landforms, v. 36, no. 9, p. 1162–1171.

Sanderson, J.S., Rowan, N., Wilding, T., Bledsoe, B.P., Miller, W.J., and Poff, N.L., 2012, Getting to Scale with Environmental Flow Assessment: The Watershed Flow Evaluation Tool: River Research and Applications, v. 28, no. 9, p. 1369–1377.

Schwenk, J., and Foufoula-Georgiou, E., 2016, Meander cutoffs nonlocally accelerate upstream and downstream migration and channel widening: Geophysical Research Letters, v. 43, no. 24, p. 12,437-12,445.

Searcy, J.K., and Hardison, C.H., 1960, Double-mass Curves: U.S. Government Printing Office, 44 p.

Shepherd, R.G., 1985, Regression Analysis of River Profiles: The Journal of Geology, v. 93, no. 3, p. 377–384.

Shobe, C.M., Hancock, G.S., Eppes, M.C., and Small, E.E., 2017, Field evidence for the influence of weathering on rock erodibility and channel form in bedrock rivers: Earth Surface Processes and Landforms, v. 42, no. 13, p. 1997–2012.

Sholtes, J.S., and Bledsoe, B.P., 2016, Half-Yield Discharge: Process-Based Predictor of Bankfull Discharge: Journal of Hydraulic Engineering, v. 142, no. 8, p. 04016017.

Sholtes, J., Werbylo, K., and Bledsoe, B., 2014, Physical context for theoretical approaches to sediment transport magnitude-frequency analysis in alluvial channels: Water Resources Research, v. 50, no. 10, p. 7900–7914.

Sichingabula, H.M., 1999, Magnitude-frequency characteristics of effective discharge for suspended sediment transport, Fraser River, British Columbia, Canada: Hydrological Processes, v. 13, no. 9, p. 1361–1380.

Smalley, M.L., Emmett, W.W., and Wacker, A.M., 1994, Annual Replenishment of Bed Material by Sediment Transport in the Wind River Near Riverton, Wyoming: U.S. Department of the Interior, U.S. Geological Survey, 34 p.

Smith, D.G., 1976, Effect of vegetation on lateral migration of anastomosed channels of a glacier meltwater river: GSA Bulletin, v. 87, no. 6, p. 857–860.

Snyder, N.P., Rubin, D.M., Alpers, C.N., Childs, J.R., Curtis, J.A., Flint, L.E., and Wright, S.A., 2004, Estimating accumulation rates and physical properties of sediment behind a dam: Englebright Lake, Yuba River, northern California: Water Resources Research, v. 40, no. 11.

Sochan, A., Bieganowski, A., Ryzak, M., Dobrowolski, R., and Bartminski, P., 2012, Comparison of soil texture determined by two dispersion units of Mastersizer 2000: International Agrophysics, v. 26, no. 1.

Spiekermann, R., Betts, H., Dymond, J., and Basher, L., 2017, Volumetric measurement of river bank erosion from sequential historical aerial photography: Geomorphology, v. 296, p. 193–208.

Stafford, D.B., 1971, Air Photo Survey of Coastal Erosion: p. 11.

Stoffel, M., Corona, C., Ballesteros-Cánovas, J.A., and Bodoque, J.M., 2013, Dating and quantification of erosion processes based on exposed roots: Earth-Science Reviews, v. 123, p. 18–34.

Stroth, T., 2020, Considering Sediment Dynamics in River Restoration Design: The Application of New Perspectives and Tools (including the Capacity/Supply Ratio [CSR] Tool), *in* 19th Annual Stream Restoration Symposium – RRNW.

Stroth, T.R., Bledsoe, B.P., and Nelson, P.A., 2017, Full Spectrum Analytical Channel Design with the Capacity/Supply Ratio (CSR): Water, v. 9, no. 4, p. 271.

Sung, C.Y., and Li, M.-H. The effect of urbanization on stream hydrology in hillslope watersheds in central Texas.

Surian, N., Barban, M., Ziliani, L., Monegato, G., Bertoldi, W., and Comiti, F., 2015, Vegetation turnover in a braided river: frequency and effectiveness of floods of different magnitude: Earth Surface Processes and Landforms, v. 40, no. 4, p. 542–558.

Torizzo, M., and Pitlick, J., 2004, Magnitude-frequency of bed load transport in mountain streams in Colorado: Journal of Hydrology, v. 290, no. 1, p. 137–151.

Turowski, J.M., Hovius, N., Meng-Long, H., Lague, D., and Men-Chiang, C., 2008, Distribution of erosion across bedrock channels: Earth Surface Processes and Landforms, v. 33, no. 3, p. 353–363.

Turowski, J.M., Lague, D., and Hovius, N., 2007, Cover effect in bedrock abrasion: A new derivation and its implications for the modeling of bedrock channel morphology: Journal of Geophysical Research: Earth Surface, v. 112, no. F4.

Turowski, J.M., Yager, E.M., Badoux, A., Rickenmann, D., and Molnar, P., 2009, The impact of exceptional events on erosion, bedload transport and channel stability in a step-pool channel: Earth Surface Processes and Landforms, v. 34, no. 12, p. 1661–1673.

US EPA, O., 2020, National Rivers and Streams Assessment 2013-14 Key Findings, accessed March 24, 2021, at US EPA at https://www.epa.gov/national-aquatic-resource-surveys/national-rivers-and-streams-assessment-2013-14-key-findings.

Verhaar, P.M., Biron, P.M., Ferguson, R.I., and Hoey, T.B., 2011, Implications of climate change in the twenty-first century for simulated magnitude and frequency of bed-material transport in tributaries of the Saint-Lawrence River: Hydrological Processes, v. 25, no. 10, p. 1558–1573.

Walling, D.E., 1977, Assessing the accuracy of suspended sediment rating curves for a small basin: Water Resources Research, v. 13, no. 3, p. 531–538.

Whipple, K.X., DiBiase, R.A., and Crosby, B.T., 2013, Bedrock Rivers: Fluvial Geomorphology, p. 550–573.

Wible, T., Lloyd, W., David, O., and Arabi, M., 2014, Cyberinfrastructure for Scalable Access to Stream Flow Analysis: International Congress on Environmental Modelling and Software.

Wilcock, P.R., 2001, Toward a practical method for estimating sediment-transport rates in gravel-bed rivers: Earth Surface Processes and Landforms, v. 26, no. 13, p. 1395–1408.

Wilcock, P., Pitlick, J., and Cui, Y. Sediment transport primer: estimating bed-material transport in gravel-bed rivers: p. 84.

Wilkinson, B.H., and McElroy, B.J., 2007, The impact of humans on continental erosion and sedimentation: GSA Bulletin, v. 119, no. 1–2, p. 140–156.

Williams, G.P., 1986, River meanders and channel size: Journal of Hydrology, v. 88, no. 1, p. 147–164.

Wilson, C.G., Kuhnle, R.A., Bosch, D.D., Steiner, J.L., Starks, P.J., Tomer, M.D., and Wilson, G.V., 2008, Quantifying relative contributions from sediment sources in Conservation Effects Assessment Project watersheds: Journal of Soil and Water Conservation, v. 63, no. 6, p. 523–532.

Wolman, M.G., 1954, A method of sampling coarse river-bed material: Eos, Transactions American Geophysical Union, v. 35, no. 6, p. 951–956.

Wolman, M.G., and Miller, J.P., 1960, Magnitude and Frequency of Forces in Geomorphic Processes: The Journal of Geology, v. 68, no. 1, p. 54–74.

Wu, B., Wang, G., Xia, J., Fu, X., and Zhang, Y., 2008, Response of bankfull discharge to discharge and sediment load in the Lower Yellow River: Geomorphology, v. 100, no. 3, p. 366–376.

Wynn, T., Mostaghimi, S., and Alphin, E., 2004, The Effects of Vegetation on Stream Bank Erosion: American Society of Agricultural and Biological Engineers.

Yalin, M.S., 1972, Mechanics of sediment transport: Pergamon Press, Oxford, New York, 290 p.

Yeager, K.M., Santschi, P.H., Phillips, J.D., and Herbert, B.E., 2005, Suspended sediment sources and tributary effects in the lower reaches of a coastal plain stream as indicated by radionuclides, Loco Bayou, Texas: Environmental Geology, v. 47, no. 3, p. 382–395.

Yen, H., Daggupati, P., White, M.J., Srinivasan, R., Gossel, A., Wells, D., and Arnold, J.G., 2016, Application of Large-Scale, Multi-Resolution Watershed Modeling Framework Using the Hydrologic and Water Quality System (HAWQS): Water, v. 8, no. 4, p. 164.

Yochum, S.E., and Collins, F., 2015, Colorado Front Range Flood of 2013: Peak Flows and Flood Frequencies: p. 12.

Yochum, S.E., Sholtes, J.S., Scott, J.A., and Bledsoe, B.P., 2017, Stream power framework for predicting geomorphic change: The 2013 Colorado Front Range flood: Geomorphology, v. 292, p. 178–192.

Yu-chun, Z., 2007, Mastersizer 2000 laser particle size analyzer and its applications, accessed August 12, 2020, at /paper/Mastersizer-2000-laser-particle-size-analyzer-and-Yu-chun/09b9fde65608fa5a2216f9527bccbadd7b6ab513.